University of Alberta

Numerical simulation of Ordovician climate using a coupled atmosphere-ocean general circulation model

by

Mika Kashiwagi

©

A thesis submitted to the Faculty of Graduate Studies and Research
in partial fulfillment of the requirements for the degree of

Master of Science

Department of Earth and Atmospheric Sciences

Edmonton, Alberta
Spring 2007

Library and Archives Canada

Published Heritage Branch

395 Wellington Street
Ottawa ON K1A 0N4
Canada

Bibliothèque et Archives Canada

Direction du Patrimoine de l'édition

395, rue Wellington
Ottawa ON K1A 0N4
Canada

Your file Votre référence
ISBN: 978-0-494-29975-3
Our file Notre référence
ISBN: 978-0-494-29975-3

NOTICE:
The author has granted a non-exclusive license allowing Library and Archives Canada to reproduce, publish, archive, preserve, conserve, communicate to the public by telecommunication or on the Internet, loan, distribute and sell theses worldwide, for commercial or non-commercial purposes, in microform, paper, electronic and/or any other formats.

The author retains copyright ownership and moral rights in this thesis. Neither the thesis nor substantial extracts from it may be printed or otherwise reproduced without the author's permission.

AVIS:
L'auteur a accordé une licence non exclusive permettant à la Bibliothèque et Archives Canada de reproduire, publier, archiver, sauvegarder, conserver, transmettre au public par télécommunication ou par l'Internet, prêter, distribuer et vendre des thèses partout dans le monde, à des fins commerciales ou autres, sur support microforme, papier, électronique et/ou autres formats.

L'auteur conserve la propriété du droit d'auteur et des droits moraux qui protège cette thèse. Ni la thèse ni des extraits substantiels de celle-ci ne doivent être imprimés ou autrement reproduits sans son autorisation.

In compliance with the Canadian Privacy Act some supporting forms may have been removed from this thesis.

While these forms may be included in the document page count, their removal does not represent any loss of content from the thesis.

Conformément à la loi canadienne sur la protection de la vie privée, quelques formulaires secondaires ont été enlevés de cette thèse.

Bien que ces formulaires aient inclus dans la pagination, il n'y aura aucun contenu manquant.

Canada

ABSTRACT

The Late Ordovician (458–443 Ma) is known as a glacial time as inferred from continental glacial deposits in South Africa, South America, and Saudi Arabia, regions that were adjacent on the super continent, Gondwana, at the time. With its high levels of CO_2, reduced solar forcing and a completely different continental configuration from today, the Late Ordovician climate presents a number of intriguing challenges that may be addressed through the use of numerical modelling, such as extensive glaciation at high southern latitudes and the possibility of large amplitude Ordovician El Niño/La Niña events and tropical monsoons. Using a coupled general circulation model (GCM) suitably configured for the Late Ordovician, the aims of this research are to diagnose and explain the factors underlying the unique geological and palaeontological archives of the late Ordovician climate and to identify some of the unique climate features that are likely to have existed in Earth's deep past.

Acknowledgement

I wish to thank Prof. Andrew B. G. Bush for giving me the opportunity to take this project and for patiently supervising me through my degree time. I am grateful to Prof. Brian D. E. Chatterton for palaeontological supervisions as well as Stacey L. Gibb and Ryan McKeller for discussions and suggestions linked to this work. This research was supported by NSERC Discovery Grant awarded to Prof. Andrew B. G. Bush. The atmosphere-only and coupled atmosphere-ocean models were at the University of Alberta and had been configured for the Silicon Graphics architecture and an SGI Origin 2200 for running the model and an SGI O2 workstation for diagnostic analysis were required. Infrastructure support from the University of Alberta is gratefully acknowledged.

Finally, I wish to thank Yasutada and Hiroko Kashiwagi, Mfon Udofia, and Dr. Ted Rose for their great supports and inspirations.

TABLE OF CONTENTS

Chapter 1 General background 1

1-1. Introduction 1

1-2. Paleogeography 3

1-2-1. Reconstruction of palaeogeography 3

1-2-2. Plate tectonics 4

1-3. Palaeoclimatology 8

1-3-1. Ordovician climates 8

1-3-2. Palaeobiology and extinction events 14

1-3-2-1. Trilobites 15

1-3-2-2. Brachiopods 17

1-3-2-3. Graptolites 18

1-3-3. Paradox of the Ordovician glaciation 20

1.4. Previous Studies 21

Chapter 2 Methodology 26

2-1. Model Description 26

2-1-1. Atmosphere model 26

2-1-2. Ocean model 28

2-1-3. Atmosphere-ocean coupled model 29

Chapter 3 Modelling results 32

3-1. Atmospheric Temperature 32

3-1-1. Atmosphere – only model 32

3-1-2. The coupled model 49

3-2. Ocean 68

3-3. Interannual variability: The El Niño Southern Oscillation (ENSO) 73

3-4. Precipitation 78

3-5. Heat transportat 82

3-6. Ordovician monsoons 84

3-7. Permanent continental ice 88

Chapter 4 Discussion and conclusions **92**

4-1. Correlation between the modeling results and geological and palaeontological evidence 92

References **98**

List of Tables

Chapter 1

Table 1-1	Ordovician time scale	2

Chapber 3

Table 3-4-1	Annual mean precipitation (cm/day) at mid-latitudes (45N and 45S) and the equator for the Ordovician and the present day.	79

List of Figures

Chapter 1

Figure1-1	Plate tectonic maps for a) Late Ordovician and b) present day.	6
Figure1-2	Late Ordovician maps. Solid lines are the continental margins under transgression conditions. (a) The Late Ordovician map with palaeocontinent and palaeocean names (b) the Late Ordovician map with modern continent names.	7
Figure1-3	The average global temperature through the geological time periods.	9
Figure1-4	Late Ordovician palaeobiogeography maps. a) Trilobite distributions. b) Brachiopod distributions.	16
Figure1-5	Distribution of graptolite faunal provinces before the first Ordovician extinction event.	19

Chapter 3

Figure 3-1-1	Time evolution of temperature (atmosphere–only simulation): in (a) global, (b) tropospheric, and (c) stratospheric atmosphere temperature (°K) as a function of time (years).	33
Figure 3-1-2	Annual and zonal mean near-surface temperature (atmospherere–only simulation) in degrees Kelvin as a function of latitude.	36
Figure 3-1-3	Annual mean near surface (about 30 m above ground) temperature (°K) as a function of longitude and latitude	37

for (a) the Ordovician, and (b) the present day.

Figure3-1-4 Annual mean net surface shortwave radiation as a function of longitude and latitude for (a) the Ordovician, and (b) the present day. 38

Figure 3-1-5 Annual mean net surface (about 30 m above ground) longwave emission as a function of longitude and latitude for (a) the Ordovician, and (b) the present day. 39

Figure 3-1-6 Annual mean relative humidity (percent/100) as a function of longitude and latitude for (a) the Ordovician, and (b) the present day 40

Figure 3-1-7 Amplitude of the seasonal cycle in near surface temperature (shaded; °K) in the atmosphere – only model for (a) Ordovician and (b) the present day. 43

Figure 3-1-8 Vertical profile of annual and zonal mean temperature (shaded) and zonal velocity (contours) as a function of height and latitude for (a) Ordovician and (b) the present day. 44

Figure 3-1-9 Annual mean tropical Hadley Cells and midlatitude Ferrel cells (times 10^{10} kg/s) for (a) the Ordovician, and (b) the present day with 10^{10} kg/s intervals 46

Figure 3-1-10 Annual mean Walker circulation (times 10^{10} kg/s) for (a) the Ordovician, and (b) the present day with 10^{11} kg/s contour intervals. 48

Figure 3-1-11 Time evolution of (a) global, (b) tropospheric, and (c) stratospheric atmospheric temperature (°K) as a function of time (years) from the coupled model results. 50

Figure 3-1-12	Annual and zonal mean near-surface temperature (coupled model simulation) in degrees Kelvin as a function of latitude.	52
Figure 3-1-13	Coupled model simulation of annual mean near surface (about 30 m above ground) temperature in °K as a function of longitude and latitude for (a) the Ordovician, and (b) the present day.	55
Figure 3-1-14	Annual mean, zonally and vertically averaged atmospheric poleward heat flux for the Ordovician and the present day.	56
Figure 3-1-15	Vertical profile of annual and zonal mean temperature and zonal velocity as a function of latitude for (a) Ordovician and (b) the present day	59
Figure 3-1-16	Annual mean net surface humidity as a function of longitude and latitude for (a) the Ordovician, and (b) the present day.	60
Figure3-1-17	Annual mean net shortwave radiation as a function of longitude and latitude for (a) the Ordovician, and (b) the present day.	61
Figure 3-1-18	Annual mean net longwave emission as a function of longitude and latitude for (a) the Ordovician, and (b) the present day.	62
Figure 3-1-19	Annual mean Hadley Cells for (a) the Ordovician and (b) the present day.	65
Figure 3-1-20	Lithological distribution map for the late Ordovician.	66
Figure 3-1-21	Annual mean Walker circulation for (a) the Ordovician and (b) the present day.	67

Figure 3-2-1	Annual mean sea surface temperature (°C) (a) in the Ordovician and (b) in the present day.	69
Figure 3-2-2	(a) Annual mean sea surface salinity for the Ordovician. (b) Stream flow of annual mean ocean currents at a depth of 15m.	72
Figure 3-3-1	Maps of the mean sea surface temperature for a) 20-22 years average, b) 24-26 years average, c) 48-52 years average, and d) 53-57 years average of the late Ordovician simulation with function of longitude and latitude.	74
Figure 3-3-2	ENSO index for a) the Panthalassic ocean, b) the Palaeo-Tethys ocean and c) the Pacific ocean.	77
Figure 3-4-1	Spatial distribution of the annual mean precipitation (cm/day) for (a) the Ordovician and (b) the present day. JJA averages are shown in (c) and (d), and the DJF averages in (e) and (f) as the Ordovician and the present day respectively.	80
Figure 3-4-2	Zonal mean precipitation rate (cm/d) for (a) the Ordovician and (b) the present day.	81
Figure 3-5-1	Annual mean, zonally and vertically averaged atmospheric poleward heat flux for the Ordovician and the present day	83
Figure 3-6-1	MAM horizontal winds in (a) the Gondwana and Laurentia monsoons and JJA horizontal winds in (b) the modern south Asian monsoon regions.	86
Figure 3-6-2	MAM precipitation in the monsoon region for (a) the Ordovician and JJA precipitation in the monsoon region for (b) the present day	87
Figure 3-7-1	Spatial distribution of the Ordovician snow accumulation in cm of water equivalent.	90

Figure 3-7-2 JJA averaged sea ice thickness for (a) Ordovician and (b) the present day. 91

Chapter 4

Figure 4-1-1 The Southern hemisphere ocean currents. 95

List of Equation

Chapter 2

2.1	The normalized pressure coordinate	24

1. GENERAL BACKGROUND

1-1. INTRODUCTION

The research presented in this thesis focuses on the use of a coupled atmosphere-ocean General Circulation Model (GCM) to investigate the interactions of the atmosphere-ocean-sea ice system during the Late Ordovician Period (458–443 million years ago (Ma), Table 1-1). With its high levels of carbon dioxide (Berner, 1998; Yapp and Poths, 1992), reduced solar forcing (Endal and Schatten, 1982; Molnar and Gutowski, 1995) and a completely different continental configuration from today, the Late Ordovician climate presents a number of intriguing challenges that may be addressed through the use of numerical modelling. For example, the presence of extensive glaciation over the region now identified with the Sahara Desert and Africa (Frakes *et. al.*, 1992; Caputo, 1998) appears to be at odds with the high levels of atmospheric carbon dioxide inferred for this time. Extensive tropical epicontinental seas harboured life but, given the continental configuration of the time, were likely to be subject to large amplitude climatic events analogous to the modern El Niño Southern Oscillation (ENSO).

The aims of this research are to diagnose and explain the factors underlying the selected unique geological and palaeontological archives of the late Ordovician climate using a coupled GCM as the primary tool. This tool will be configured and constrained by existing knowledge of the climatic forcing factors of that time.

	Period / Semi-Period		Epoch		Age	Ma
Paleozoic	Permian					248
	Carboniferous					290
	Devonian					354
	Silurian	Late	Pridolian			417
			Ludlovian		Ludfordian	
					Gorstian	423
		Early	Wenlockian		Gleedonian	
					Whitwellian	
					Sheinwoodian	
			Llandoverian		Telychian	
					Aeronian	
					Rhuddanian	443
	Ordovician	Late	Ashgillian		Hirnantian	
					Rawtheyan	
					Cautleyan	
					Pusgillian	449
			Caradocian		Onnian	
					Actonian	
					Marshbrookian	
					Longvillian	
					Soudleyan	
					Harnagian	
					Costonian	458
		Middle	Llandeilian		Late	
					Middle	
					Early	
			Llanvirnian		Late	
					Early	470
		Early	Arenigian			
			Tremadocian			490
	Cambrian	Late	Sunwaptan	Merioneth	Dolgellian	
			Steptoean		Maentwrogian	500
		Middle	Majuran	St David's	Menevian	
			Delamaran		Solvan	512
		Early	Dyeran	Caerfai	Lenian	
			Montezuman		Atdabanian	
					Tommotian	549

Table 1-1. Ordovician time scale. (After Palmer and Geissman, 1999; Harland *et. al.*, 1990)

1-2. PALAEOGEOGRAPHY

1-2-1. RECONSTRUCTION OF PALAEOGEOGRAPHY

A number of researchers using various methods including geology, palaeomagnetism, isotope records, and palaeobiogeography have determined the distribution of palaeocontinents through time (Scotese, 2001; Ziegler, 1988; Cocks, 2001; McCormick and Fortey, 1999; and, Cocks and Fortey, 1990). Although the accuracy of such palaeogeography maps decreases farther back in time, estimates of continental positions are believed to be reasonable back to the Cambrian (543-490 Ma).

Isotopic evidence from stratigraphy and fossil records is used to demonstrate the position of palaeoclimatic belts and suggest the latitudinal positions of the palaeocontinents. Correlations between sea level fall during global cooling and carbon isotope excursions, as well as between sea level rise and a fall in oxygen isotope values were observed in Upper Ordovician lithological and palaeobiological records from the modern U.S and South China (Wang, *et. al.*, 1997; Brenchley *et. al.*, 2003; Saltzman and Young, 2005). However, in such studies there are many assumptions needed because of complicated relationships between the preservation of the chemical components and the palaeoenvironmental changes. In the case of carbon isotopes, when the host rocks, carbonates, had additions or losses of carbon isotopes from partial metamorphoses, or alterations due to tectonics, the original isotopic amount cannot be calculated (Nichols, 1999). This makes it difficult to rely on results based purely on isotope geochemistry.

However, the combination of palaeobiological distributions and geochemical data increases the accuracy of palaeogeographic arrangements. For example, palaeobiotic events (inferred from the distribution of brachiopods, trilobites, graptolites, etc.) on Gondwana have been observed from various geographic locations in the modern world, such as the modern U.S. (in Laurentia during the Ordovician) and modern South China (in Gondwana; Cocks, 2001; Brenchley, *et. al.*, 2003) and give an idea of where biota that had certain environmental preferences lived.

1-2-2. PLATE TECTONICS

The most recent Late Ordovician palaeogeography (Cocks, 2001; Scotese, 2001; Scotese, *et. al.*, 1999; McCormick and Fortey, 1999; Cocks and Fortey, 1990) took a number of steps to produce. The base map was created using knowledge of plate tectonics. Figure 1-1-a and 1-1-b are plate tectonic maps for the end of the Ordovician (450Ma) and today (modified from Skinner and Porter, 1987; Scotese 2001; Ziegler, 1988). The sources of the Late Ordovician palaeogeography applied to this research were selected as an example of the reconstructed Late Ordovician world.

The orientation of the palaeocontinents was deduced from studies of palaeomagnetism. Palaeomagnetism determines the latitudinal positions of the palaeocontinents. A disadvantage of this method is that the longitudinal positions of the continents are not constrained (Scotese, 2001). In addition, it is often difficult to find undisturbed sediments from this time that have kept their

original magnetic orientations to provide useful palaeomagnetic data, so the database is sparse.

Lithological, palaeoclimatological and palaeobiological data also aid in determining the latitudinal positions of the palaeocontinents. For example, evaporites are likely to have been formed in the subtropics under the descending branches of the Hadley circulation (Ziegler, *et. al.*, 1981)

These multidisciplinary methods produced our current understanding of Late Ordovician palaeogeography. During the Ordovician, the major continents (Laurentia, Siberia, Baltica, and Gondwana) were concentrated in the southern hemisphere, and open oceans covered the northern hemisphere (Figure 1-2). In Figures 1-1-a, 1-2-a, and 1-2-b, solid lines are the coastlines of the Ordovician continents, whereas the dashed lines show the edge of the continental shelf. The locations of shallow epicontinental seas may be inferred from the areal difference between the solid and dashed lines.

Even though mountains are believed to have existed during the Late Ordovician, very little is known about topographic heights at this time. However, there is evidence of subduction zones and volcanic island arcs. An Appalachian orogeny (Wildley 1995) and the Pan-African orogenies (Qing, *et. al.*, 1998) are believed to have existed, because of the patterns of dispersion of Ordovician organisms (Scotese, 2001; Hallam, 1994; Windley, 1995; McKerrow, *et. al.*, 1991) and strontium isotope components in the palaeocean (Qing, *et. al.*, 1998). Nevertheless, precise locations and heights are not known.

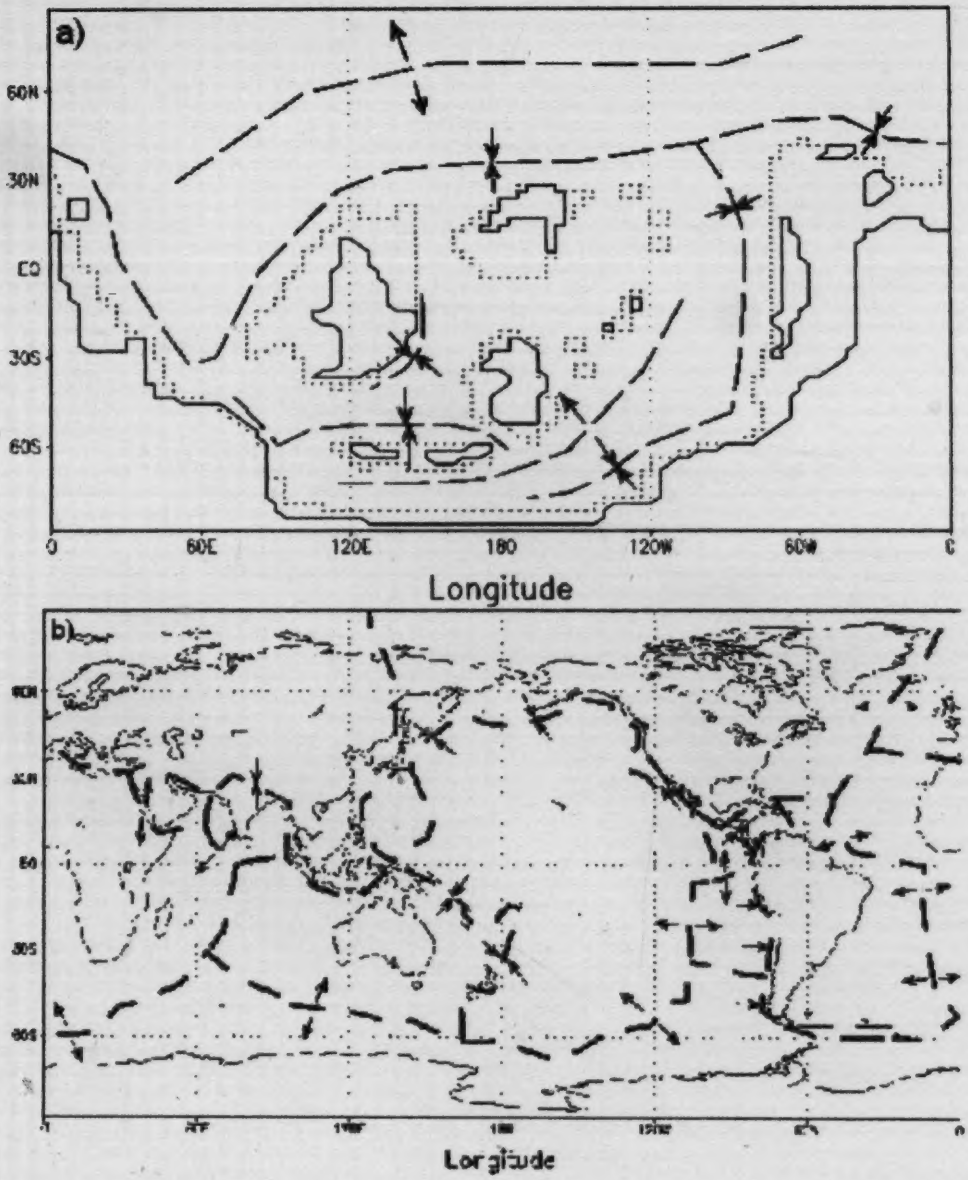

Figure 1-1. Plate tectonic maps for a) Late Ordovician and b) present day (modified from Skinner and Porter, 1987; Scotese 2001; Ziegler, 1988). Dashed lines are plate boundaries and arrows are the direction of plate movements.

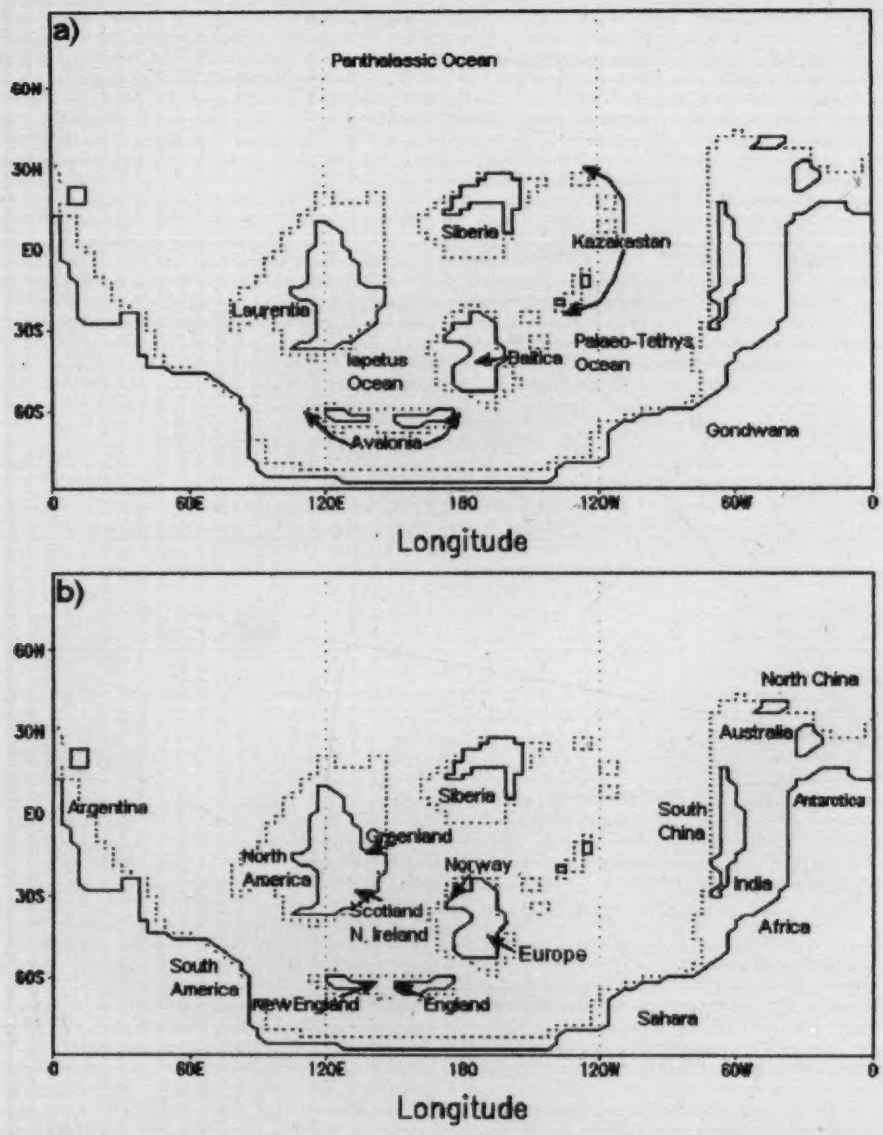

Figure 1-2. Late Ordovician maps. Solid lines are the continental margins under transgression conditions. Dashed lines are the continental margins, which were the coastlines when sea level was lower. (a) The Late Ordovician map with palaeocontinent and palaeocean names (b) the Late Ordovician map with modern continent names (modified from Scotese, 2001 and Cocks, 2001).

1-3. PALAEOCLIMATOLOGY

Weather is constantly changing through time and averaging the weather over a long period of time is defined as climate. Relatively recent climate changes have been recorded by humans over the past 150 years from direct measurement (Lowe, *et. al.*, 2001). Palaeoclimate proxy indicators (e.g. ice cores, ocean cores and tree rings) extend the record of palaeoclimate conditions back to about 3 million years before present (Lambeck, *et. al.*, 2002; Petit *et. al.*, 1999). Knowledge of climates prior to this time, however, is necessary in order to place the evolution of life in context with the evolution of the planet's climate system. The use of coupled atmosphere-ocean General Circulation Models (GCMs) has immense potential for providing reasonably accurate estimates of past and future climates because the models incorporate the earth's total energy budget by simulating in approximate fashion the overall linkage of oceanographic, atmospheric, cryospheric, and land surface processes.

1-3-1. ORDOVICIAN CLIMATES

The Ordovician period spans 490 Ma to 443 Ma and its climate is believed to be a relatively warm one that experienced a rapid temperature drop and glaciation over the last few million years of the Ordovician (Figure1-3, e.g. Saltzman and Young 2005; Brenchley *et. al.*, 2001; Sheehan, 2001b). Glaciation is inferred from continental glacial deposits in a region now occupied by the Sahara Desert and North, South, and, West Africa (Frakes *et. al.*, 1992; Caputo, 1998; Scotese, *et. al.*, 1999), all of which were regions adjacent to one another on the super continent Gondwana (Figure1-2; Brenchley and Newall, 1984).

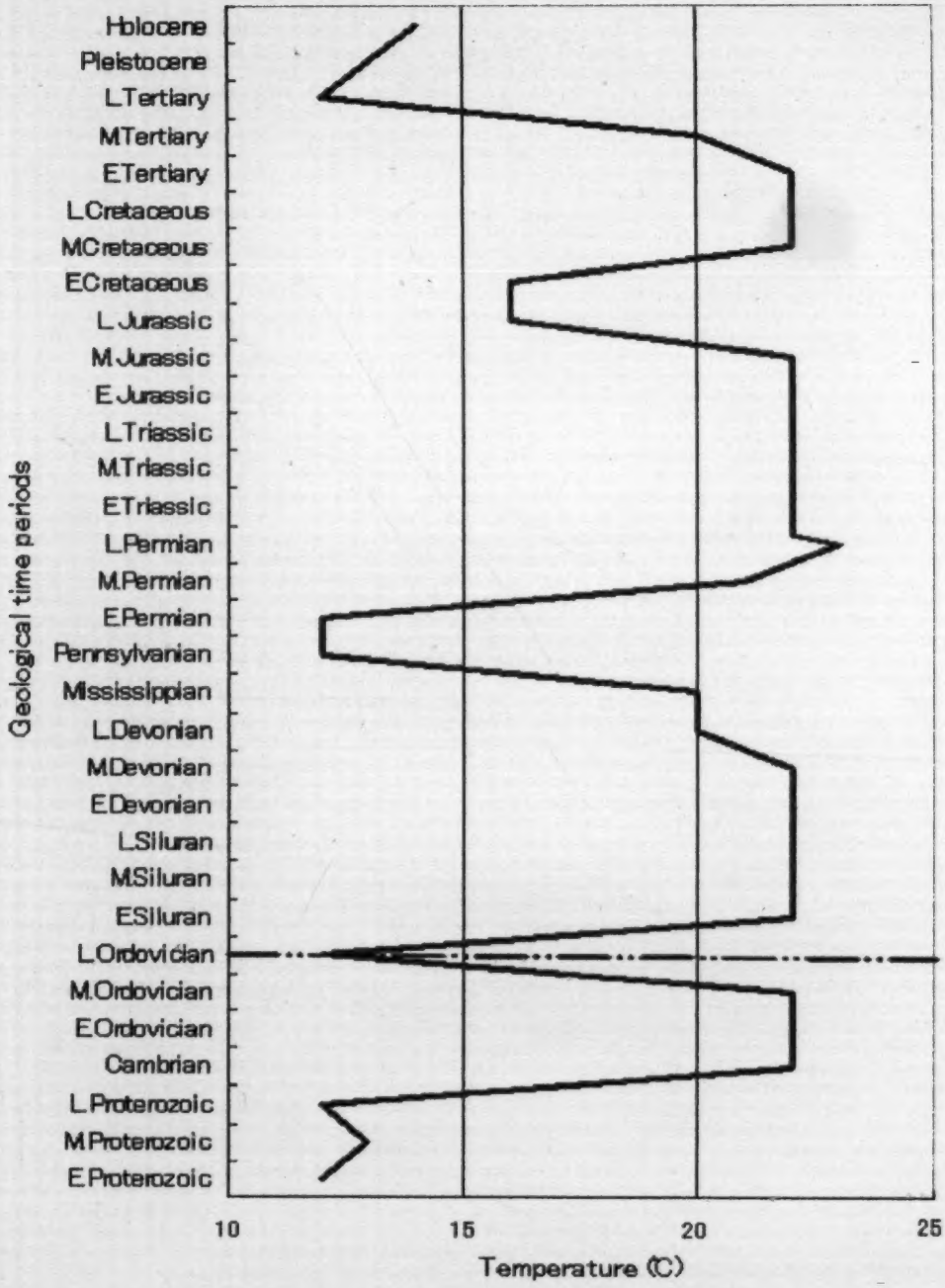

Figure 1-3. The average global temperature through the geological time periods. The dashed line represents the Late Ordovician (after Scotese *et. al.*, 1999, Scotese, 2001).

Glacial deposits from Gondwana suggest a latitudinal ice distribution of 60 degrees to 40 degrees in the southern hemisphere and it is believed that sea ice reached 10 degrees North (Scotese, *et. al.*, 1999; Royer *et. al.*, 2004; Brenchley and Newall, 1984). Extensive evaporite deposits from Laurentia and Siberia (Ronov, *et. al.*, 1984; cited in Scotese, *et. al.*, 1999) suggest drier conditions and that these regions were located under the descending branches of the Hadley cells. The locations of carbonate rock formations suggest that warm moist tropical conditions extended further poleward than today. Ronov *et. al.* (1980) noted that there were latitudinal differences in the distribution of the carbonate sediments between the Caradocian and the Wenlockian (458-423Ma; cf. Table 1-1), during which sediments formed between 35°N and 35°S, and the pre-Caradocian (≥458Ma) and post-Wenlockian (≤423Ma), during which carbonate rock formations expanded to 50°S (there is no data from the north hemisphere). The latitudinal shift in these deposits support the hypothesis of colder temperatures during the Caradocian to Wenlockian periods (Ronov *et. al.*, 1980). The lithological evidence therefore supports the notion of a dry-cold (glaciated) environment at the end of the Ordovician. However, the northern hemisphere is believed to have remained mostly ice-free during the Late Ordovician due to the presence of open oceans and a lack of large continental landmasses in that hemisphere. Possible explanations that have been proposed for the appearance of glaciation at this time are plate tectonics, which changed the palaeocontinents' positions (Scotese *et. al.*, 1999; Scotese, 2001), changes in oceanic heat transport (Sheehan and Coorough, 1990), and changes in atmospheric CO_2 and O levels (Saltzman and Young, 2005, Brenchley, *et. al.*, 2001).

The duration of glaciation during the late Ordovician is under debate. Nevertheless, this glacial cycle has been suggested as the major cause of two Late Ordovician extinction events by numerous authors (Brenchley, *et. al.*, 2001, 2003; Brenchley and Newall, 1984; Cocks and Fortey, 1990; Fortey and Cocks, 2005; Sepkoski, 1998; Sheehan, 2001a, b; Sheehan and Coorough, 1990) and there is to date no evidence (e.g. geochemical evidence) for a bolide impact during the Late Ordovician (Sheehan, 2001b). The first phase of extinction, which eliminated 80% of graptolites, chitinozoa, and 50% of benthic fauna (Brenchley, *et. al.*, 2001) was coincident with rapid cooling and a regression of sea level near the beginning of the Hirnantian age (≥ 443 Ma; Brenchley, *et. al.*, 2001; Sheehan, 2001b) and was followed by the gradual appearance of *Hirnantia* fauna (Brenchley *et. al.*, 2003). Brenchley *et. al.* (2003) inferred the Hirnantian glaciation from carbon and oxygen isotope data from brachiopods and ostracodes. Their data demonstrated a single major positive isotope excursion in δ^{13} C starting at the beginning of the Hirnantian. δ^{18} O values concur with the carbon isotopic results and these are correlated with the mark of glacio-eustatic sea level fall in the facies. Using isotopes derived from Nevada conodonts and graptolites, Saltzman and Young (2005) used δ^{13} C and δ^{18}O values from the middle of the Caradocian (458-449 Ma, Chatfieldien Stage) to infer that there was a long (about 10 Ma) icehouse period before the Hirnantian (443 Ma) glacial maximum. Villas *et. al.* (2002) and Fortey and Cocks (2005) supported this long duration of glaciation preceded by an episode of pre-Hirnantian global warming, called the Boda event, using lithologic evidence (from carbonates) and data from brachiopods and trilobites. If this hypothesis is true then the glaciation length must be extended

to be the length of the Caradocian and the Ashgillian (about 15 Ma; Harland *et. al.*, 1990), with an interglacial period in the middle Ashgillian, just before the Hirnantian. The proposed Boda event therefore suggests an interglacial period within the episode of glaciation, and is supported by other carbon and oxygen isotopes studies (Marshall *et. al.*, 1997), stratigraphic sequences (Paris *et. al.*, 1995), and inferred eustatic sea level changes (Brenchley and Newall, 1980).

The second phase of extinction, which eliminated *Hirnantia* fauna (Brenchley *et. al.*, 2003) such as cnidarians (e.g. Genera *Eocatenipora*), brachiopods (e.g. Genus *Philhedrella*, *Hirnantia*, *Eostropheodonta*, *Plectothyrella*, *Hindella*), trilobites (e.g. Genera *Salterolithus*, *Mucronaspis*), echinoderms (e.g. Genera *Brightonicystis*, *Gomphocystites*, *Heliocrinites*; Harper and Owen, 1996) was coincident with global warming and sea level rise in the middle to the end of the Hirnantian age (≥ 443 Ma; Brenchley, *et. al.*, 2001; Sheehan, 2001b). δ^{18} O values dropped at the boundary of the Ordovician and the Silurian, as did δ^{13} C values (Brenchley *et. al.*, 2003), and indicate sea level rise and the end of the Hirnantian glaciation.

Gibbs *et. al.*, (2000) proposed that palaeocontinental distribution and the southward movement of Gondwana triggered the glaciation with CO_2 levels over 10 times pre-industrial atmospheric levels (x PAL) with low sea level. Herrmann *et. al.* (2004b) supported the hypothesis that palaeogeography had an impact on the initiation of Late Ordovician glaciation and addressed the amount of CO_2 in the atmosphere was a preconditional factor to control the Late Ordovician climate.

Herrmann *et. al.* (2004a, 2004b) showed that the Boda event may have occurred from Caradocian and Ashgillian numerical simulations. The changes in sea level and poleward ocean heat transport had significant roles in these simulations to initiate glaciation (section 1-4).

An additional factor that has been invoked to cause the glaciation at the end of the Ordovician is lower solar luminosity. Solar luminosity during the Ordovician is believed to have been about 2.5-5% less than the modern level (Crowley and North, 1991) so that the Ordovician climate system received less energy from incoming solar radiation. According to a two-dimensional Energy Balance Model (EBM) that includes a nonlinear ice-albedo feedback the global annual mean temperature would be 11.6°C when the solar constant is reduced to 0.975 of today's compared with 16.4°C when the solar constant is today's value (Crowley and North, 1991). A 5°C drop in global mean temperature is of approximately the same magnitude as the difference between today and the Last Glacial Maximum, 21,000 years ago (Bush and Philander, 1999). However, because of low insolation such a drop in global temperature would be made smaller by the higher levels of atmospheric CO_2 during the Late Ordovician.

The causes of glaciation during this time are therefore not yet fully understood. One contribution that can be made in the context of numerical modeling and energy balances is whether the Ordovician climate could support year round ice in a high CO_2 environment. This idea will be addressed in chapter 3.

1-3-2. PALAEOBIOLOGY AND EXTINCTION EVENTS

The past distribution of organisms and important palaeobiotic events may aid in inferring the latitudinal positions of the continents, as well as their proximities and relative positions (Cocks, 2001; Scotese, 2001). In this section, 3 palaeobiological examples, trilobites, brachiopods, and graptolites, are simply described.

The Ordovician period was a time of rapid expansion of diversity (Sepkoski, 1981, 1998; Sheehan, 2001a). Following this "great Ordovician radiation" was the two-phased extinction event at the end of the Ordovician. Possible causes of the Ordovician radiation have been discussed by numerous authors and may be related to the Ordovician glaciation (Cocks and Fortey, 1990; Sheehan and Coorough, 1990; Sepkoski, 1981, 1998; Sheehan, 2001a). However, some authors suggest that the first phase of the extinction started before the positive excursion of carbon and oxygen isotopes (Brenchley *et. al.*, 2003; Smit, 2006) and that the unstable climate signified by the interglacial Boda event (Fortey and Cocks, 2005) does not provide a direct link between climate and extinction. Nevertheless, trilobites and brachiopods are well documented during the Ordovician and are good examples of groups that suffered during the two extinction events. A large proportion of graptolites went extinct during the first phase, and 80% or more of conodont species went extinct during the second phase (Brenchley *et. al.*, 2001; Sweet, 1990 cited in Sheehan, 2001b; Barnes and Zhang, 1999). Their distributions helped in the reconstruction of the positions of the palaeocontinents during that period (Bulman, 1971; Cocks and Fortey, 1990).

Figure 1-4 shows palaeobiogeographic maps for a) trilobite and b) brachiopod distributions at the end of the Ordovician (after Cocks and Fortey, 1990; Sheehan and Coorough, 1990; McCormick and Fortey, 1999).

1-3-2-1 TRILOBITES

The life modes of trilobites include benthic (attached to the substrates and/or sediments) or nektonic (free swimmers). *Carolinites* were nektonic trilobites, similar to today's fairy shrimp. The distribution of all trilobite fossils recovered is plotted on Figure 1-4-a (after Cocks and Fortey, 1990; McCormick and Fortey 1999). The samples were found in various places such as Utah, Alberta, Spitsbergen, Australia, and Montagne Noire in the south of the central Massif (Cocks and Fortey, 1990; McCormick and Fortey, 1999). Most samples of *Carolinites* were therefore in the palaeoequatorial region, with the exception of the Montagne Noire site, which was at a higher southern latitude. *Ampyxina*, *Calyptaulax*, *and Panderia* were benthic trilobites. *Ampyxina* is found in modern North America, Greenland, Russia, and Europe. *Calyptaulax* is found in modern North America, Russia, Europe, and Kazakhstan. *Panderia* is found in modern Europe, Kazakhstan, Middle East Asia, and South China (Cocks and Fortey, 1990; McCormick and Fortey 1999). When these samples are placed on the Ordovician map, they are all shown to have lived in the shallow epicontinental seas.

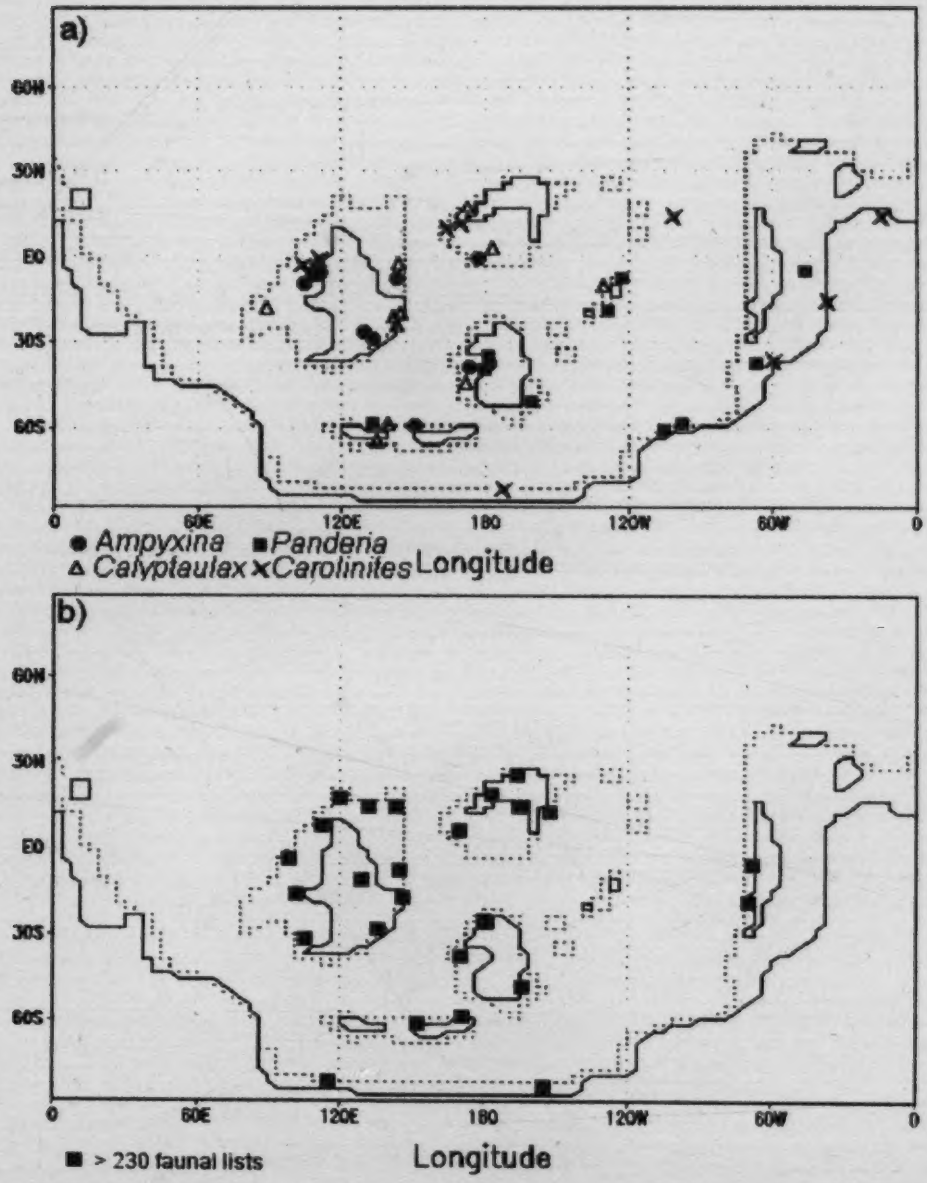

Figure 1-4. Late Ordovician palaeobiogeography maps. a) Trilobite distributions. Solid circles are *Ampyxina*, open triangles are *Calyptaulax*, solid squares are *Panderia*, and crosses are *Carolinites* (after Cocks and Fortey, 1990; McCormick and Fortey 1999). b) Brachiopod distributions. Solid squares represent the sum of more than 230 faunal lists from Coorough (1986) and Sheehan and Coorough (1990)

The dispersion of benthic trilobites was postulated to have been by palaeoceanic currents (Cocks and Fortey, 1990). The palaeoceanic current circulations were in turn suggested by hypothesized surface wind directions. Gyre circulations in the southern Palaeo-Tethys Ocean (between Gondwana and Baltica and Siberia) and the Iapetus Ocean (between Laurentia, Baltica and Avalonia) have been hypothesized to disperse the benthic trilobites and their planktonic larvae within warm water currents (Cocks and Fortey, 1990). Ocean gyre circulations are therefore one aspect of the numerical simulations that will be examined here and this hypothesis may therefore be tested.

1-3-2-2. BRACHIOPODS

Brachiopods were an important part of benthic communities living on the tropical continental shelves of Laurentia, Baltica, Siberia, and part of Gondwana. The *Foliomena* fauna was a distinctive brachiopod assemblage. It was primarily found in Laurentia, Baltica-Avalonia, and North Gondwana. The *Foliomena* fauna is also believed to have been dispersed by ocean currents and distributed across these separate continental shelves. This fauna lived in the tropical band between 30S and 30N. The rapid cooling near the beginning of the Hirnantian wiped out most of the brachiopods of this fauna in the first phase of extinction, and most of the survivors, who were then in the higher latitudes, migrated to the tropics. However, collections of such brachiopod faunas as *Foliomena* are not uniform around the world and data are simply not available for some regions (e.g. from modern South America). The 230 brachiopod faunas used to construct Figure 1-4-b include 200 brachiopod faunas provided by Coorough (1986), cited

in Sheehan and Coorough (1990), and an additional 30 faunas provided by Sheehan and Coorough (1990) that were sampled from 10 modern regions (Greenland, the British Isles, north, south, and central Europe, North Africa, Kazakhstan, Siberia, Kolyma, and South China). These faunal lists indicate that some brachiopods dispersed into the southern polar region during the Hirnantian, likely carried by palaeocean currents, and slowly adapted to the colder environment. However, they subsequently disappeared during the 2nd phase of extinction as the climate warmed.

1-3-2-3. GRAPTOLITES

Graptolites were both benthic and planktonic organisms living in the tropical marine realm. Pelagic graptolites radiated during the Ordovician and were a part of the great Ordovician diversity, hence becoming one of the more abundant and diverse groups of organisms during this period. However, an important extinction event occurred in the early Ashgillian (Clarkson, 1986; Hallam, 1994) and only five or six species of pelagic graptolites (the earliest monograptids) appear to have survived this event.

There are two major faunal provinces for pelagic graptolites. One is the Atlantic realm which is characteristic of Ordovician rocks in Europe and along the North Atlantic margins (e.g., didymograptids with pendent stipes; Clarkson, 1986). The Pacific realm is another faunal province whose faunas are more diverse than those of the Atlantic realm. Examples are *Isograptus, Oncograptus,* and *Cardiograptus* (Clarkson, 1986; Hallam, 1994). The Pacific faunas lived in the

tropical oceans between 30N and 30S; the Atlantic faunas lived in the palaeolatitudes poleward of 30S (Figure 1-5) before the first phase of extinction took place (Clarkson, 1986). The distribution of graptolites is also believed to have been influenced by oceanic gyres as well as by sea surface temperature (SST). Their distributions are similar to those of trilobites, suggesting that they were carried by the same gyres in the southern Palaeo-Tethys Ocean and Iapetus Ocean. After the first extinction event, Ordovician graptolites lived only between 30N and 30S (Clarkson, 1986).

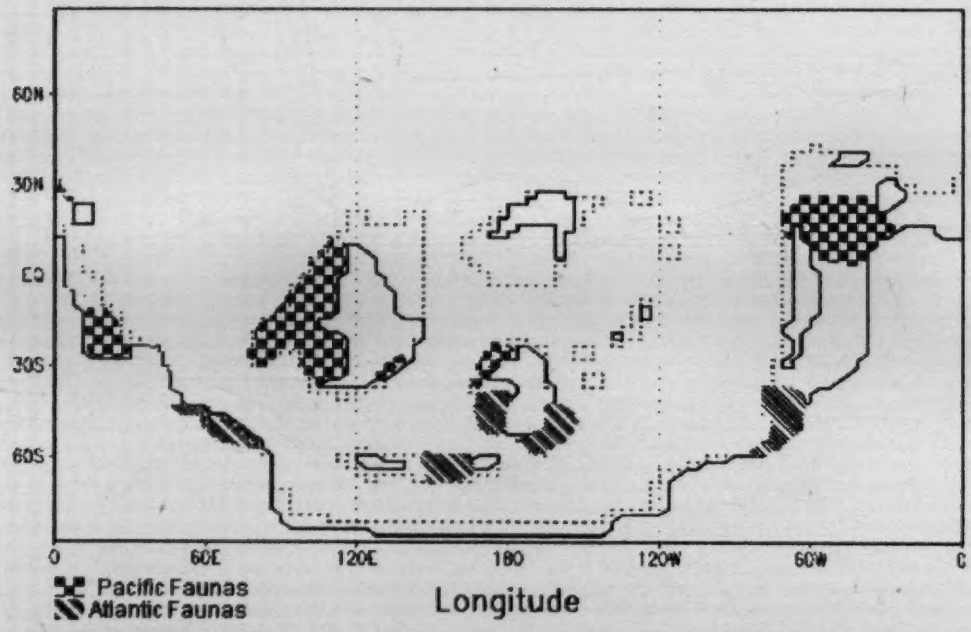

Figure1-5. Distribution of graptolite faunal provinces before the first Ordovician extinction event. Diagonal shading is for the Atlantic faunal province found in modern England, Wales, SE Ireland, Europe, North Africa, Peru, and Bolivia. The checker-board shading is for the Pacific faunal provinces found in modern N. America, Argentina, Australia, Australasia, Scotland, NW Ireland, and W Norway (after Clarkson, 1986; Hallam, 1994)

1-3-3. PARADOX OF THE ORDOVICIAN GLACIATION

Climate forcing during the Ordovician was very different from that of the present day. Previous geochemical (Berner, 1998; Yapp and Poths, 1992) and palaeosol (Brenchley and Newall, 1984) studies stated that CO_2 levels in the Late Ordovician were about 8-20 times higher than pre-industrial levels of 280 parts per million. There is some geochemical evidence to suggest that atmospheric CO_2 decreased during the Hirnantian glaciation period (Saltzman and Young, 2005; Wang *et. al.*, 1997) although specific values are not known. The well-known greenhouse effect associated with high levels of CO_2 at the end of the Ordovician is paradoxical because of the existence of extensive continental glaciation at the same time. Given the discussion in the previous section, Ordovician glaciation was likely the product of continental configuration (Scotese, 2001) and the smaller amount of solar radiation emitted by the younger Sun (Endal and Schatten, 1982; Molnar and Gutowski, 1995), since solar luminosity is estimated to have increased 20-30% through the 4.6 billion years of Earth history (Endal and Schatten, 1982; Molnar and Gutowski, 1995).

Another possible cause of the Late Ordovician glaciation is the Earth's orbital parameters. Some authors suggested that not only atmospheric CO_2 levels were important but also that the orbital forcing had an important role at this time (Williams, 1991; Sutcliffe *et. al.*, 2000; Herrmann, *et. al.*, 2004b) because when orbital forcing was changed, the latitudinal and seasonal distribution of solar radiation differed and thus the seasonal cycle and the equator to pole insolation gradient were altered (Herrmann and Patzkowsky, 2003). Numerical climate modeling is one tool with which this apparent paradox may be explored.

1-4. PREVIOUS STUDIES

There are several previous modeling studies that have simulated the Late Ordovician period using a variety of different numerical models.

Crowley and Baum (1995) simulated the presence of permanent ice on the south pole at the end of the Ordovician with the Global Environmental and Ecological Simulation of Interactive Systems (GENESIS) model with a mixed layer slab ocean model in which meridional heat transport is specified and ocean dynamics are ignored. The conditions they used in their experiments were 12–14 (x PAL) of CO_2, 4.5 – 5% reduced solar luminosity, an orbit that minimized the amount of insolation in austral summer (termed a "cold summer" orbit) and 2 different palaeogeographic distributions (Silurian (443~ Ma) and Ashgillian (449-443 Ma)) with and without 500m elevated topography on Gondwana. Sensitivity tests showed that permanent ice was formed only when the palaeogeographic map had 500m topographic heights, the atmosphere had 12 x PAL CO_2 and solar luminosity was reduced 5%. Under these conditions, the freezing line was lowered to sea level.

Poussart *et. al.* (1999) analyzed the Late Ordovician glaciation with an energy/moisture balance atmospheric model (EMBM) coupled to an ocean general circulation model (OGCM). The initial conditions in their experiments for the ocean model were a simplified temperature structure adapted from modern observations (Levitus and Boyer, 1994), and globally constant salinity. The initial atmospheric temperature was 0°C everywhere, and there was no atmospheric moisture. Sensitivity experiments were carried out using different values of atmospheric CO_2, orbital configurations, and magnitudes of ice-snow albedo feedback. The values of atmospheric CO_2 levels were 10 x PAL, 14 x PAL, and 18 x PAL, which are representative of the estimated range of Ordovician CO_2 levels. The orbital configurations were defined as a hot summer orbit (HSO) and a cold summer orbit (CSO) for two extreme configurations, and as a warm fall/cool spring orbit (WFCS) and a cold fall/warm spring (CFWS) for two intermediate configurations. An ice albedo was tested for values of 0.7, 0.8 and 0.9. Solar luminosity was decreased by 4.5% from the present day so that the solar constant equaled 1.306×10^3 Wm^{-2}.

Results showed that it was possible to maintain a significant (14.5×10^6 km^2) permanent snow cover in the southern high latitudes of Gondwana when the atmospheric CO_2 concentration was 10 x PAL, the orbital configuration was WFCS forcing, and the ice albedo was at least 0.7. CSO forcing also produced a smaller region of permanent snow with atmospheric $CO2_2$ concentration at 10 x PAL, and an ice albedo of 0.9.

An interesting result was the presence of permanent sea-ice extending from 60°-70°N. Minimum simulated sea-ice coverage in the northern

hemisphere was 12.3 x 10^6 km^2 when CO_2 was 18 x PAL with WFCS forcing, and an ice albedo of 0.9. Maximum simulated sea-ice coverage in the northern hemisphere was 59.4 x 10^6 km^2 when CO_2 was 10 x PAL with WFCS forcing and the ice albedo 0.7 and 17.70 x 10^6 km^2 in southern hemisphere. There is no geological or palaeontological evidence for northern hemisphere ice in the Late Ordovician because there were no continents there at the time, nor can there be any evidence supporting the existence of sea ice. However, Poussart *et. al.* (1999) argued that because of the lack of continents in the northern hemisphere, the poleward ocean heat transport became weak enough to isolate the northern polar latitudes from the warm equatorial region. They suggested that an atmospheric general circulation model (AGCM) modeling studies need to include ocean heat transport values directly calculated by an OGCM.

Poussart *et. al.* (1999) concluded that the combination of orbital forcing and summer atmospheric temperature could play an important role in creating permanent continental ice during times of high atmospheric CO_2.

Another recent numerical simulation of the Late Ordovician was carried out by Herrmann *et. al.* (2004a). They used the GENESIS atmospheric model coupled with a 3-D ice sheet model. As in previous studies, the sensitivity tests they used were aimed at exploring the boundary conditions necessary to maintain permanent ice on the South Pole. The initial conditions were snow/ice free, a motionless atmosphere, and present-day annually averaged zonal mean temperatures. Their coupled model adapted the 2 different palaeogeographic maps for the Caradocian (458-449 Ma) and the Ashgillian (449-443 Ma) with

shoreline positions for low and high sea levels (Scotese and McKerrow 1990, 1991; Scotese, 1997). Topography was set to 250m for coastal grid points and 500m for all other land grid points. Atmospheric CO_2 levels in their sensitivity tests were 8, 10, 12, 15, and 18 x PAL. The orbital parameters were set to CSO and solar luminosity was reduced by 4.5%. There was no vegetation on the land, which had intermediate soil colour values for the surface albedo. Two different values of the oceanic heat transport diffusion coefficient were used in this simulation, one was the same as the modern climate value and the other was 50% of the modern value.

Lower CO_2 values delivered lower global mean temperatures, similar to the studies of Crowley and Baum (1995) and Poussart *et. al.* (1999). Permanent ice was simulated under the conditions of 8 x PAL CO_2 level, lower sea level, and modern heat transport using both Caradocian palaeogeography ($58x10^6$ km^3 of ice) and Ashgillian palaeogeography ($168x10^6$ km^3 of ice). The same CO_2 level combined with high sea level and low oceanic heat transport produced $67x10^6$ km^3 of ice during the Caradocian and $35x10^6$ km^3 during the Ashgillian. Unlike Poussart *et. al.* (1999), there was no ice simulated with 10 x PAL CO_2 under the same conditions. However, 22 x 10^6 km^3 of ice volume was simulated with 15 x PAL CO_2 level during the Caradocian when both sea level and oceanic heat transport were low.

Herrmann *et. al.* (2004a) concluded that atmospheric CO_2 levels and changes in the palaeogeographic distributions of land masses were not necessary to trigger the initial formation of permanent continental ice individually. In the case of lower CO_2, sea level controlled the annual mean temperature. The

difference between Caradocian and Ashgillian ice sheets was influenced by the palaeogeographic changes, which reduced the poleward ocean heat transport. Notably, the Caradocian simulation with a low sea level, 15 x PAL CO_2 level and a lower heat transport simulated glaciation but not in the Ashgillian since Gondwana was less exposed in the higher southern hemisphere and the global annual mean temperature was higher. Therefore Herrmann *et. al.* (2004a) stated the importance of sensitivity tests of different sea levels and poleward ocean heat transport for the formation of permanent ice.

This study focuses on the use of a fully coupled atmosphere-ocean GCM to investigate the interaction of atmosphere-ocean-sea ice system during the late Ordovician. The importance of the coupled GCM is the close interaction of the ocean and atmosphere since they influence each other and influence the global climate system. This study represents the first attempt to simulate Late Ordovician climate using a model that includes the full dynamics and thermodynamics of both the atmosphere and the ocean. It improves on Poussart *et. al.* (1999) by incorporating a full atmospheric GCM and it improves on Herrmann *et. al.* (2004a) by including a full ocean GCM. A unique aspect of this study is the simulation of dynamic atmosphere – ocean interactions that can give rise to such global phenomena as the El Niño Southern Oscillation. Chapter 2 describes the numerical models used and the assumptions made in their configurations. Chapter 3 presents the results of the simulations and compares them with available proxy data. Finally, Chapter 4 provides a discussion and conclusions.

2. METHODOLOGY

2-1. MODEL DESCRIPTION

The model used in this study consists of two separate models (detailed below) coupled together to simulate the atmosphere, ocean, sea ice system. The model is global and three-dimensional and describes the physical processes within the atmosphere and oceans and their interaction with sea ice and the land surface. The Grid Analysis and Display System (GrADS; Doty and Kinter III, 1995) was used to visualize the output data from the atmosphere-ocean coupled GCM.

2-1-1. ATMOSPHERE MODEL

The atmospheric component (Gordon and Stern 1982) was developed at the Geophysical Fluid Dynamics Laboratory (GFDL) in Princeton, New Jersey, and is a global spectral model. It has 14 vertical sigma (σ) levels and rhomboidal spectral truncation at wave number 30. The equivalent Gaussian grid therefore has a resolution of 2.25° in latitude and 3.75° in longitude.

The normalized pressure coordinate (σ) is defined as;

$$\sigma = \frac{P - P_T}{P^* - P_T} \qquad (2.1)$$

Where P is the atmospheric pressure, P* is a spatially and temporally varying surface pressure and P_T is the pressure at the top model level (15mb). The 14 levels of σ are 0.015, 0.05, 0.101, 0.171, 0.257, 0.355, 0.46, 0.568, 0.676, 0.777, 0.866, 0.935, 0.979, and 0.997. In the following results, "near surface" variables were taken from the σ = 0.997 surface, which is approximately 30 m above ground in a standard atmosphere (Bush and Philander, 1997). The advantage of using the σ-coordinate system rather than pressure is that σ-surfaces follow the topography. First, the atmospheric model was run for 19 years in order to adjust to the altered radiative forcing. Initial sea surface temperatures (SST) were modern temperatures (Levitus and Boyer, 1994) plus 3 degrees everywhere to account for the enhanced radiative forcing from high CO_2 levels. Land topography is set to zero. There are proposed orogenies during the Ordovician (Windley, 1995; Qing, *et. al.*, 1998); however, there does not exist any detailed topographic reconstruction for this time. Gravity wave drag and continental runoff, which are related to the topographic and palaeogeographic information, were therefore also neglected. It should be noted however, that where steep topography existed then regional climate and local hydrology would be affected through orographic precipitation upwind of mountains and rain shadow effects downwind of mountains. For example, Hahn and Manabe (1975) examined the role of the higher topography in the south Asian summer monsoon circulation and concluded that the presence of the mountains had a great influence on the south Asian monsoon circulation. The Tibetan Plateau was controlled the northward expansion of the monsoon over India (Hahn and Manabe, 1975) and this plateau takes a role of maintaining the dryness of the Eurasian interior (Manabe and

Holloway, 1975). Nevertheless, without gridded topographic data any numerical simulation that includes topography is a "best guess" scenario. In the simulations reported here no topography is assume but it needs to be addressed that a sensitivity test including topography would change regional climates.

2-1-2. OCEAN MODEL

GFDL's Modular Ocean Model (MOM 2; Pacanowski, *et. al.*, 1991) is used in this study. MOM 2 evolved from an original model by Bryan (1969) and Cox (1984) and has improved continually in its ability to represent ocean circulation on a global scale. A detailed model description is given in Pacanowski *et. al.*, (1991) but the main features are described here. This 3-dimensional model includes a finite difference version of the primitive fluid equations with a ∇^4 horizontal diffusion operator.

The model uses a discretization based on decomposition of the ocean into rectangular boxes of variable size. Therefore it requires additional smoothing in high latitudes where grid boxes converge. Vertical mixing is based on the Richardson number scheme developed by Pacanowski and Philander (1981). The grid resolution for latitude is 2° and for longitude is 3.62°, which is nearly equal to the equivalent spatial grid of the global spectral atmospheric model (Bush and Philander, 1997). There are 15 unevenly spaced vertical levels with the grid centers positioned at depths of 15, 52, 104, 180, 289, 441, 648, 924, 1279, 1724, 2264, 2898, 3620, 4416 and 5265m. There is higher resolution in the upper kilometer in order to resolve better the tropical thermocline and the wind driven

circulation. A constant ocean depth of 5700m was applied and a flat ocean bottom is employed, since there exists no information on bathymetry during this time. The shallow epicontinental seas were included since they have been estimated through a combination of palaeomagnetic and fossil reconstructions (Scotese, 2001) and they were assigned a constant depth of 500m.

2-1-3. ATMOSPHERE-OCEAN COUPLED MODEL

There are significant dynamic interactions between atmospheric and oceanic motions, particularly in the tropics. In the coupled model, the atmospheric model is dynamically and thermodynamically coupled with the ocean model with a 1-day coupling interval. Boundary condition data from one model are spatially interpolated for input onto the grid of the second model and passed across on this 1-day timescale. Boundary condition variables required by the atmospheric model are SST and sea surface current velocities. Boundary condition variables required by the ocean model are vector components of wind stress, net heat flux, net freshwater flux and net short-wave radiation. The duration of this coupled model integration is 65 years, which is sufficient for the wind-driven gyre circulations to be established.

In configuring the model for the Late Ordovician, some of the physical parameters in the model such as the orbital parameters of the planet, the rotation speed of the Earth, and the total atmospheric mass are set to be the same as today for simplicity and for a complete lack of data. The obliquity, eccentricity and longitude of perihelion orbital parameters were therefore assigned the modern values (23.47°, 0.0167, and 282°, respectively). Although it is believed that the

oxygen levels were about 15-20% of present levels (Barnes, 1999) there is a lack of detailed ozone (O_3) data during this period and the distribution of O_3 is therefore assumed to be identical to the present day.

Since major land plant evolution occurred after the Ordovician, albedo values on land are set to 0.2, which is the value for dry soil and medium coloured stone (Stormont, 2003; Young, 2004). Ocean albedos on the equator are set to be the same value as the present day, (0.06), and the higher latitude ocean albedos are calculated using that value plus knowledge of the solar zenith angle (Bush and Philander, 1997). The land-sea distribution during the Late Ordovician was made to be consistent with the model grid resolution (Figure 1-1).

As an initial experiment, an atmosphere-only configuration of the model was used in which the SST and sea ice extent were prescribed. In order to do this, present day SST was zonally averaged for each month then increased by 3 degrees everywhere. In the epicontinental seas, the imposed SST value was set to be 5 degrees higher than the modern zonal average for that latitude. These higher values of SST were estimates to take into account the fact that the atmosphere contained a very large amount of greenhouse gases that would significantly heat up shallow seas. For the same reason, the initial sea ice condition was set to zero. When the coupled atmosphere-ocean model was used, of course, both SST and sea ice became model-predicted quantities, but the initial distribution was prescribed as above.

The true level of atmospheric CO_2 is obviously under debate. The range of it is between 8 to 20 times higher than PAL (Berner, 1994; Yapp and Poths, 1992). $\delta^{13}C$ data suggest there was a short term interval of lower CO_2 levels in the Late Ordovician (Brenchley *et. al.*, 1994; Gibbs *et. al.*, 1997; Villas, *et. al.*, 2002). Therefore, the CO_2 level in this study was chosen to be 10 x PAL and is the lower average of previous studies of palaeosols (Brenchley and Newall, 1984) and geochemical models (Berner, 1998).

The solar constant value for the present day is approximately 1356 W/m2. This experiment used a value that is 2.5% less than present (Crowley and North, 1991). The combination of a reduced solar constant with high levels of atmospheric CO_2 will be examined with the intent of determining whether such a reduced solar constant is sufficient to explain the continental glaciations during this time using a relatively low estimate of CO_2 but including full atmosphere-ocean dynamics.

Continental ice must be prescribed in all current atmosphere GCMs, and if prescribed it is not allowed to change. I therefore do not prescribe any continental ice and use the proxy of year-round snow accumulation to indicate the possibility of ice sheet existence (as in Poussart *et. al.*, 1999) under the chosen model conditions. It is noted that the length of time required for coupled atmosphere–ocean simulations (~1 month for 30 years of simulated climate) precludes a suite of sensitivity tests from being performed. However, the coupled atmosphere – ocean coupled simulation presented here is unique and explores the phenomena that only coupled models can produce, such as ENSO.

3. MODELLING RESULTS

3-1. ATMOSPHERIC TEMPERATURE

3-1-1. ATMOSPHERE – ONLY MODEL

Figure 3-1-1 is the time evolution of global (Figure 3-1-1-a), troposphere (Figure 3-1-1-b), and stratosphere (Figure 3-1-1-c) atmospheric temperatures simulated by the atmosphere-only model. The global temperature is relatively stable indicating that the atmosphere adjusts very quickly to the altered radiative forcing. The tropospheric temperature responses are also stable through the 19 year simulation. Fluctuations of the Ordovician stratosphere temperatures are smaller than those of the Ordovician troposphere. The average Ordovician global temperature is 253.365 °K compared with 251.47 °K for today (approximately 1.9 degree difference; the near surface average difference is 4.8 degree). The Ordovician tropospheric temperature is on average about 4.8 °K higher than today and the Ordovician stratospheric temperature is on average about 6.8 °K lower than today. Stratospheric cooling is consistent with that simulated for future climate scenarios (Boer *et. al.*, 1992) since the increased greenhouse gases in the troposphere absorb more of the outgoing longwave radiation emitted by the Earth. Manabe and Wetherald (1975) studied a doubling of CO_2 concentration in a GCM for today and stated that even this relatively small increase resulted in a colder stratosphere. In the model, CO2 amount is a constant everywhere so with higher values less and less longwave radiation emitted by the surface reaches the higher altitudes.

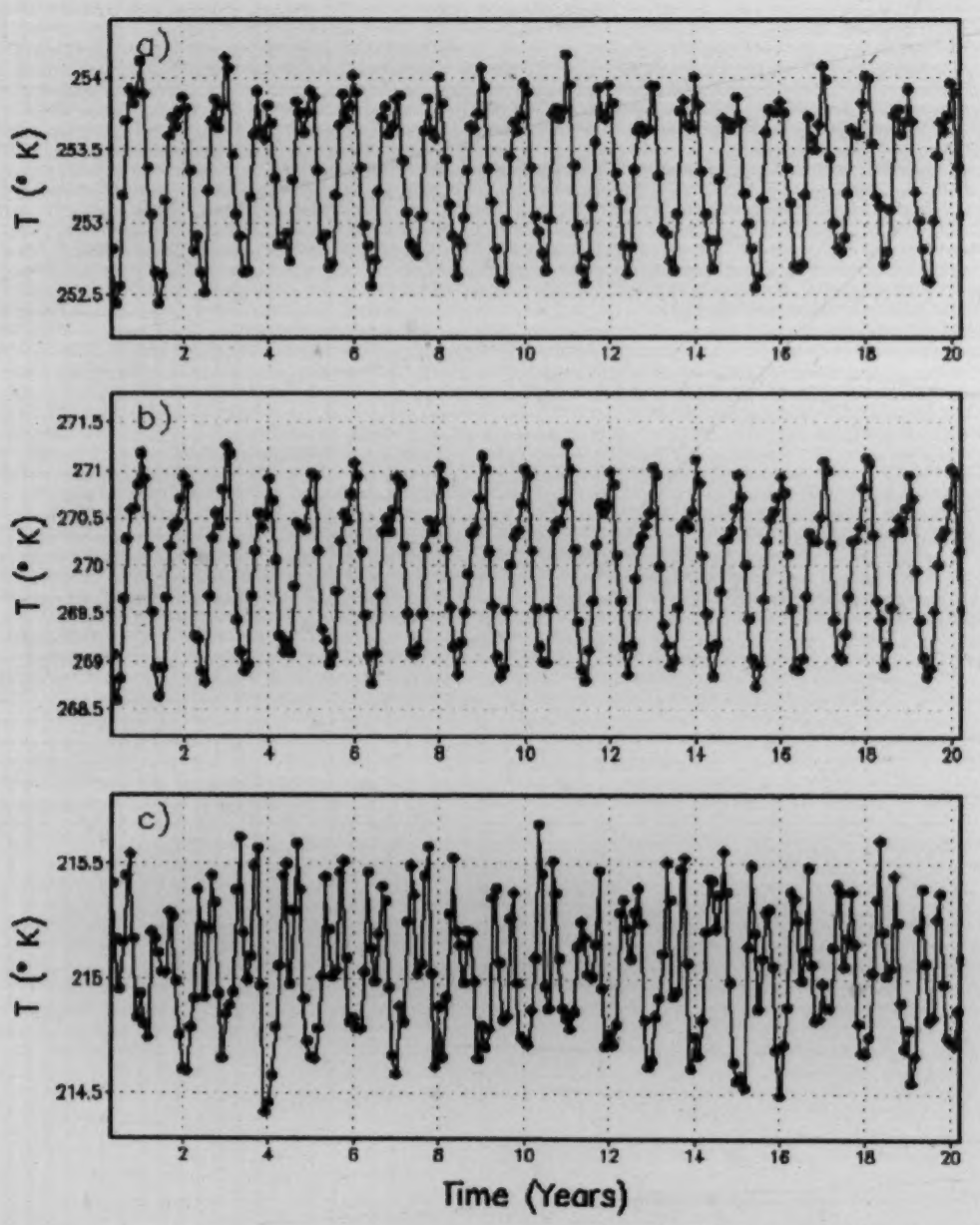

Figure 3-1-1. Time evolution of temperature (atmosphere–only simulation): in (a) global, (b) tropospheric, and (c) stratospheric atmosphere temperature (°K) as a function of time (years).

The simulated near surface (about 30 m above ground) annual and zonal mean temperature as a function of latitude in the Ordovician and present day are shown in Figure 3-1-2. The Ordovician near surface temperature is generally higher than the present day with equatorial temperatures about 303°K, ~2.8° higher than today. High latitude temperatures in the northern hemisphere in the Ordovician are approximately 9.2°K higher than the present day, whereas in the southern hemisphere temperatures are about 28.3°K greater than the present day. The lower temperature of both polar areas in the present day is caused by massive Arctic and Antarctic ice sheets, with positive ice albedo feedback encouraging the low temperatures. Such permanent ice is absent in the Ordovician simulation. Midlatitude temperatures in the Ordovician simulation are ~3 – 6.5°K warmer than today. The South midlatitude temperature is 3.5°K warmer than the North midlatitude in the Ordovician because of the presence of the palaeocontinents, which tend to amplify the seasonal cycle as compared to the oceans.

Figure 3-1-3-a shows the spatial distribution of annual mean surface temperature in the Ordovician simulation. The highest temperatures (307°K) are found in the tropics over west Gondwana (35W 20S) and the second highest (306°K) at west Laurentia (115E 15S) whereas the highest temperature in the present day simulation (Figure 3-1-3-b) is 304°K over west equatorial Africa and northern South America. The Ordovician tropical zone (roughly defined to have temperatures over 300°K) has a 10-15 degree expansion towards the poles. This is comparable with the Late Cretaceous (~75 – 65 Ma) simulation with the conditions of 4 x PAL CO_2 (Bush and Philander, 1997). The annual mean near

surface temperature over the high latitudes of both hemispheres (higher than ~70S, 70N) in the Ordovician simulation are below the freezing point of 273.16°K.

Where the maximum net shortwave radiation (incoming minus reflected) is simulated (Figure 3-1-4), the average atmospheric temperature in the lower latitudes is greater, because of the absorption of the solar radiation by the surface. In general, net surface shortwave radiation (incoming minus reflected) is higher over the oceans because of the high absorptivity of water compared to land. In the present day, the highest continental temperatures are found where the net shortwave is greatest over land (e.g. Northern South America, sub-Saharan Africa, and Northern Australia).

The net longwave emission from the surface (outgoing minus incoming) in Figure 3-1-5 indicates that the hottest regions of today's climate (Saharan Africa and the Australia desert) emit the most in accordance with the Stefan-Boltzman relation ($E=\sigma T^4$). The Ordovician simulation also indicates that the most longwave emission is from the hottest continental regions (cf. Figure 3-1-3).

The annual mean relative humidity (Figure 3-1-6) is anticorrelated with atmospheric temperatures (cf. Figure 3-1-3). The lower humidity indicates drier atmospheric conditions. Lower humidity in the Ordovician (Figure 3-1-6-a) correlates with higher temperatures (Figure 3-1-3-a) and lower humidity in the modern simulation is (Figure 3-1-6-b) located above deserts. On the other hand, higher humidity implies relatively wet conditions and includes regions with high precipitation rates (section 3-5) such as under monsoon regions (see section 3-7).

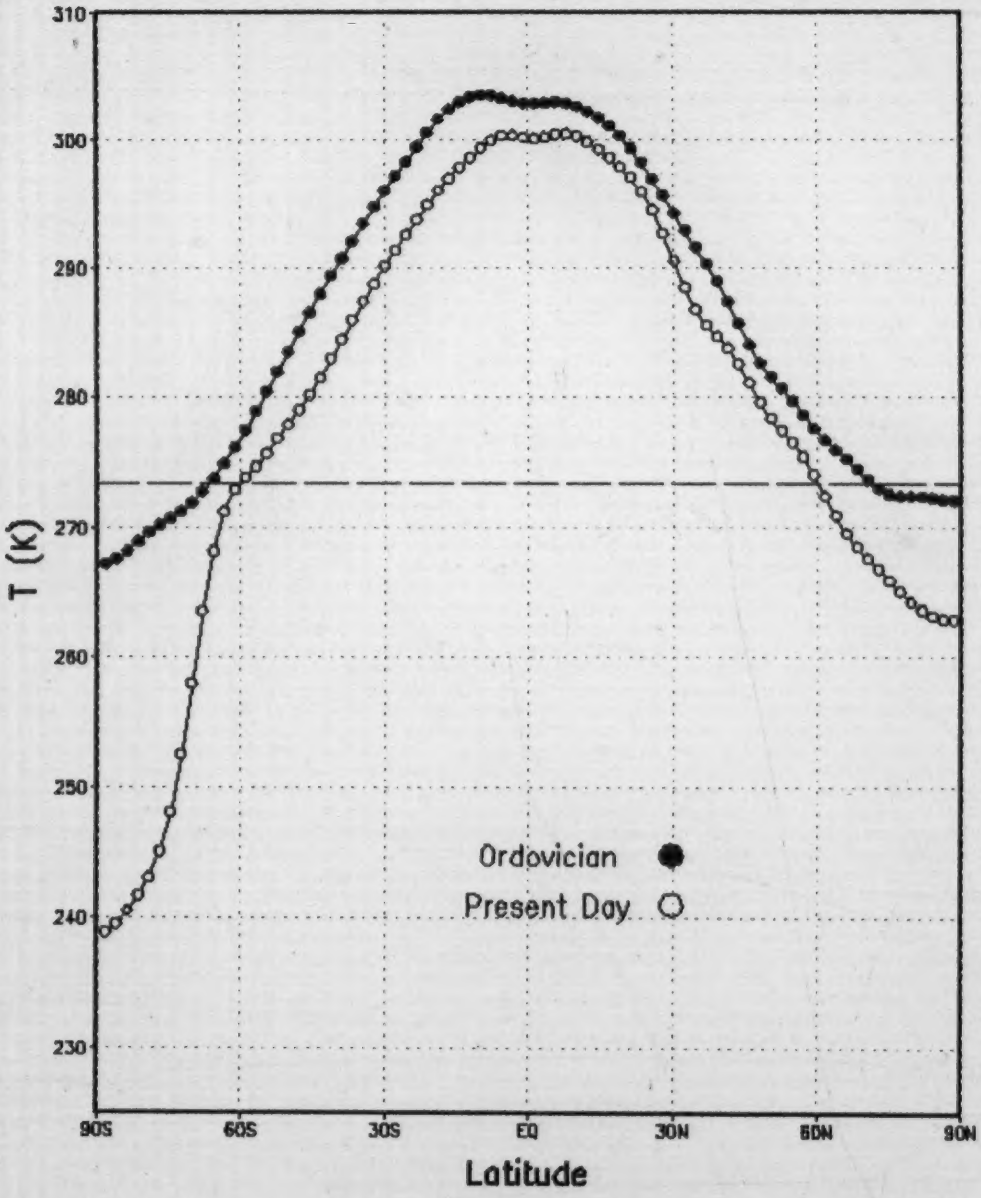

Figure 3-1-2. Annual and zonal mean near-surface temperature (atmospherere–only simulation) in degrees Kelvin as a function of latitude. For the Ordovician (solid circle) and present day (open circles). The dashed line is the freezing line of 273.15°K.

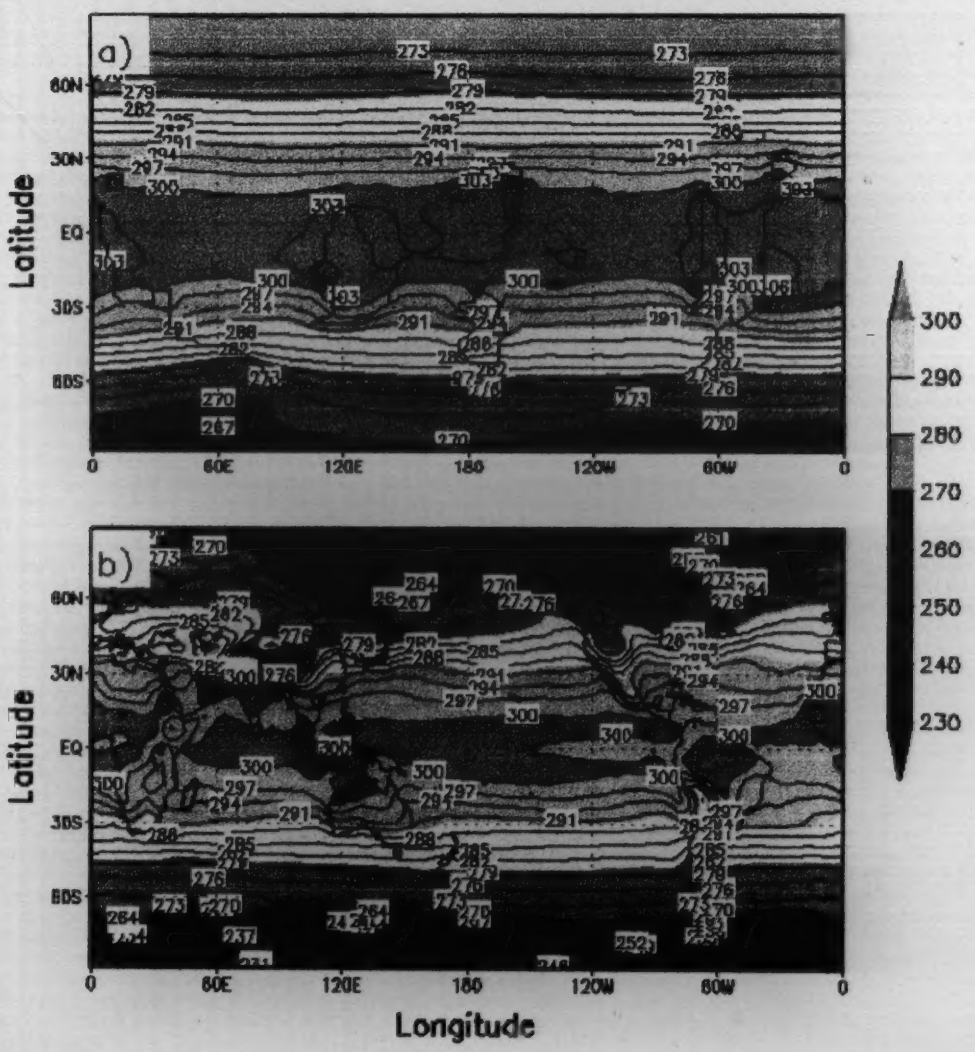

Figure 3-1-3. Annual mean near surface (about 30 m above ground) temperature (°K) as a function of longitude and latitude for (a) the Ordovician, and (b) the present day. The shading has an interval of 10 °K whereas contours have a 3 °K interval.

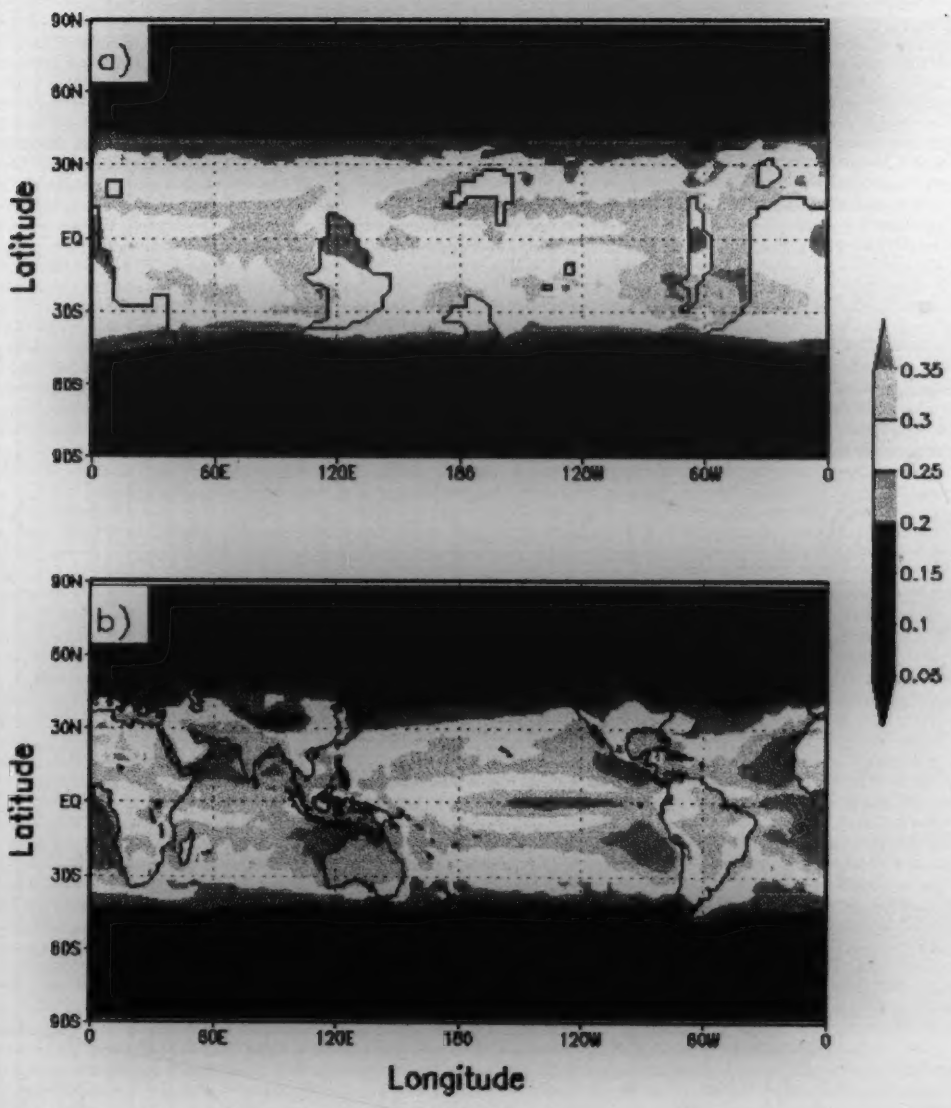

Figure 3-1-4. Annual mean net surface shortwave radiation as a function of longitude and latitude for (a) the Ordovician, and (b) the present day. The shaded colour is the annual mean near surface shortwave with units of cal/cm^2/min and 0.05 cal/cm^2/min intervals.

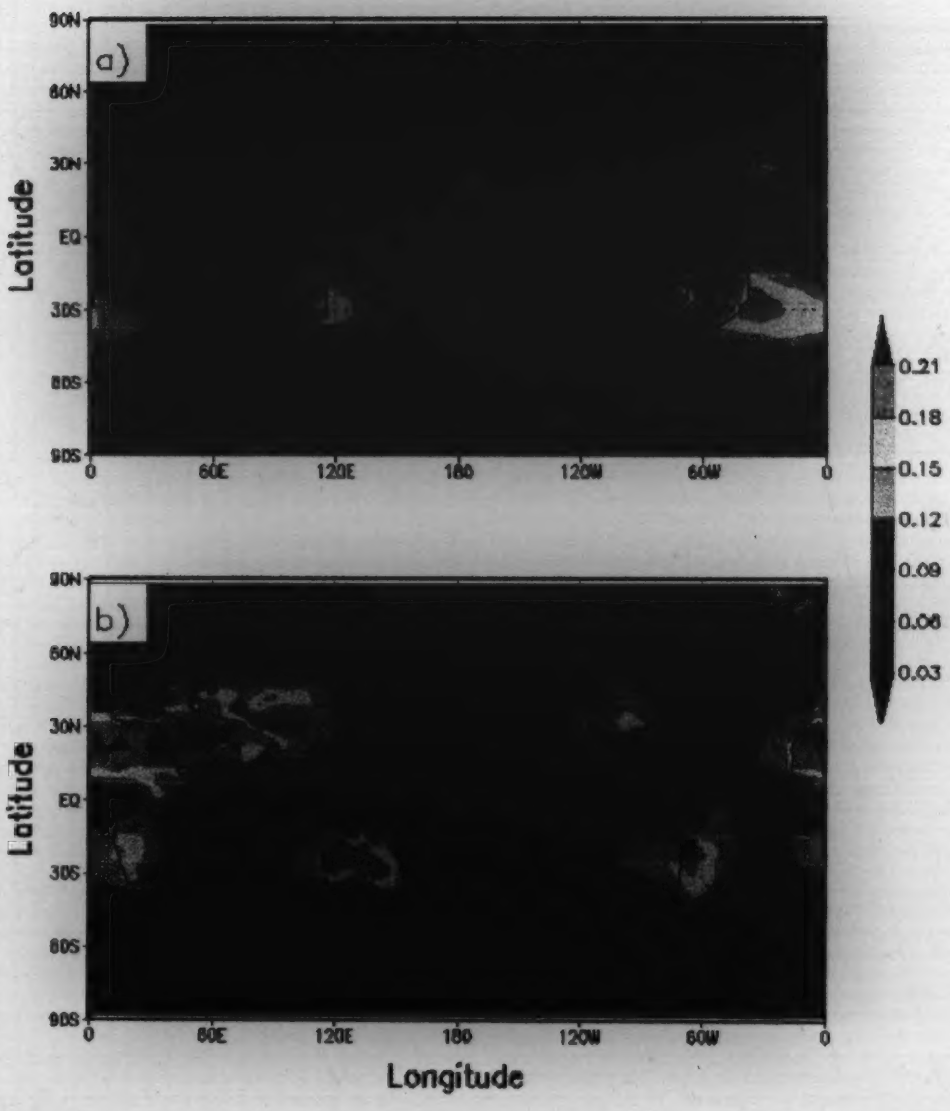

Figure 3-1-5. Annual mean net surface (about 30 m above ground) longwave emission as a function of longitude and latitude for (a) the Ordovician, and (b) the present day. Units are cal/cm^2/min with 0.03 cal/cm^2/min intervals.

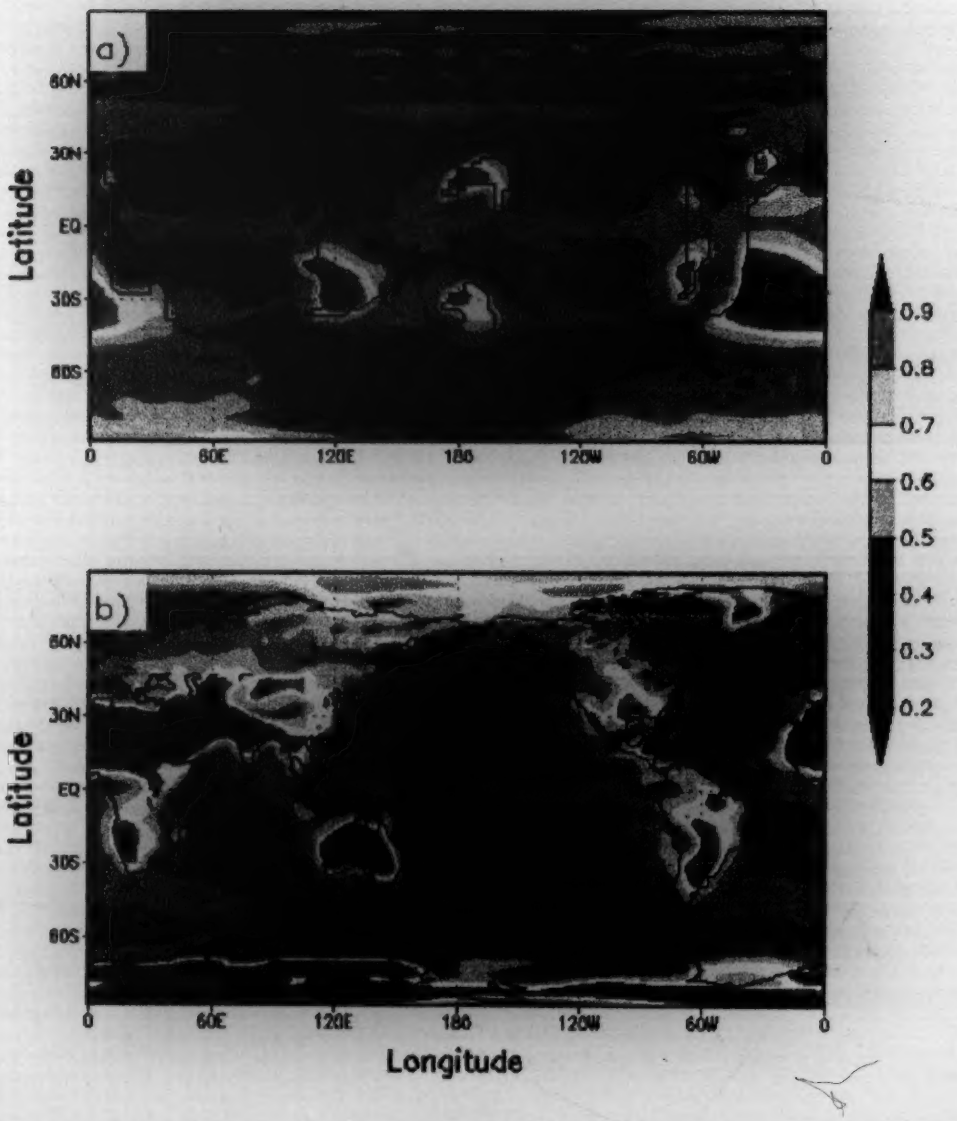

Figure 3-1-6. Annual mean relative humidity (percent/100) as a function of longitude and latitude for (a) the Ordovician, and (b) the present day with 0.1 percent/100 intervals.

The amplitude of the Ordovician seasonal cycle is shown in Figure 3-1-7-a. The amplitude of the seasonal cycle is given by the magnitude of the mean June-July-August (JJA) near surface temperature minus the mean December-January-February (DJF) near surface temperature. The interior of Gondwana experienced a very large seasonal cycle, with temperatures fluctuating more than 45° over the course of a year over a large geographic area. In contrast, only Siberia experiences such conditions today. The seasonal cycle in the high northern latitudes (30N to poleward) is longitudinally uniform with a low magnitude (less than 10 degrees) because of the absence of Ordovician continents. The Ordovician freezing lines are shifted poleward in both hemispheres compared with the present day and are consistent with the global temperature increase.

The vertical – latitudinal annual mean temperature in the Ordovician simulation (Figure 3-1-8-a) indicates that the most pronounced warming compared with the present day (Figure 3-1-8-b) is in the lower troposphere. The meridional temperature gradients in the lower troposphere are stronger today than in the Ordovician because of the strong ice albedo feedback that reduces modern polar temperatures. The middle troposphere meridional temperature gradients in the Ordovician, however, are comparable with the present day, especially in the northern hemisphere. This fact, also seen in simulations at the Cretaceous (Bush and Philander, 1997), has implications for the strength of the midlatitude jet streams through the thermal wind balance relation.

The Ordovician annual mean temperature in the upper troposphere and stratosphere (approximately 12km) is colder than the present day because of the higher atmospheric CO_2, which prevents longwave radiation emitted by the surface from reaching the upper atmosphere.

The Ordovician midlatitude westerly jets are slightly faster than the modern simulation even though the temperature gradient in the lower troposphere is reduced. There are two explanations for this feature. Since there is no continental topography, surface wind speeds are faster, which through thermal wind balance should increase the speeds of the jets. Also, the lack of gravity wave drag, normally generated by topography, would increase the speed of the jet.

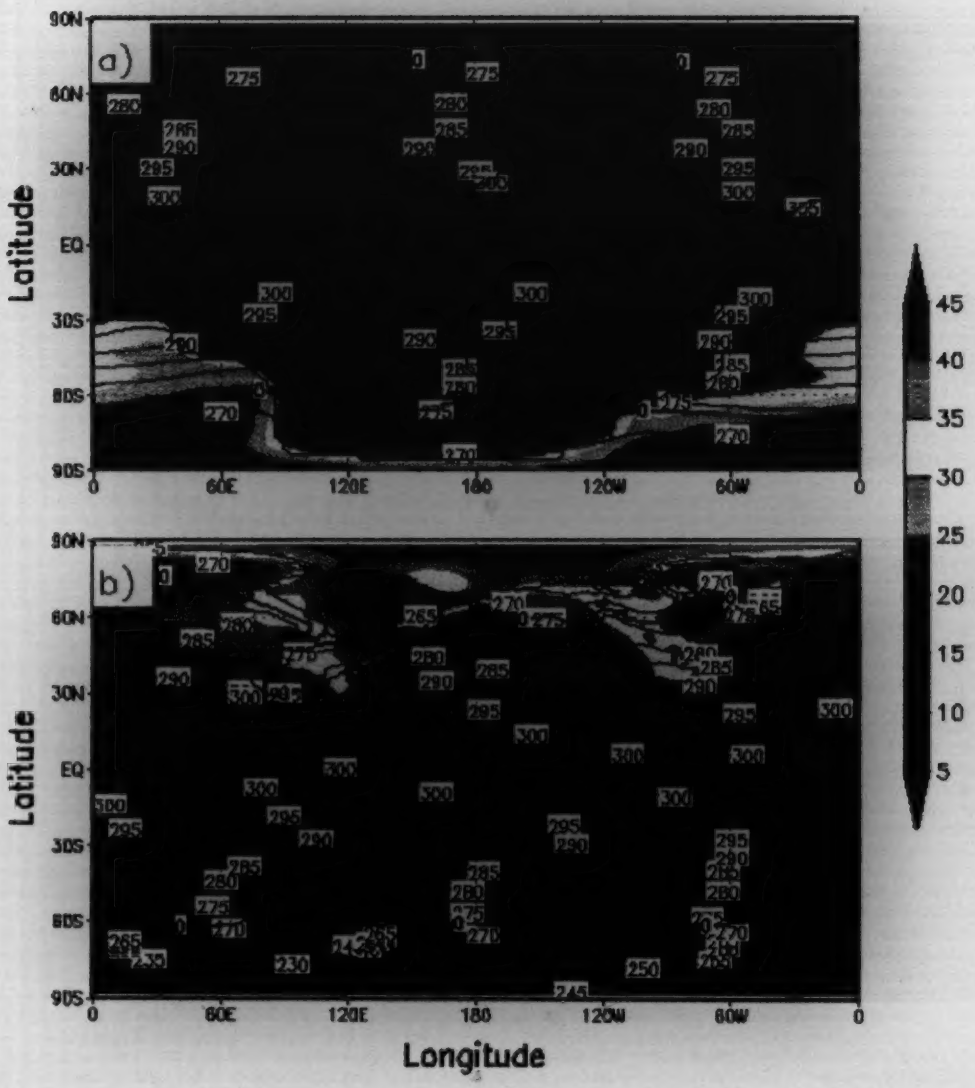

Figure 3-1-7. Amplitude of the seasonal cycle in near surface temperature (shaded; °K) in the atmosphere – only model for (a) Ordovician and (b) the present day with an interval of 5 °K. Contours are the annual mean temperature with 5 °K interval. The bold line is the freezing line and poleward of this line the annual mean near surface temperature is below freezing.

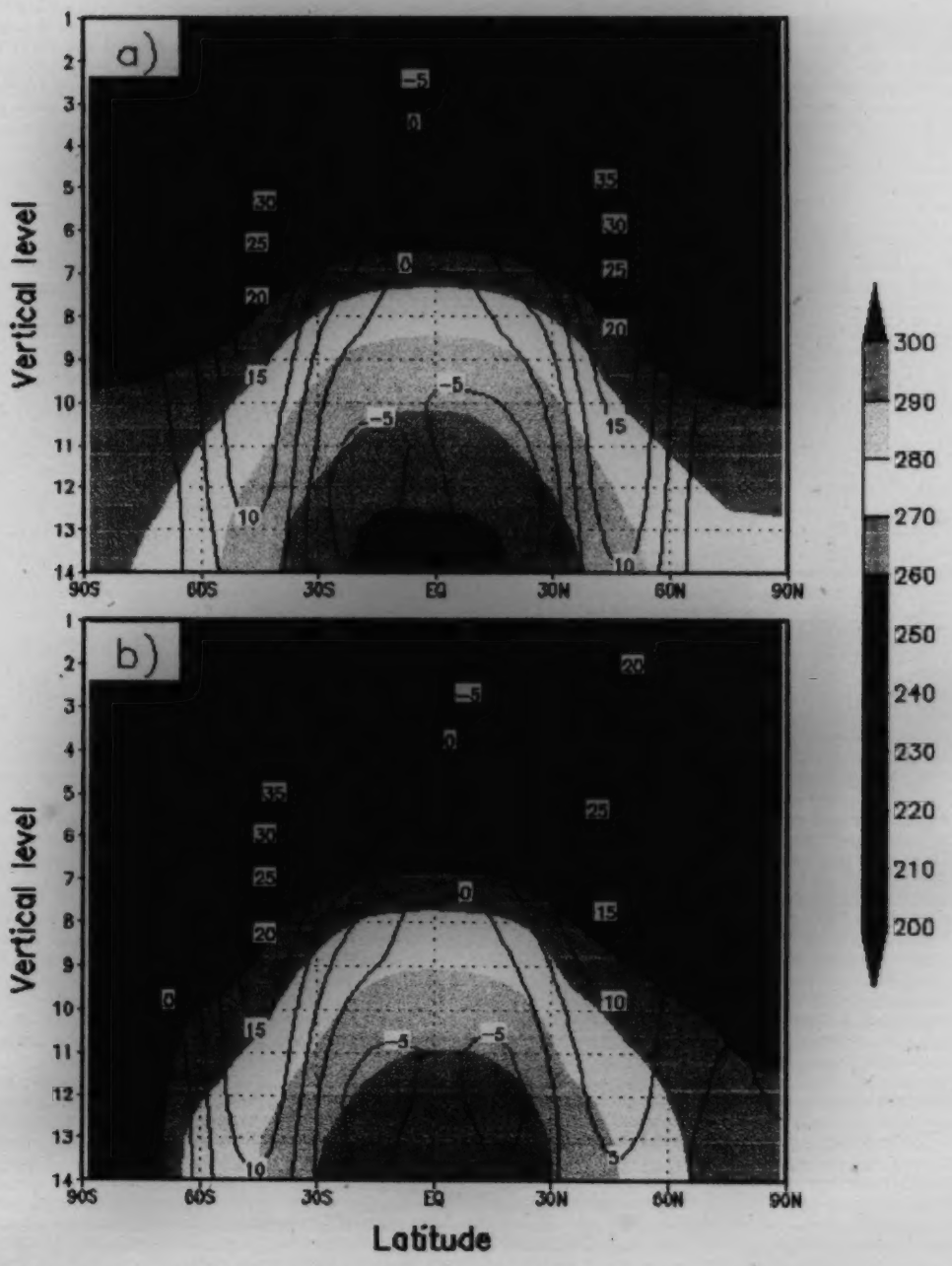

Figure 3-1-8. Vertical profile of annual and zonal mean temperature (shaded) and zonal velocity (contours) as a function of height and latitude for (a) Ordovician and (b) the present day. The contour intervals are 10°K for temperature and 5m/s for zonal velocity.

The mean meridional atmospheric circulation has significant control over latitudinal climate belts. The mean atmospheric circulation controls sedimentary deposition such as evaporite, and calcrete, which are representative rock types of dry semi-arid conditions. The Hadley cell is one of the major tropical atmospheric mean circulations. Winds in the Hadley cells converge at the surface in the intertropical convergence zone (ITCZ), which is shifted towards the south in the Ordovician simulation and towards the north in the modern simulation (Figure 3-1-9). Through longwave radiative cooling in the upper troposphere, air in the Hadley cells sink at ~30 degrees in both hemispheres in both the Ordovician and modern simulations. The strength of the Ordovician Hadley cells differ, with the northern hemisphere Hadley cell being stronger than both the southern hemisphere cell and both modern Hadley cells. The strong north hemisphere cell is related to the strong jet stream, which through baroclinic instability drives a stronger mean meridional circulation (Kim and Lee, 2001; Lee, 1997).

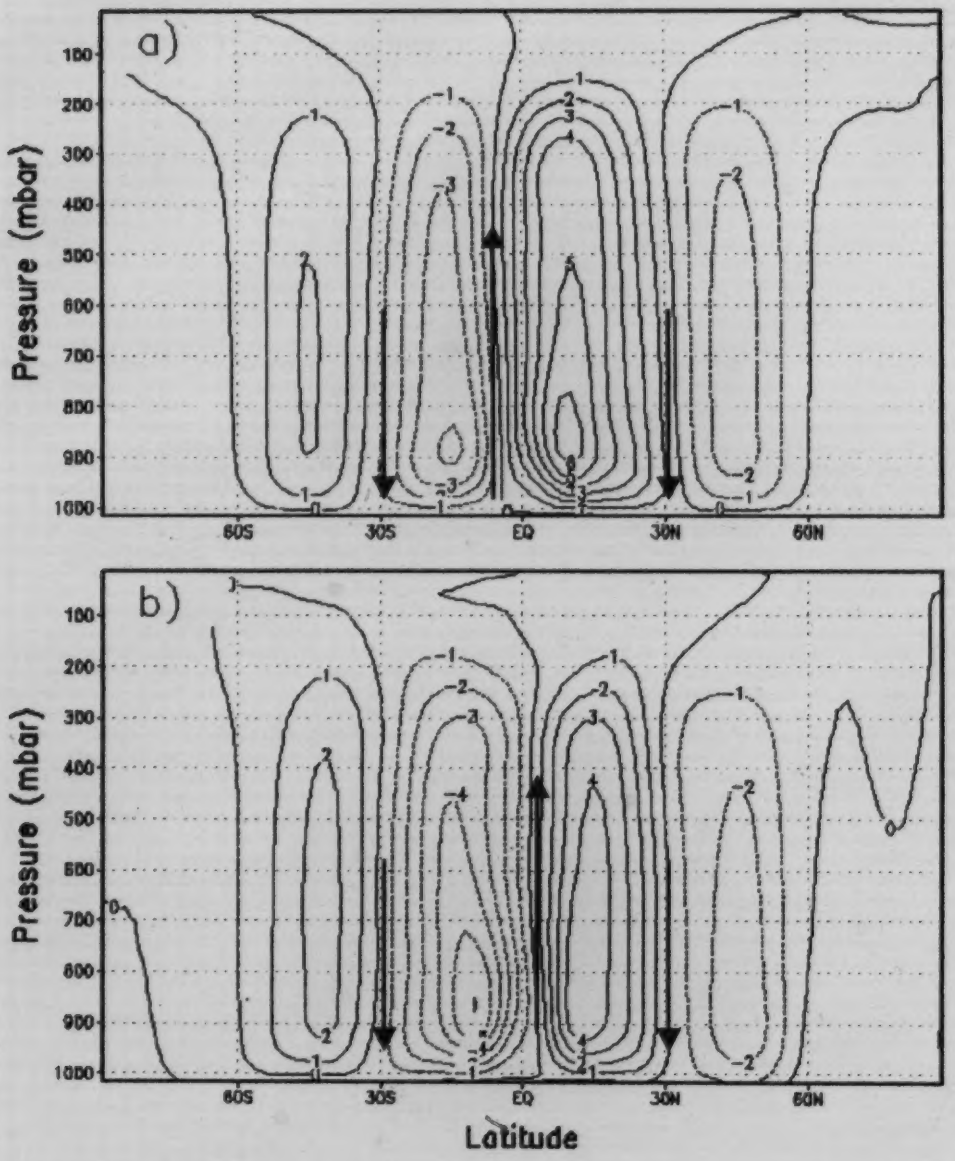

Figure 3-1-9. Annual mean tropical Hadley Cells and midlatitude Ferrel cells (times 10^{10} kg/s) for (a) the Ordovician, and (b) the present day with 10^{10} kg/s intervals. The negative values indicate counterclockwise flow in the diagrams.

In contrast to today's dominant Pacific Walker circulation, there are 2 Walker circulations above the Panthalassic ocean and the Palaeo-Tethys ocean in the simulated Ordovician climate (Figure 3-1-10-a). The Palaeo-Tethys ocean Walker circulation is larger and stronger than both the Panthalassic cell and the modern Pacific Walker cell (Figure 3-1-10-b). The strength of the Walker cells are related to the strength of the Hadley cells (through angular momentum) as well as to the strength of tropical convection over warm SST. It is expected that these circulations to change when coupled atmosphere-ocean processes are included in the model.

The atmosphere–only model simulations preclude physical interactions between the atmosphere and oceans. The next section (section 3-1-2) describes the coupled model simulations in which these atmosphere-only results are modified by the inclusion of ocean dynamics.

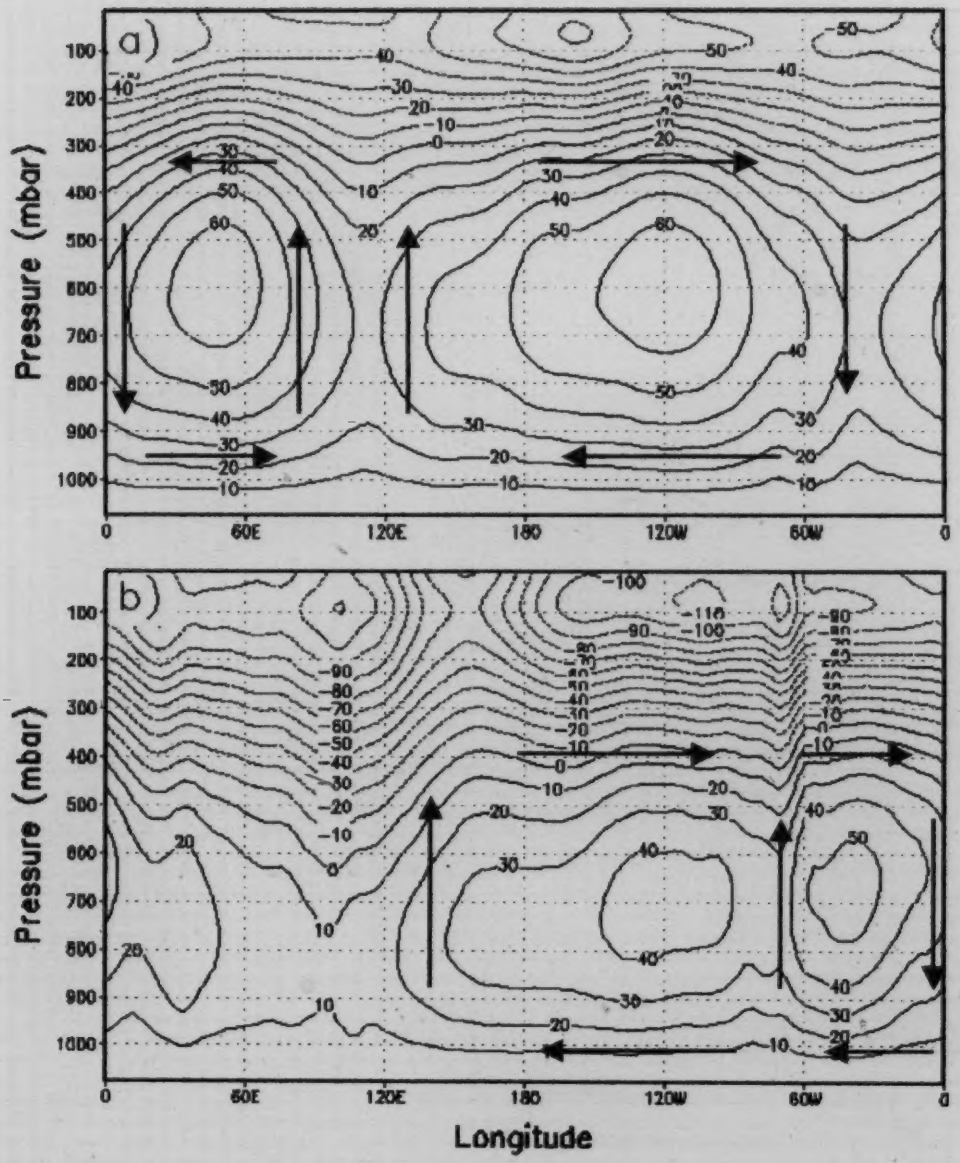

Figure 3-1-10 Annual mean Walker circulation (times 10^{10} kg/s) for (a) the Ordovician, and (b) the present day with 10^{11} kg/s contour intervals. The negative values indicate clockwise flow in the plane of the diagrams. Arrows indicate the flow directions for clarity.

3-1-2. THE COUPLED MODEL

The atmosphere – only and the coupled model have different response times to the Ordovician forcing parameters because of the presence in the latter of an active ocean and sea ice. Figure 3-1-11 shows the time evolution of global (Figure 3-1-11-a), troposphere (Figure 3-1-11-b), and stratosphere (Figure 3-1-11-c) atmospheric temperature simulated by the coupled model. The thermal response is slower than in the atmosphere-only simulation and takes about 15 years to adjust to 10 times higher atmospheric CO_2. There is a slower thermal response over the next 10 years due to stabilization of high latitude SST by the wind driven circulation. The global temperature becomes relatively stable after 25 years of simulation (Figure 3-1-11-a). In comparing Figure 3-1-1 with Figure 3-1-11, it is evident that SST is a major force controlling atmospheric temperature. The average global temperature (253.457°K) is about 1.987°K higher than today (251.47 °K). The Ordovician tropospheric temperature average increased about 4.8°K and the Ordovician stratospheric temperature average decreased about 6.7°K from the modern values, respectively.

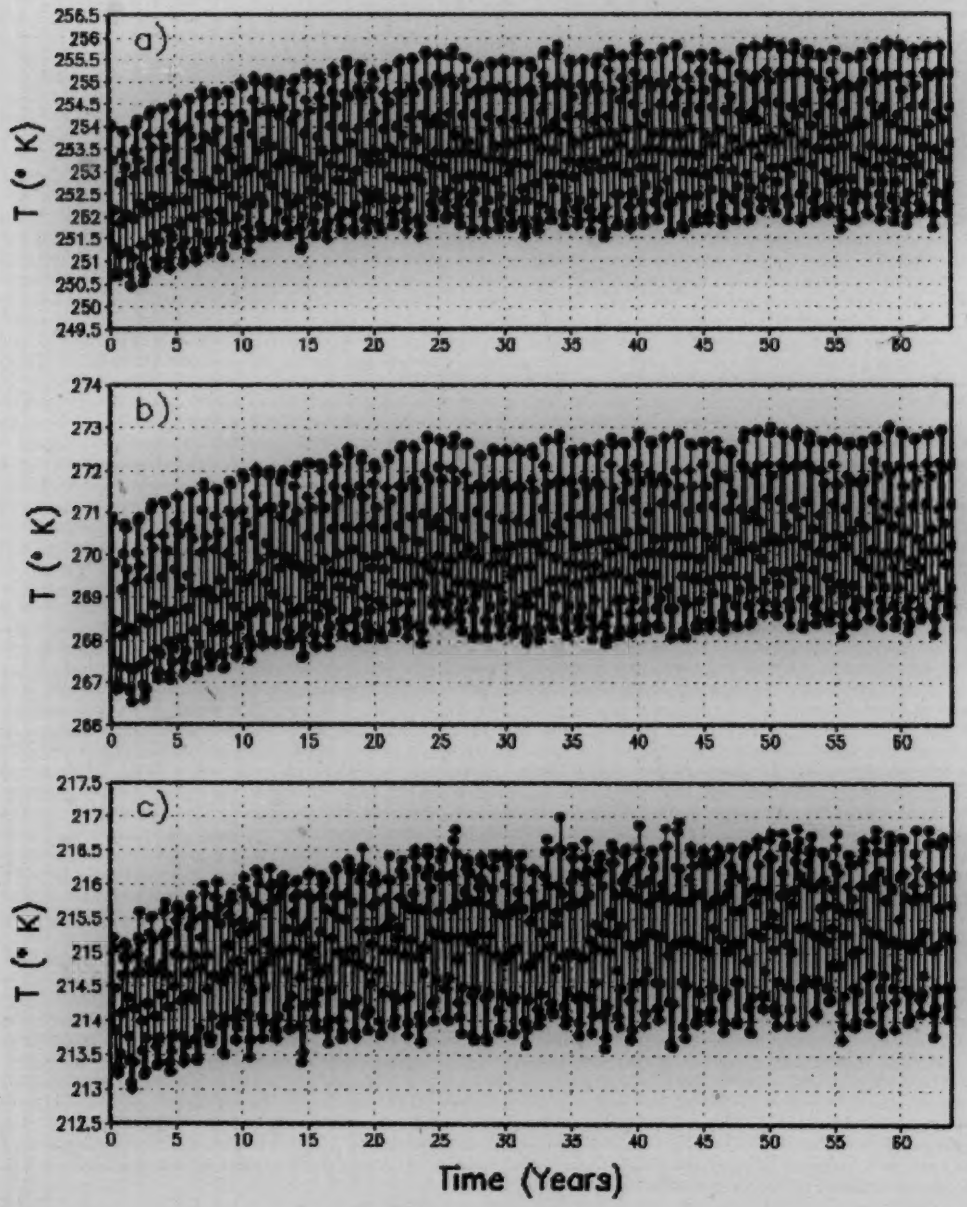

Figure 3-1-11. Time evolution of (a) global, (b) tropospheric, and (c) stratospheric atmospheric temperature (°K) as a function of time (years) from the coupled model results.

The simulated near surface (about 30 m above ground) annual and zonal mean temperature as a function of latitude in the Ordovician and present day coupled model results are shown in Figure 3-1-12. The coupled model results (Figure 3-1-12) are quite similar to the atmosphere-only model results (Figure 3-1-2) indicating that in a zonal mean the assumed SST in the atmosphere-only simulation was reasonable. The Ordovician near surface temperature is generally higher than the present day with tropical temperatures 3-4° higher with values of ~303.4°K. At 20N, the simulated Ordovician and modern temperatures are very similar to each other.

High latitude temperatures in the northern hemisphere in the Ordovician are approximately 11°K higher than the present day, whereas in the southern hemisphere temperatures are about 31.5°K greater than the present day. The lower temperature of both polar areas in the present day is explained by the same reason as that described for the atmosphere–only results (i.e., caused by massive Arctic and Antarctic ice sheets in the modern climate). The difference between the midlatitude temperature of the Ordovician and of the present day is ~2.5 – 7°K. The Southern midlatitude (45S) temperature is 4.5°K warmer than the North midlatitude (45N) in the Ordovician because the palaeocontinents are absent in the northern hemisphere.

Generally, the coupled simulations resulted in higher atmospheric temperatures than in the atmosphere-only simulation (cf. Figure 3-1-2) and show the effects of poleward heat transport by the ocean circulation. For example, polar temperatures are ~3°K warmer when ocean currents are included.

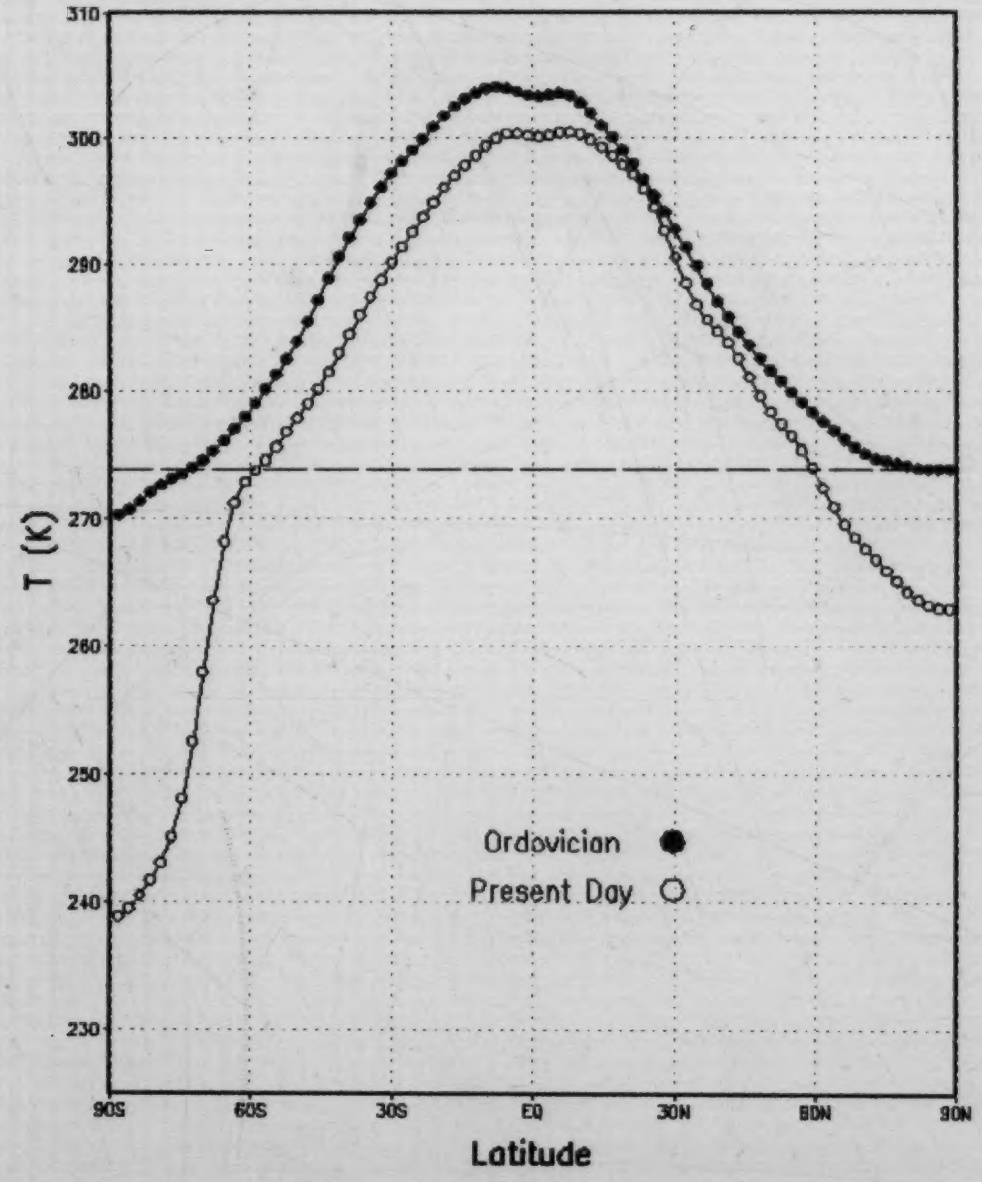

Figure 3-1-12. Annual and zonal mean near-surface temperature (coupled model simulation) in degrees Kelvin as a function of latitude. For the Ordovician (solid circle) and present day (open circles). The dashed line is the freezing line of 273.15°K.

The spatial distribution of annual mean surface temperature in the Ordovician (Figure 3-1-13) indicates that the highest temperatures (306°K) are still found in the tropics over west Laurentia and west Gondwana (Figure 3-1-13-a). The annual mean near surface temperature over the southern high latitudes in the Ordovician simulation are below the freezing point of 273.15 °K. The coupled simulation shows a general increase of the spatial annual mean near surface temperature of about 3 degrees more than the atmosphere–only result (Figure 3-1-3) and it becomes more apparent in the northern high latitudes, where the coupled simulation has a temperature above freezing in the annual mean. This indicates that ocean heat transport plays a strong role in regulating sea ice in this region.

The amplitude of the Ordovician seasonal cycle (Figure 3-1-14-a) shows that Gondwana experienced a very large seasonal cycle, with temperatures fluctuating more than 45 degrees over the course of a year as in the atmosphere–only simulation. The earliest evidence for land plants, embryophyte spores, are reported from Avalonia, Baltica, Laurentia, and N. Gondwana in the early Llanvirnian (Middle Ordovician; 470-464 Ma) to Llandoverian (Early Silurian; 443-428 Ma; Wellman and Gray, 2000; Wellman, *et. al.*, 2003). Their depositional environments, are inferred from their occurrence in continental and near shore marine deposits and their abundances usually decrease offshore (Wellman and Gray, 2000). Since early life on land had 40 Ma of relative stasis at the margin of the continent and the megafossil records of relatively complete land plants (e.g. tracheophytes, rhyniophytoids, nematophytes) predate at least the

Wenlock (Late Silurian; 428~ Ma; Wellman and Gray, 2000) this extreme environment on Gondwana could be the unpopular habitat for the primitive land life. The freezing line is about 25 degrees poleward in the Ordovician compared with the present day because of the warmer mean temperature.

The coupled simulation (Figure 3-1-13-a) shows a poleward expansion of the tropical zone (roughly defined to be the region where temperatures are over 300°K) by about 5 degrees further than in the atmosphere–only simulation (cf. Figure 3-1-3-a), and thus there is a further poleward shift of the freezing zones (below 273.15 °K) in the coupled simulation.

The amplitude of the seasonal cycle in the Ordovician northern hemisphere and in the area above the oceans in the southern hemisphere become stronger in the coupled simulation (Figure 3-1-14-a) than in the atmosphere – only simulation (Figure 3-1-7-a). However, the higher southern latitude continental region (South Gondwana) has a reduced seasonal cycle amplitude. Poleward ocean heat transport therefore significantly influences the atmospheric temperature over continental high latitudes. It is reiterated that this simulation captures the poleward heat transport of both the atmosphere and the oceans, unlike any previous study, and I find both transport mechanisms to be important to high latitude climate.

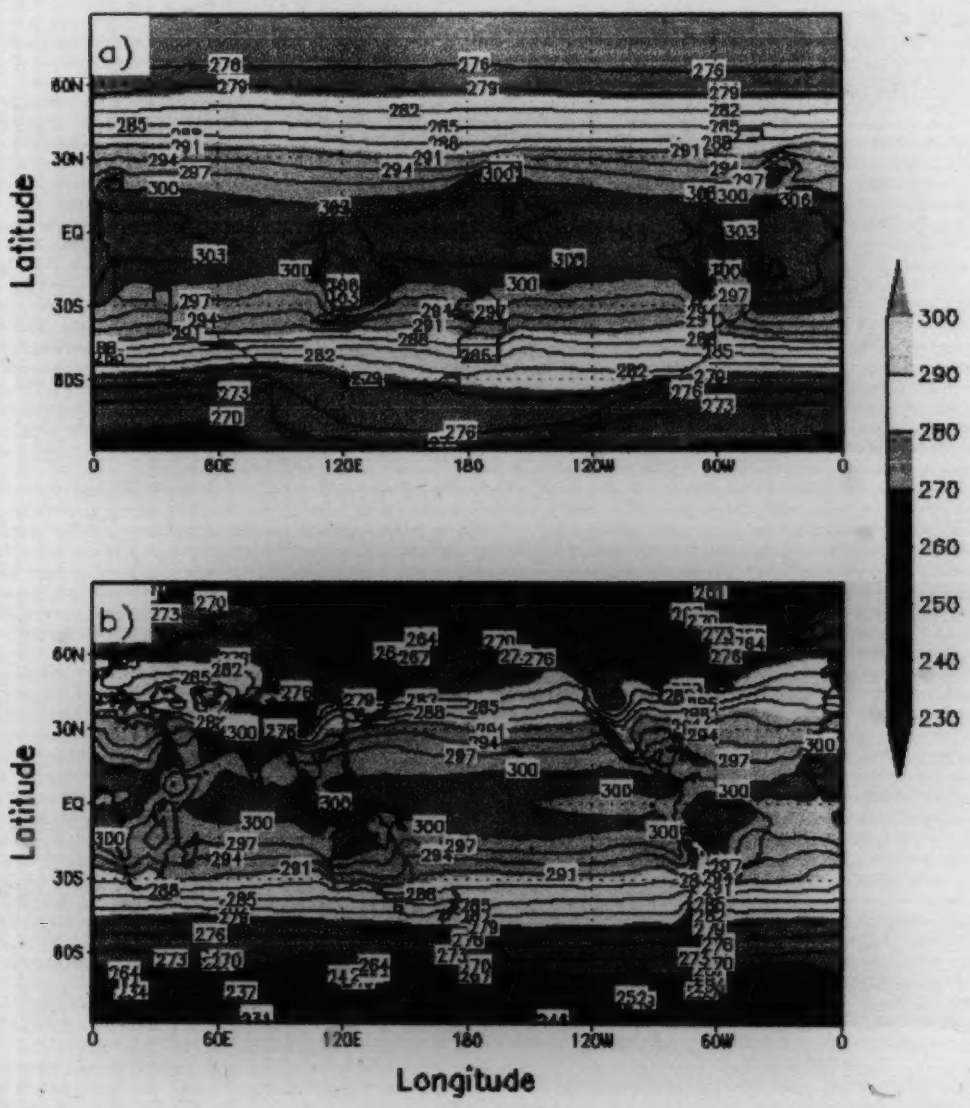

Figure 3-1-13. Coupled model simulation of annual mean near surface (about 30 m above ground) temperature in °K as a function of longitude and latitude for (a) the Ordovician, and (b) the present day. Shading has a 10 °K interval and contour lines have a 3°K interval.

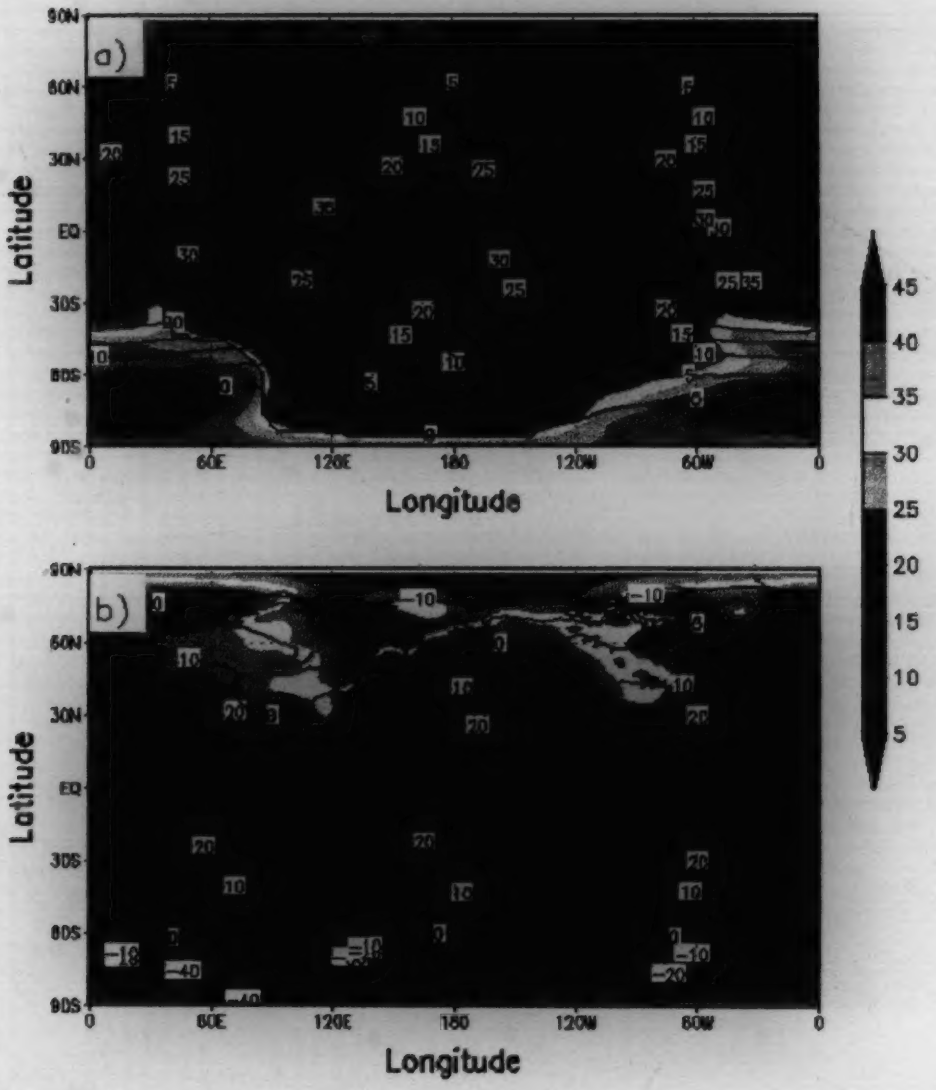

Figure 3-1-14. Amplitude of the seasonal cycle in near surface temperature in the coupled model. The shaded values are the amplitude of the seasonal cycles for (a) Ordovician and (b) the present day. The contour lines are the annual mean near surface temperature in degrees Kelvin. The contour intervals are 5°K in (a) and 10°K in (b). The bold blue line is the freezing line and poleward of this line the annual mean near surface temperature is below freezing.

The vertical-meridional structure of the Ordovician annual mean temperature (Figure 3-1-15-a) indicates a weaker meridional temperature gradient in the lower troposphere compared with today (Figure 3-1-15-b) but it is even weaker than in the atmosphere-only simulation (cf. Figure 3-1-8) because of the oceanic poleward heat transport. There is an equatorward shift of the northern hemisphere jet core which, through the thermal wind relation, increases the wind speeds in the jet core.

The simulated temperature increase is related not only to higher CO_2 levels but also to atmospheric water vapour content and latent heat release in the Ordovician atmosphere. The change in atmospheric temperature influences both the absolute and relative humidity (Figure 3-1-16), the latter of which has lower minimum values compared to the atmosphere-only simulation. The net shortwave radiation at the surface (Figure 3-1-17) is increased where oceanic upwelling occurs and the maximum values of net surface longwave radiation (Figure 3-1-18) are increased since atmospheric temperatures are greater in the coupled model.

The regional pattern of simulated relative humidity from the coupled model (Figure 3-1-16-a; above Siberia, Southern Laurentia, Northern Baltica and Northern Gondwana Islands and North Gondwana), correlates with the increased net longwave emissions (Figure 3-1-18-a). Where the atmosphere is hottest there is the most outgoing longwave radiation and a minimum in relative humidity. The net surface shortwave radiation (Figure 3-1-17-a) is higher in the ocean regions that are adjacent to the paleocontinents and where cold deep ocean water is upwelled to the surface.

The middle troposphere meridional temperature gradients in the Ordovician and the present day are similar to each other, especially in the northern hemisphere, even though there is a decreased temperature gradient at the surface. The zonal velocity in Figure 3-1-12 shows the midlatitude jet streams. The Ordovician core jet speed is faster than the present day and is stronger in the northern hemisphere. The meridional width of the jets is smaller in the Ordovician, especially in the northern hemisphere, and the jet core is displaced equatorward by ~7-8 of latitude compared to today and ~5 degrees compared to the atmosphere-only simulation. This demonstrates the effect that palaeogeographic distribution has on the jet streams. When there are no continents or no topographic barriers, stronger zonal surface winds occur and the jet is shifted equatorward. Additionally there is no topographic gravity wave drag in the Ordovician simulation, therefore the jet velocity is enhanced in the upper atmosphere (McFarlane and Manzini, 1997).

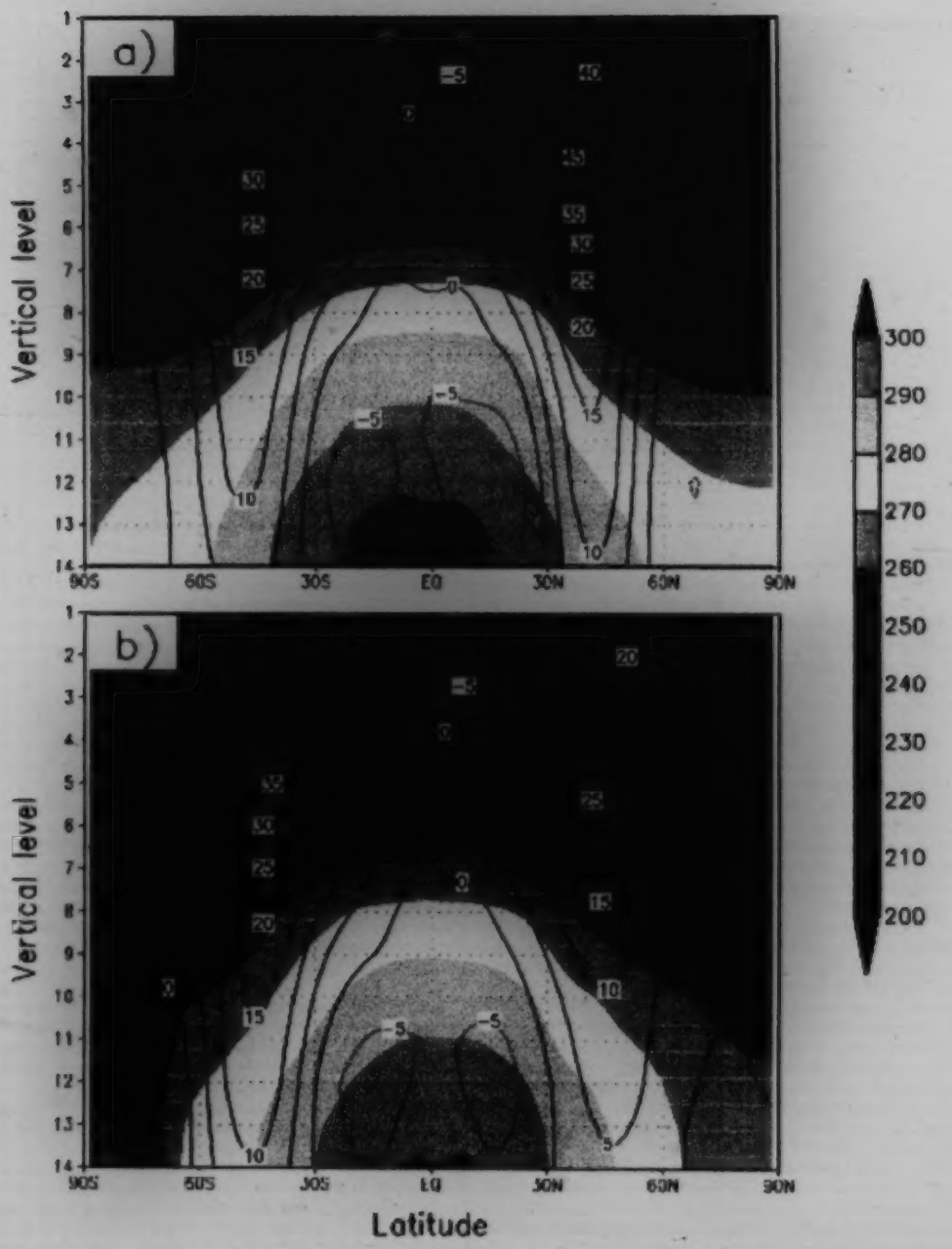

Figure 3-1-15. Vertical profile of annual and zonal mean temperature (shaded) and zonal velocity (contours) as a function of latitude for (a) Ordovician and (b) the present day. The contour intervals are 10°K for temperature and 5m/s for zonal velocity.

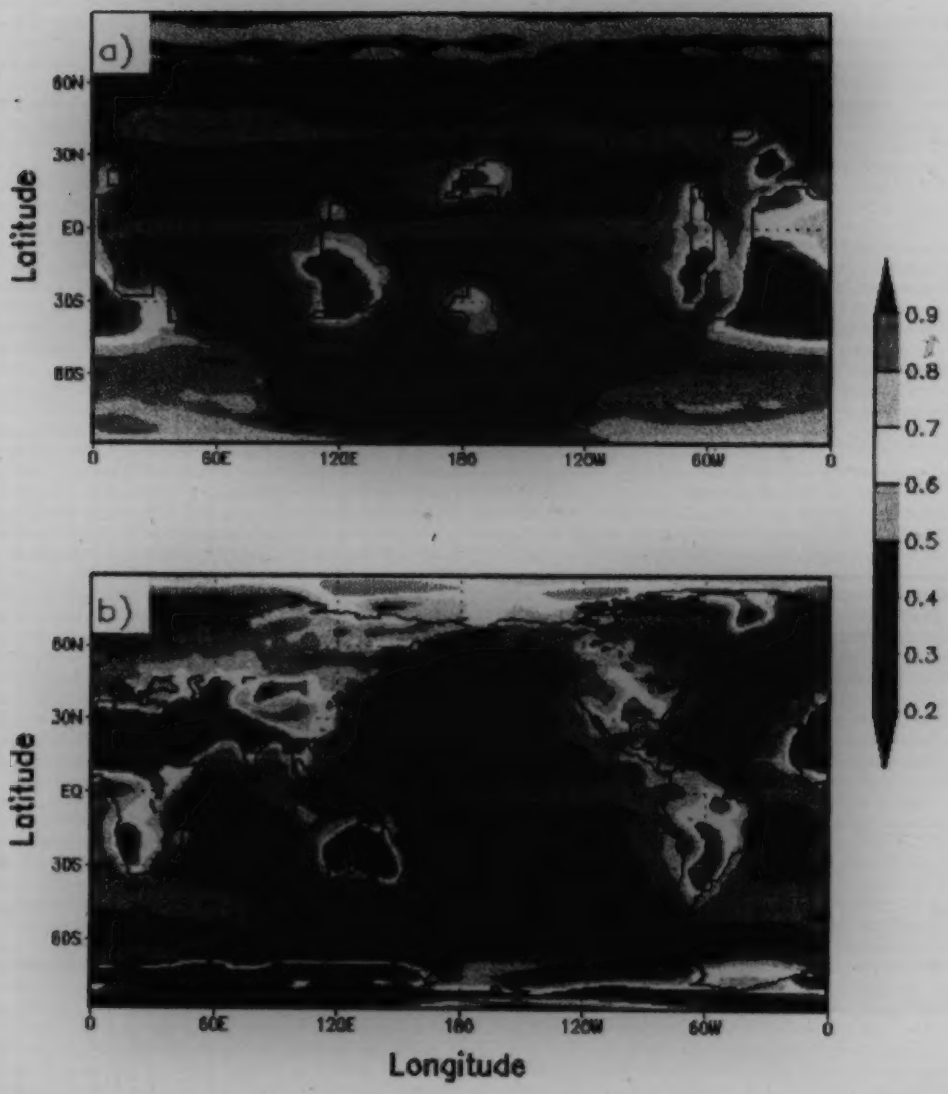

Figure 3-1-16. Annual mean net surface humidity (percent/100) as a function of longitude and latitude for (a) the Ordovician, and (b) the present day with 0.1 percent/100 intervals.

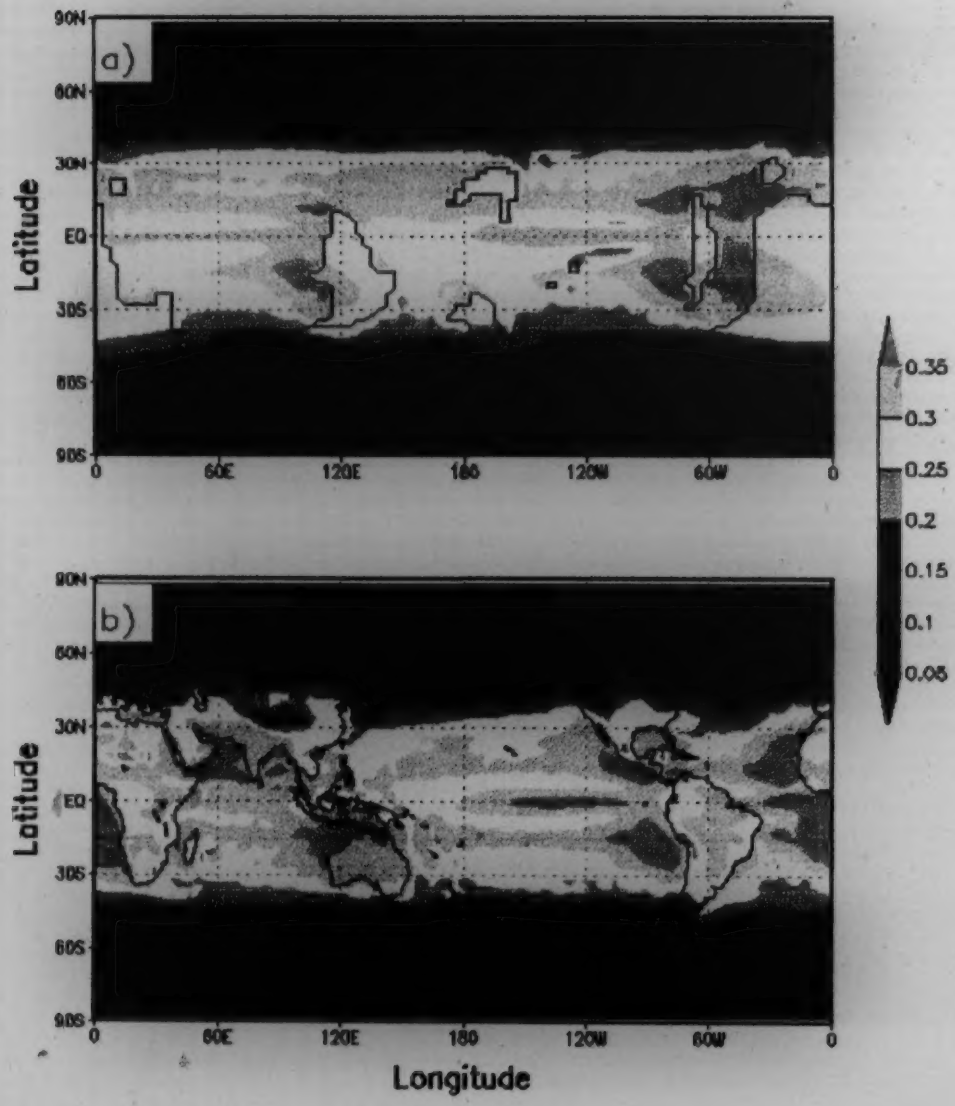

Figure 3-1-17. Annual mean net shortwave radiation as a function of longitude and latitude for (a) the Ordovician, and (b) the present day in units of cal/cm^2/min with 0.05 cal/cm^2/min intervals.

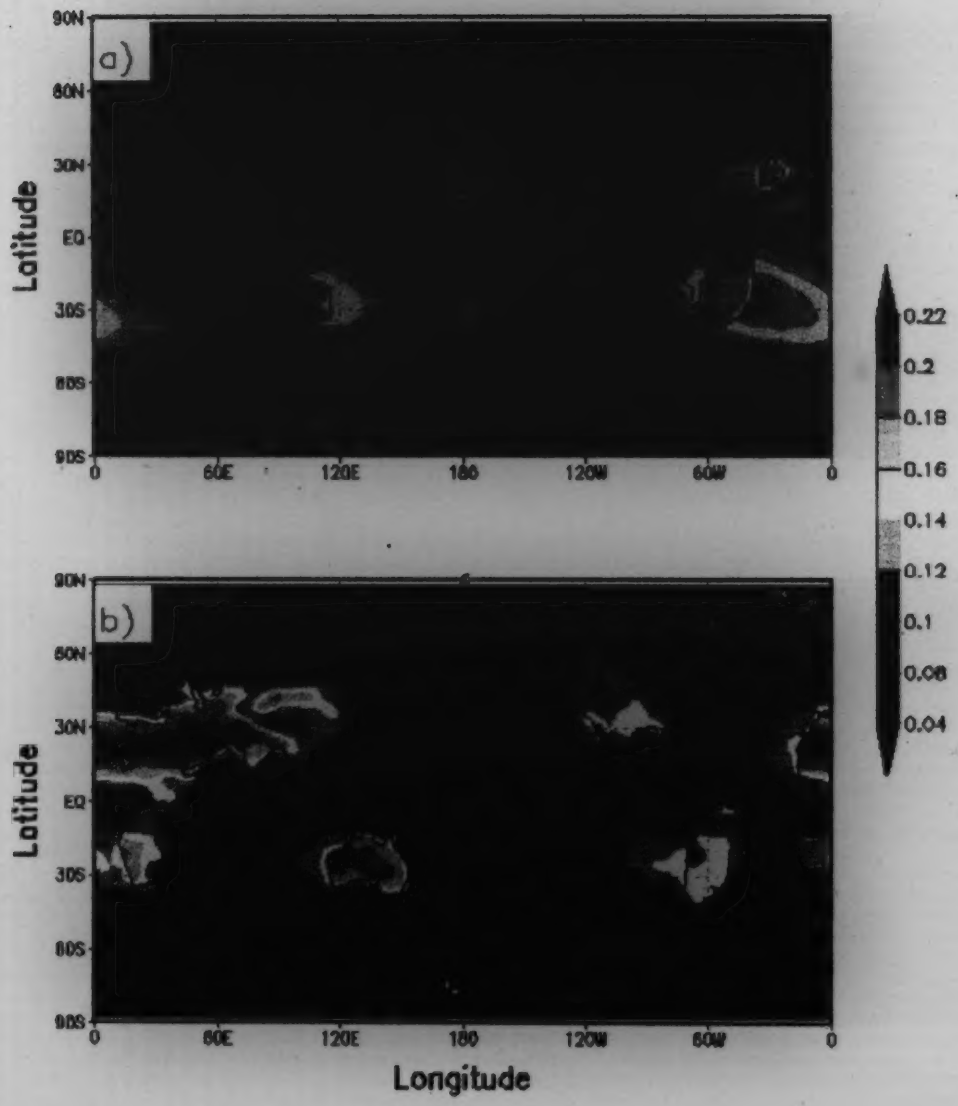

Figure 3-1-18. Annual mean net longwave emission as a function of longitude and latitude for (a) the Ordovician, and (b) the present day in units of cal/cm^2/min with 0.02 cal/cm^2/min intervals.

Winds in the modern Hadley cells converge at the surface in the ITCZ and through longwave radiative cooling in the upper troposphere sink at 30 degrees in both hemispheres (Figure 3-1-19-b). In contrast, the atmosphere-only Ordovician Hadley cells rise at about 5S and sink at about 30N and 30S (cf. Figure 3-1-19-a). The Ordovician north equatorial Hadley cell is stronger than both the southern hemisphere cell and either of the present day cells. These major features are also true in the coupled model simulation (Figure 3-1-19) although the strength of the Hadley and Ferrell cells are different. In the coupled model, poleward heat transport in the southern hemisphere reduces the jet strength and hence baroclinic instability, the Ferrell cell, and the Hadley cell are also all weaker. In the northern hemisphere, the stronger jet produces stronger Ferrell and Hadley cells. Underneath the descending branches of the Hadley cells are regions of high evaporation and high ocean salinity. These salty ocean regions correlate well with a map of evaporites and calcretes (Figure 3-1-20, Scotese, 2002). An Island of NW Gondwana has produced a large amount of evaporite findings. Evaporites and calcretes have been found in places that would have been roughly between 25N and 30S in the Ordovician (Scotese, 2002), which correlates with the simulated descending branches of the Hadley cells. There would have been even more arid conditions under the stronger northern Hadley cell, but there were few landmasses there at that time from which to find evidence.

The position of the Walker circulations from the coupled simulations are relatively similar to the atmosphere – only simulations (Figure 3-1-21). Two strong cells arise because the Panthalassic ocean and the Palaeo-Tethys ocean are

each large enough to support distinct western warm pools and eastern cold tongues, while in the modern oceans this structure is not as pronounced in the Atlantic Ocean. The size of the Pacific Ocean is comparable with the Palaeo-Tethys ocean. However, modern SST in the western warm pool is lower than in the Ordovician warm pools and this reduces the strength of the Walker circulation through reduced atmospheric convection. Additionally, the strength of the upward branch of the Walker circulations in the Ordovician is partially increased by enhanced latent heat release over the warm pools during convection in the warmer and moister climate (cf. Figure 3-1-13). These enhanced Walker cells also imply that the easterlies in the lower troposphere were stronger during the Ordovician as well as the westerlies in the upper troposphere over the ocean basins.

There is a seasonal fluctuation of the zonal extent of the simulated Walker circulations. During JJA, the Palaeo-Tethys ocean Walker circulation is at its maximum zonal extent (between 120E-30W) and during DJF, the Panthalassic ocean Walker circulation is at its maximum (30E-150E).

Continental heating of Siberia and north Laurentia during JJA could induce warmer SST in the western Palaeo-Tethys ocean, whereas heating of Gondwana during austral summer induces warmer SST in the western Panthalassic ocean. As will be shown in the next section, these changes correlate with seasonal precipitation changes.

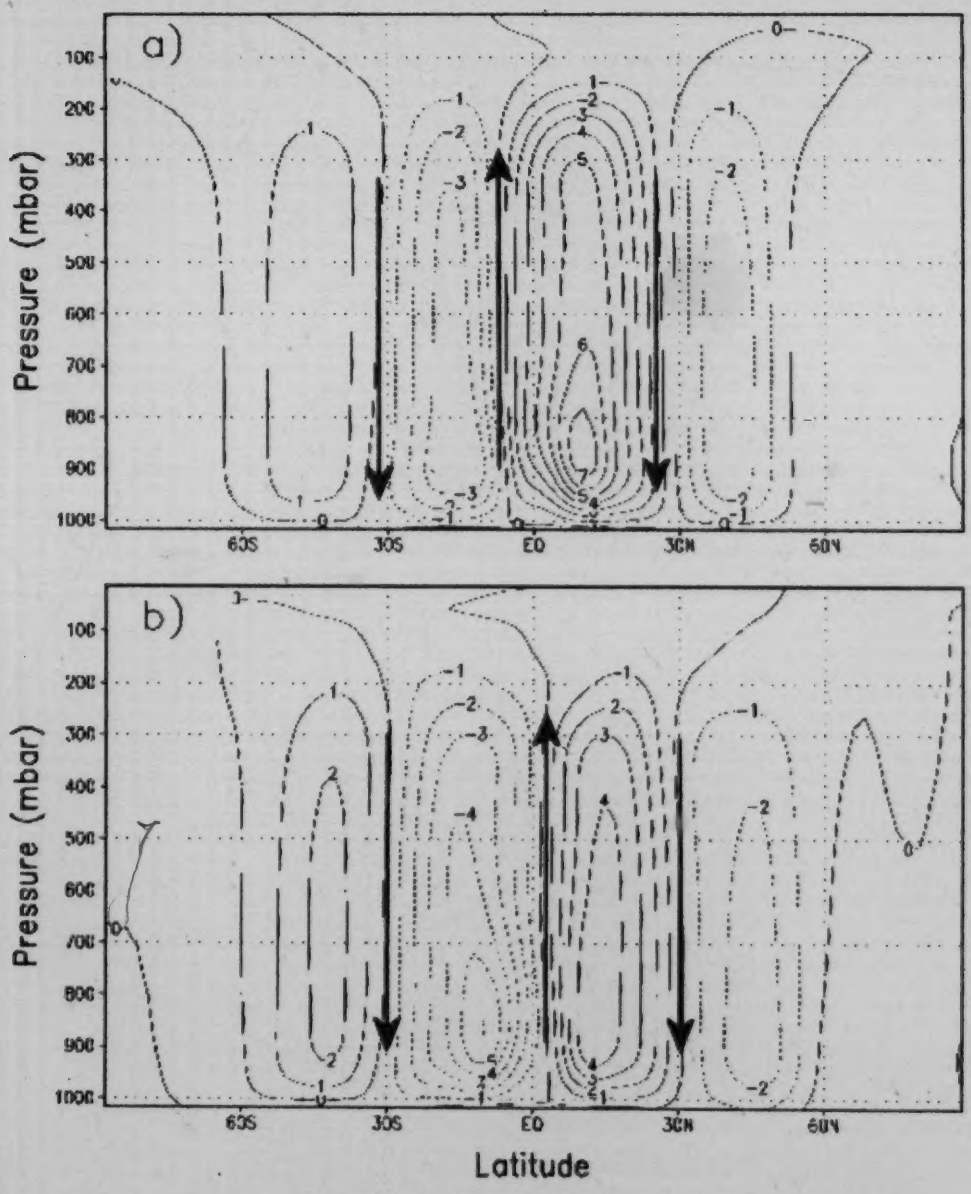

Figure 3-1-19. Annual mean Hadley Cells (times 10^{10} kg/s) for (a) the Ordovician and (b) the present day. Contour interval is 10^{10} kg/s and the negative values indicate counterclockwise flow in the diagrams.

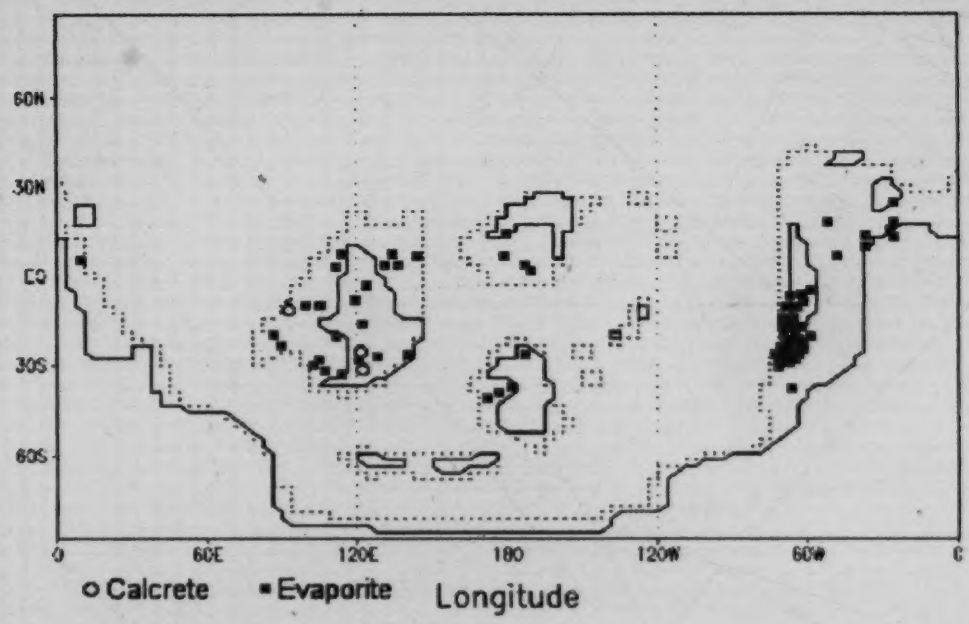

Figure 3-1-20. Lithological distribution map for the late Ordovician. Solid squares are evaporites and open circles are calcretes. (modified from Scotese 2002)

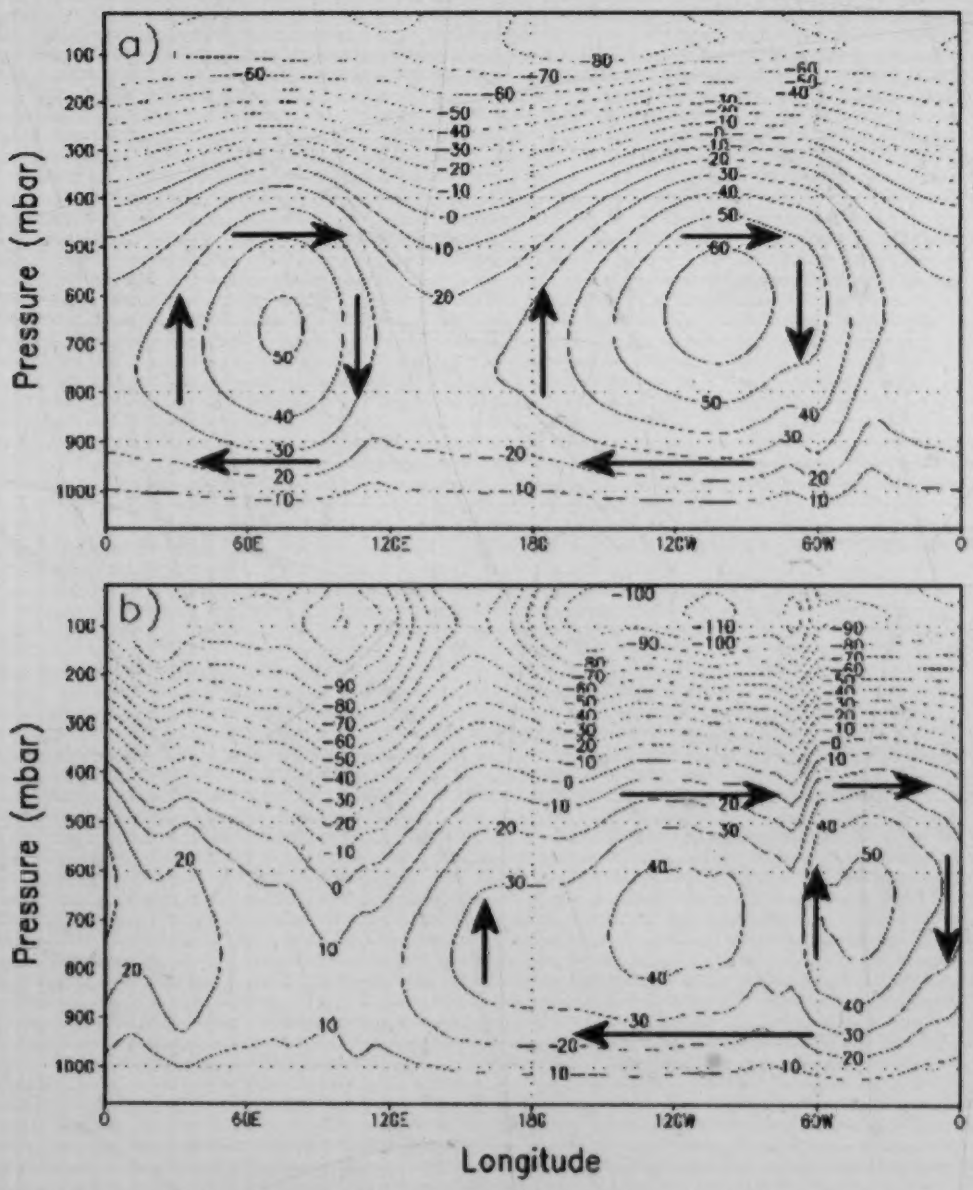

Figure 3-1-21. Annual mean Walker circulation (times 10^{10} kg/s) for (a) the Ordovician and (b) the present day. Contour interval is 10^{11} kg/s and positive values indicate clockwise flow in the plane of the diagram. Arrows indicate the flow directions for clarity.

3-2. OCEAN

There is a rapid SST response over the first 13 years followed by a slower response over the next 12 years as the wind driven circulation adjusts and stabilizes after the first 25 years of the simulation. The Ordovician annual mean sea surface temperature is warmer than the present day (Figure 3-2-1). The Ordovician global SST mean is about 2.5 degree higher than the present day and gives justification for the use of 3°C above modern SST in the atmosphere–only simulation.

SST in the high northern latitudes in the Ordovician simulation is fairly zonally uniform because of strong zonal currents driven by the strong jet stream with no continental barriers. SST in the higher northern latitudes (about 65N~) is below freezing point, therefore there is a potential to form seasonal sea ice. SST in the high southern latitudes is more complex because of the landmass barriers and consequent current movement.

The simulated Ordovician tropical ocean has a wider poleward expansion than today as determined by the 27°C isotherm. The Walker circulations affect the equatorial ocean circulation and SST. Deep cold water is upwelled to the surface because of the strong easterly zonal winds over the East Panthalassic Ocean (West Laurentia) and East Palaeo-Tethys Ocean (West Gondwana), similar to the east Pacific cold tongue of today (Figure 3-2-1-b). Upwelling deep water therefore forms two strong tropical cold tongues in the Ordovician. The Palaeo-Tethys ocean cold tongue, with a minimum temperature 24°C, is stronger than the one in the Panthalassic Ocean.

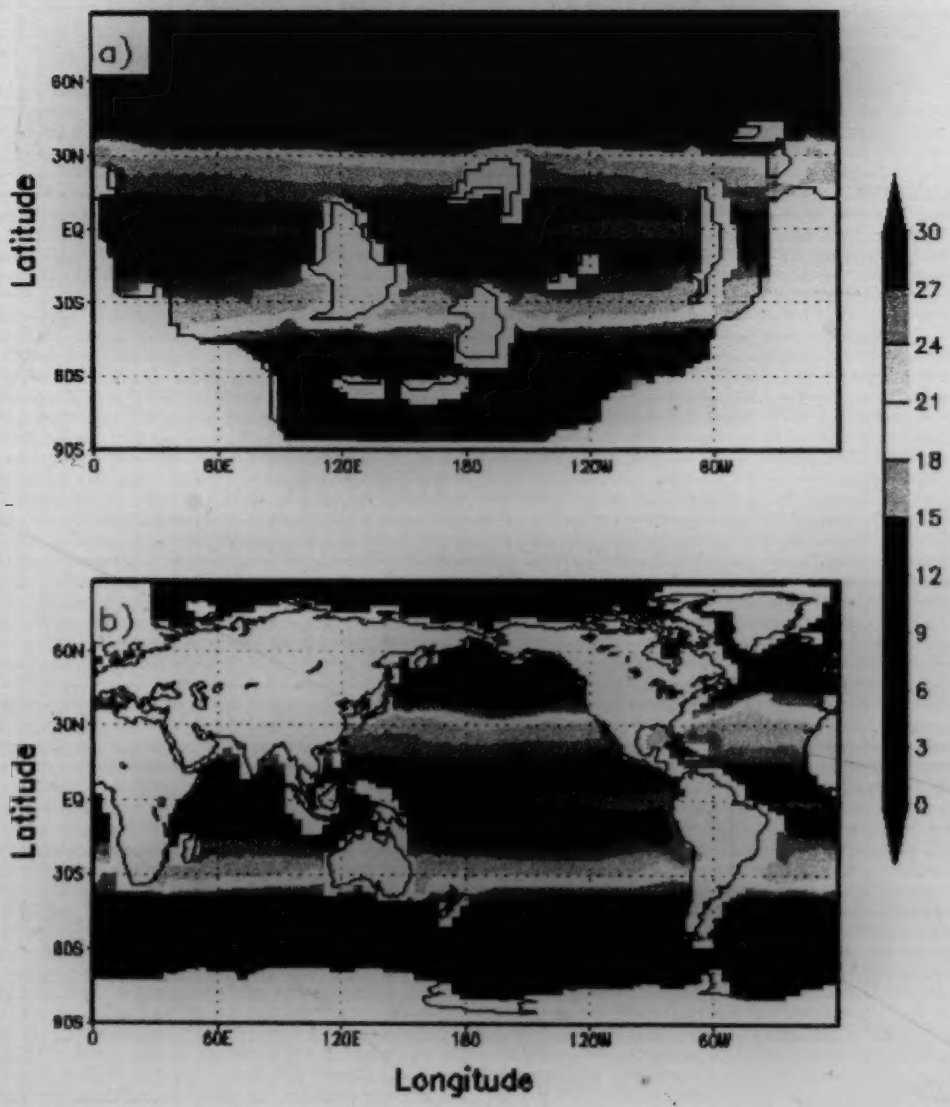

Figure 3-2-1. Annual mean sea surface temperature (°C) (a) in the Ordovician and (b) in the present day with a contour interval of 3 degrees centigrade.

Concurrent with these two cold tongues are two western warm pools above which most of the tropical convection takes place, similar to the west Pacific warm pool of today. This cold-tongue/warm pool structure is analogous to that of the present day Pacific and Atlantic oceans, although the structure in the Atlantic is not as pronounced because of the relatively small size of the basin. Given this climatological mean state, the possibility exists that both oceans undergo interannual variability analogous to the modern El Niño Southern Oscillation (ENSO). This interesting point will be examined in more detail in section 3-3-2.

The simulated SST, when combined with biogeographic reconstructions, suggests that graptolite Pacific faunas preferred SST above 18 °C and that the Atlantic faunas existed in SST of between 18 °C and 0 °C (cf. Figure 1-5). The majority of graptolites were likely preserved under anoxic and low turbulence environments because of their organic exoskelton being complete (Clarkson, 1986; Harper and Owen, 1996), since the upwelling of deep water would break it up. The equatorial East Palaeo-Tethys and East Panthalassic oceans have simulated oceanic upwelling and this result is therefore a likely cause for the lack of specimens recovered from these upwelling regions. The mean ocean surface salinity is changed by atmospheric temperature, wind speed and the continental distribution, which affects the winds and precipitation patterns. The higher salinity (>36 ‰) regions are observed near SW Laurentia, and NE Gondwana in the south equatorial regions, and E Siberia and N Gondwana in the northern hemisphere (Figure 3-2-2-a). Both belts of high salinity occur under the descending branches of the Hadley cells. The higher salinity waters of the northern hemisphere correlate with a stronger Northern Hadley cell and enhanced

subsidence and evaporation. The higher salinity values of the southern hemisphere arise because of both the higher annual mean atmospheric near surface temperature and the continental distribution.

The annual mean ocean current directions are shown in Figure 3-2-2-b. In the northern hemisphere midlatitudes there are strong zonal winds and strong zonal currents, which create shear eddies in the ocean. There are also strong boundary currents in the Panthalassic and Palaeo-Tethys oceans, which are analogous to eastern boundary currents of the modern oceans. In the tropics there is an easterly current driven by the trade winds analogous to the modern South equatorial current in the Pacific Ocean. Given these easterly currents and the cold tongue/warm pool structure of both Ordovician oceans, interannual variability is therefore likely in this coupled simulation.

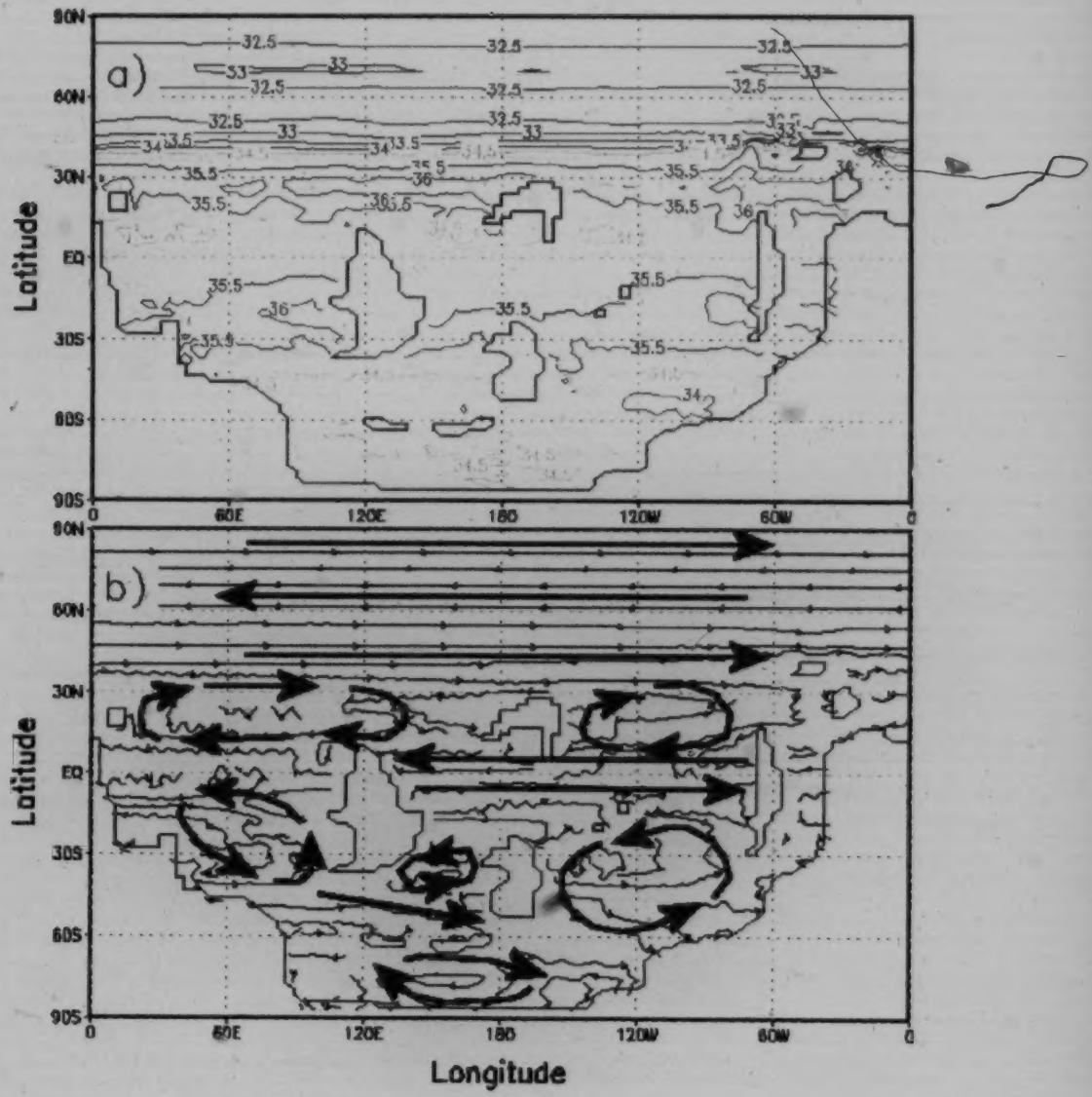

Figure 3-2-2. (a) Annual mean sea surface salinity for the Ordovician. The contour interval is 0.5 practical salinity unit (PSU). (b) Stream flow of annual mean ocean currents at a depth of 15m. Arrows indicate the current directions for clarity.

3-3. INTERANNUAL VARIABILITY: THE EL NIÑO SOUTHERN OSCILLATION (ENSO)

The El Niño Southern Oscillation (ENSO) phenomenon is observed in the modern tropical Pacific Ocean. The tropical atmospheric winds have an important influence on the tropical Pacific SST through oceanic upwelling along the equator (e.g., Trenberth, 1997a). El Niño (the Child Jesus; Philander, 1990) was the original name for a warm ocean current that ran southward along the coast of Peru during Christmas time. Now, it applies to the more extensive anomalous ocean warming in the central-eastern Pacific Ocean that triggers anomalous global climate patterns (Philander, 1990). La Niña is the opposite phase of El Niño and is characterized by strong easterly winds over the tropical Pacific Ocean, and anomalously cold eastern Pacific SST due to stronger upwelling of cold deep ocean water. The fluctuation of the modern tropical Pacific ENSO phenomenon repeats in 3-6 years cycles (e.g., Trenberth, 1997a).

The coupled model does indeed give rise to such interannual variability in both oceans that is analogous to the modern ENSO. Representative maps of Ordovician SST for La Niña and El Niño events are shown in Figure 3-3-1. Figure 3-3-1-a and -d are representative of El Niño-like events in the Panthalassic ocean and La Niña-like events in the Palaeo-Tethys ocean, respectively. Figure 3-3-1-b and -c are characteristic of El Niño-like events in the Palaeo-Tethys ocean and La Niña-like events in the Panthalassic ocean, respectively.

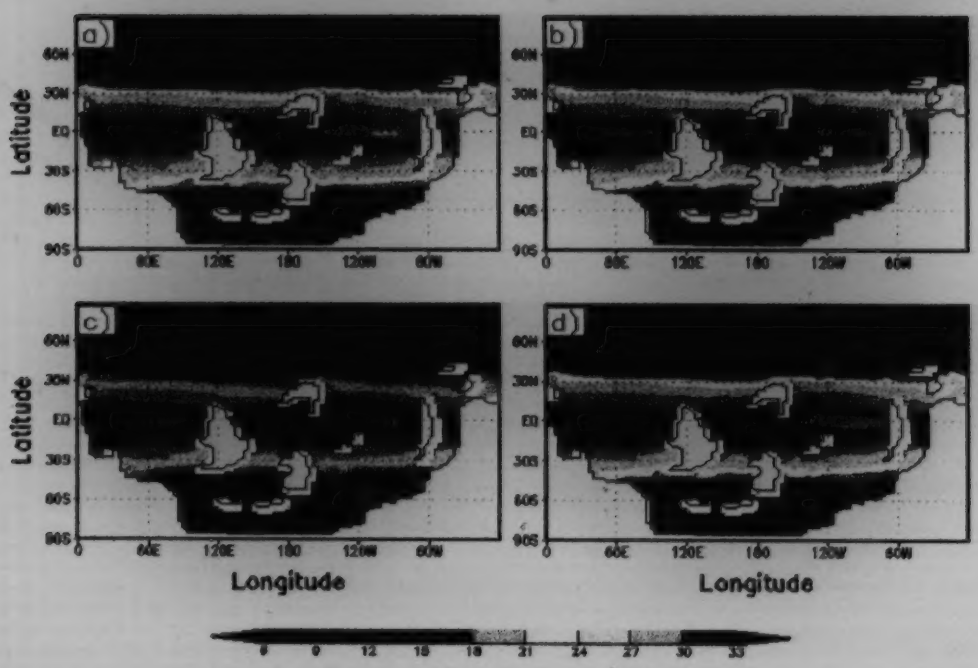

Figure 3-3-1. Maps of the mean sea surface temperature for a) 20-22 years average, b) 24-26 years average, c) 48-52 years average, and d) 53-57 years average of the late Ordovician simulation with function of longitude and latitude. The shaded colour interval is 3 °C.

The areas of significant SST change are defined as the ENSO regions, such as the Panthalassic region as 5N-5S, 80-100E, Palaeo-Tethys region as 5N-5S, 130-110W from the Ordovician simulations, and Pacific region as 5N-5S, 170-120W (Trenberth and Stepaniak, 2001) from the present simulations. The intensity of ENSO from the stated regions is demonstrated by using the deviation of SST in regions, with monthly SST means subtracted from normalized mean of SST as ENSO indices. Normalized ENSO indices are calculated from the

deviation of SST in regions divided by the standard deviation. Figure 3-3-2 shows ENSO indices using 5 months running means, which purpose is for smoothing out the intraseasonal variations as a function of time. The duration of ENSO indices are 15-64 years of the Ordovician simulations and 15-62 years of the present simulation. Trenberth (1997b) defined ENSO events with positive and negative anomaly values exceeding thresholds of ±0.4°C for 6 months or more.

There are 2 interesting results from the simulation. One is that the duration of the Ordovician ENSO-like events are longer than the modern ENSO. Yah *et. al.* (2006) and Bush (2006) simulated doubling atmospheric CO_2 levels in different climate system models to analyze the changes of ENSO amplitude and period. Both studies concluded that with higher atmospheric CO_2, the amplitude of ENSO becomes greater and events last longer. A second notable point is that the Panthalassic and Palaeo-Tethys oceans have ENSO cycles anti-phased such that when one basin is in an El Niño state the other is in a La Niña state. A similar relationship is observed between the modern Pacific and Atlantic oceans, although Handoh *et. al.* (2006) hypothesize that the Atlantic ENSO events appear to be a passive response to Pacific ENSO forcing. Changes in the easterly trade winds and latent heat flux from the Pacific Ocean controls the Atlantic SST anomalies. The Panthalassic and Palaeo-Tethys ocean ENSO-like events appear to be distinct and are closely related to the Walker circulations. When the Palaeo-Tethys is in a La Niña state and its Walker circulation is strong, the trade easterlies over the equatorial Panthalassic are weakened by increased surface convergence over the Palaeo-Tethys warm pool. This weakening of the

Panthalassic trade winds generates an El Niño state in that basin. A similar argument applies for the other phase of Ordovician interannual variability. The annual cycle in the tropics of the Ordovician simulation is more pronounced than today (as evident in Figure 3-3-2). Reasons for this are not clear but are likely to be related to the continental distribution and its interaction with seasonal radiation. Ordovician ENSO cycles appear to be very long-lived but very infrequent compared to today. This result is consistent with the trend towards less frequent but longer-lasting ENSO cycles in a climate with doubled atmospheric carbon dioxide (Bush, 2006).

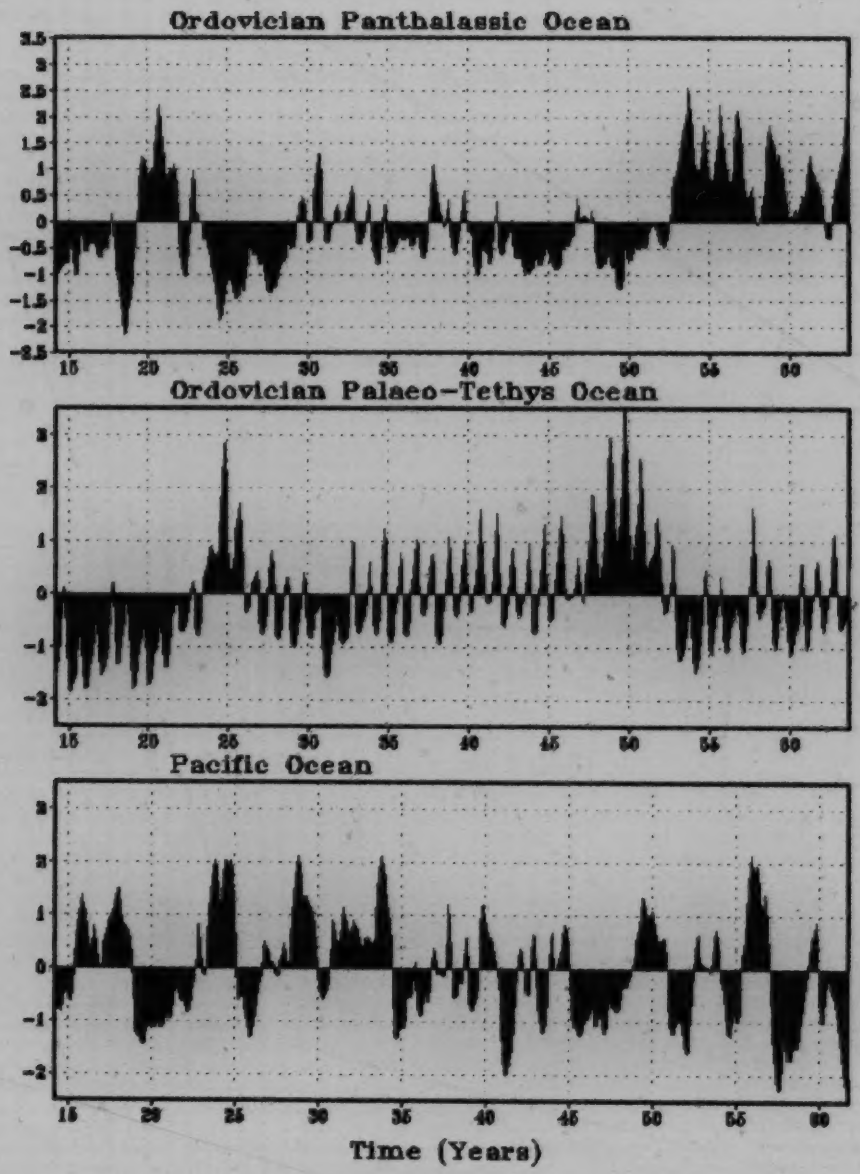

Figure 3-3-2. ENSO index for a) the Panthalassic ocean, b) the Palaeo-Tethys ocean and c) the Pacific ocean. High amplitude red and blue colours indicate El Niño and La Niña respectively.

3-4. PRECIPITATION

The simulated precipitation maps (Figure 3-4-1) demonstrate the influence of the Hadley and Walker circulations on regional precipitation. Annual mean precipitation in the Ordovician simulation from the equator to 10S (Figure 3-4-1-a) is higher than in higher latitudes. The Ordovician JJA and DJF averaged precipitation show seasonal fluctuations of the ITCZ (Figure 3-4-1-c and 3-4-1-e). Precipitation is greatest under the convective branches of the two Walker circulations, which occur over the two western "warm pools" of high SST. When the Palaeo-Tethys ocean Walker circulation is larger and stronger during JJA, higher precipitation rates are simulated over ~120E. The global annual mean precipitation for the Ordovician and for the present day simulations are 1.04m/year and 0.93m/year, respectively, so there is a ~12% increase in the warmer climate. The average rainfall in mid-latitudes (~45N) in the Ordovician (0.3 cm/d) is also higher than the present day (0.24cm/d). This implies that synoptic eddies in the warmer climate generate ~25% more precipitation and release more latent heat, a result consistent with climate predictions for increased CO_2 (Boer *et. al.*, 1992). Under the higher precipitation regions (~40-60 degrees North and South latitude), the regional salinity is lower because of fresh water input (cf. Figure 3-2-2-a) and this exerts a partial control over the midlatitude ocean circulation.

Figure 3-4-2 shows the zonal mean rates of precipitation (cm/day) as a function of latitude. The equatorial peak of the annual mean precipitation for the

Ordovician (Figure 3-4-2-a) is further from the equator than the modern equatorial peak (Figure 3-4-2-b) because the Ordovician ITCZ is shifted into the southern hemisphere. The Ordovician annual mean and JJA average of the equatorial precipitation peaks are higher than the present day (Table 3-4-1). These imply that the latent heat release is increased and the poleward heat flux is stronger in mid-latitudes, especially in the northern hemisphere where the Ordovician jet stream is very strong.

	45N	Equator	45S
Ordovician	0.368618	0.632594	0.300591
Present	0.249675	0.49005	0.29912

Table 3-4-1. Annual mean precipitation (cm/day) at mid-latitudes (45N and 45S) and the equator for the Ordovician and the present day.

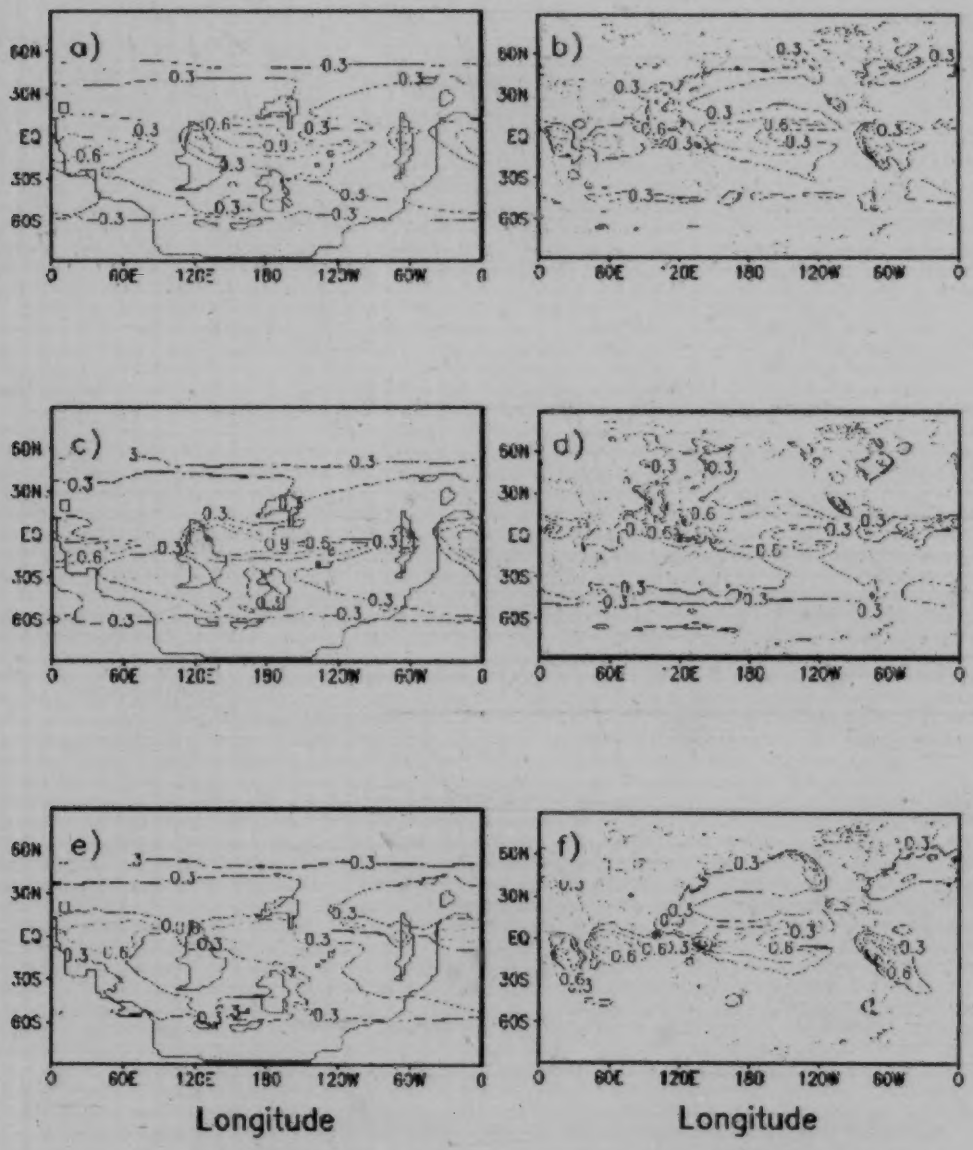

Figure 3-4-1. Spatial distribution of the annual mean precipitation (cm/day) for (a) the Ordovician and (b) the present day. JJA averages are shown in (c) and (d), and the DJF averages in (e) and (f) as the Ordovician and the present day respectively. Contour intervals are 0.3, 0.6, 1, 1.4, and 1.8

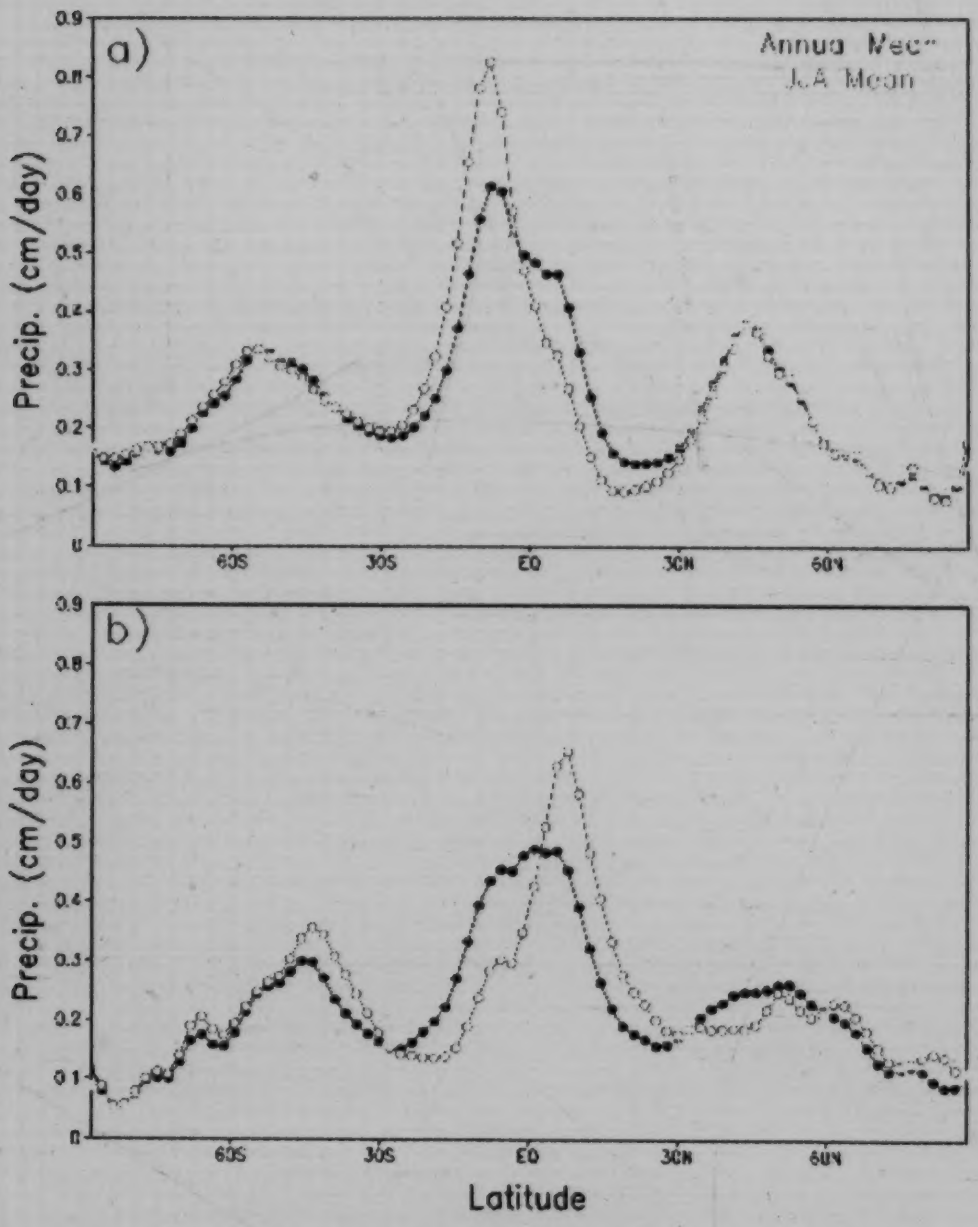

Figure 3-4-2. Zonal mean precipitation rate (cm/d) for (a) the Ordovician and (b) the present day. In each panel are shown the annual mean, (solid circle), the JJA (open circles), and the DJF mean (crosses).

3-5. HEAT TRANSPORT

The net poleward heat transport in the climate system is completed by both the atmosphere and the ocean with the atmosphere transporting most of the heat in the modern climate (Trenberth and Caron, 2001). However, in the northern hemisphere of the Ordovician there are no continents and hence no oceanic western boundary currents to transport heat poleward. Oceanic flow is therefore primarily zonal and most of the heat transport is done by the synoptic eddies generated by the strong atmospheric jet stream. The net poleward heat flux in the atmosphere as a function of latitude is shown in Figure 3-5-1 and displays the distinct rise in atmospheric heat transport in the northern hemisphere. As a comparison, the southern oceanic poleward heat transport becomes higher where the stronger eastern boundary currents are (Figure 3-2-2-b).

There are significant differences between the heat fluxes of the Ordovician and the present day climates. The simulated atmospheric heat transport demonstrates large negative heat fluxes at 12S and 15N associated with the tropical Hadley cells (Figure 3-1-19-a) which carry warmer air equatorward. Southern hemisphere heat fluxes from the present day simulation are stronger (about 35-60 Kms^{-2} stronger) because of the stronger southern midlatitude jet and Ferrell cell (cf. Figures 3-1-15 and 3-1-19). In the simulated Ordovician heat fluxes are stronger (~110 Kms^{-2} more) than the present day in the northern hemisphere because of enhanced midlatitude baroclinic eddy activity arising from the stronger jet stream (cf. Figure 3-1-15).

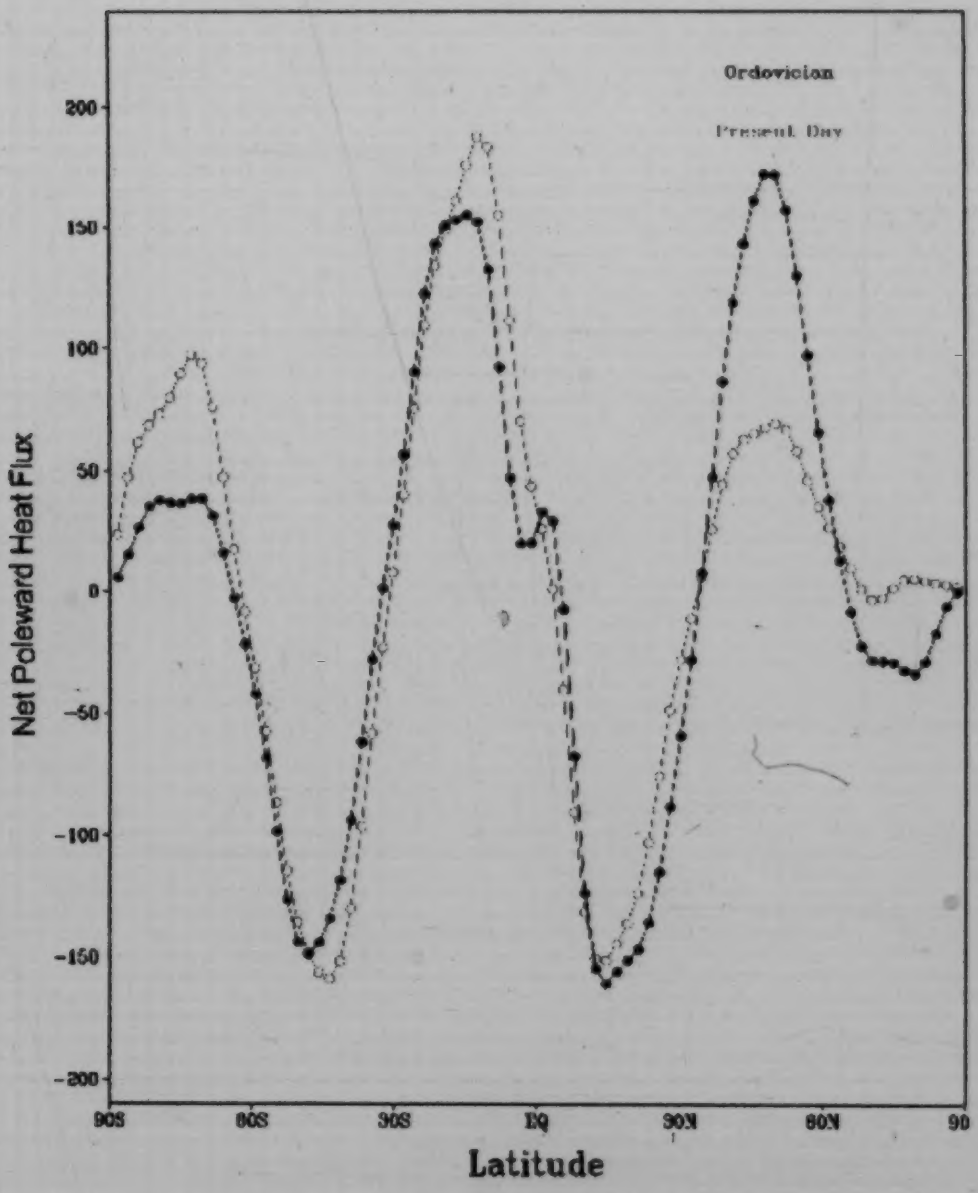

Figure 3-5-1. Annual mean, zonally and vertically averaged atmospheric poleward heat flux for the Ordovician (solid circle) and the present day (open circle). The unit for total heat flux is Kelvin per meter per second ($°Kms^{-1}$).

3-6. ORDOVICIAN MONSOONS

The Monsoon is a seasonal wind driven by the thermal contrast between landmasses and the surrounding oceans. For example, the temperature above the modern Indian landmass increases during JJA whereas temperature over the Indian ocean does not increase as much. This generates the horizontal temperature/pressure gradients that produce the monsoon winds which blow from the coast of Africa to the coast of China (Figure 3-6-1-b). The south Asian monsoon over the Indian ocean is simulated for the present day (Figure3-6-2-d) as is the summer monsoon over west Africa (Figure 3-4-1-f). The maximum local precipitation in the modern monsoon is over 2.2cm/d during JJA.

In comparison, the Ordovician climate exhibits equinox monsoon flows over both equatorial Gondwana and Laurentia (Figure 3-6-1-a; continental monsoons) with March-April-May (MAM) precipitation exceeding 1. cm/d over E. Laurentia to Palaeo-Tethys ocean (Figure 3-6-2-a). When the Ordovician equatorial continents become hot, which is twice a year at the equinoxes, monsoon flow is generated. The Gondwana equatorial monsoon is stronger than the Laurentia monsoon because of the larger landmass of Gondwana, where temperatures can exceed 315°K. Therefore the magnitude of the pressure gradients becomes higher and the monsoon wind above Gondwana is stronger. There are relatively higher rainfall rates (above 1.2 cm/d) over the region on Gondwana where near surface temperature exceeds 309°K. The Ordovician annual mean sea surface salinity under the Ordovician monsoon regions is

relatively low (34.5 practical salinity unit (PSU; cf. Figure 3-2-2-a) because of the intense seasonal precipitation. In the modern Indian monsoon (Figure 3-4-1-b) precipitation is high because of orographic precipitation induced by the Himalayas. The maximum Gondwana and Laurentia monsoon precipitations are nevertheless comparable to the modern monsoon precipitation. Despite the lack of topographic forcing in the Ordovician simulation, peak precipitation rates are comparable to today. If topography existed in these monsoon regions then precipitation rates would be expected to be much greater than today. In this sense, I can conclude that the Ordovician monsoons were much stronger than today's. Similar large scale summer and winter monsoons, "mega-monsoons", were demonstrated by Kutzbach and Gallimore (1989) along the Tethyan coasts of Pangea from Late Permian to Early Jurassic (250-200 Ma) simulation.

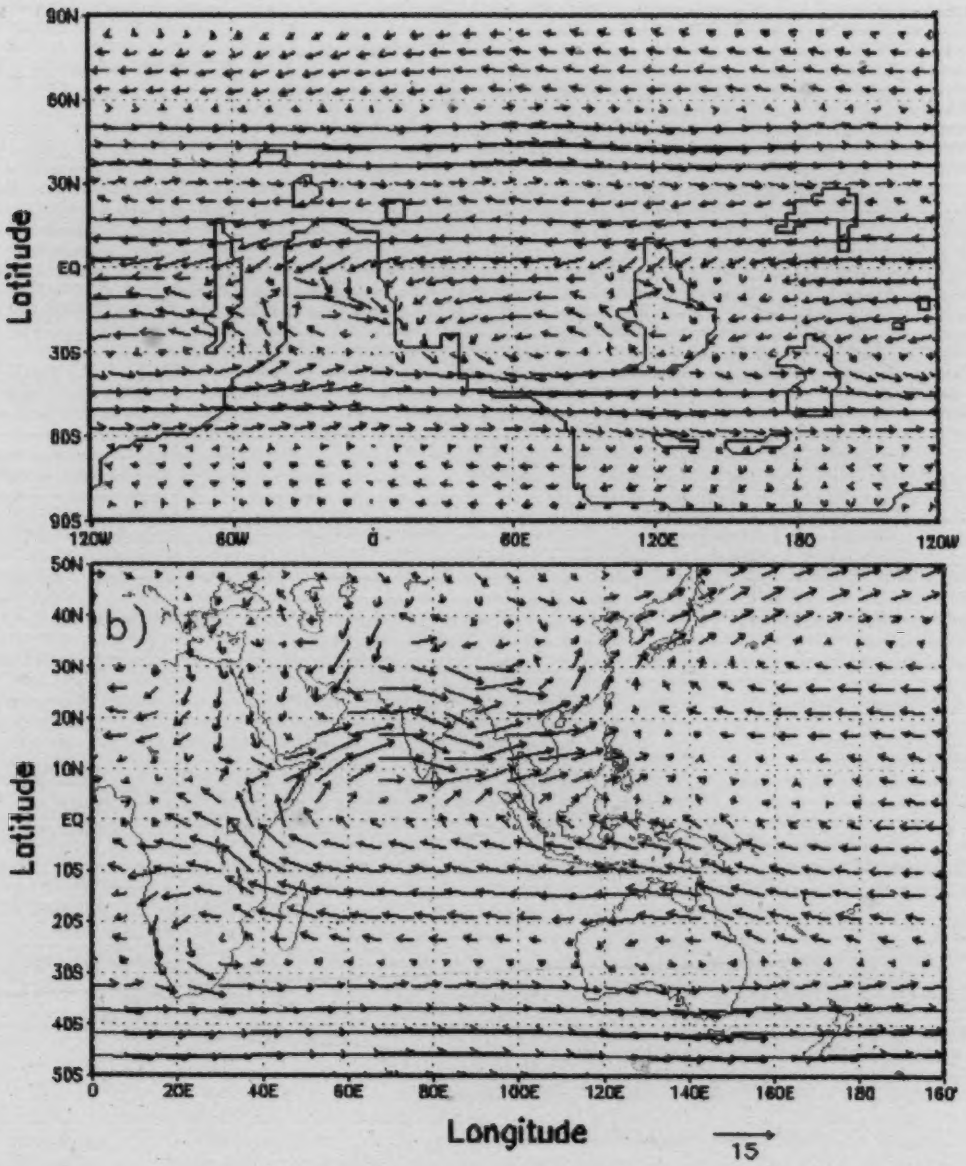

Figure 3-6-1. MAM horizontal winds in (a) the Gondwana and Laurentia monsoons and JJA horizontal winds in (b) the modern south Asian monsoon regions. The vertical level is the σ=0.866 surface (lower troposphere). Velocity vectors are scaled in both panels in m/s as indicated in the bottom right.

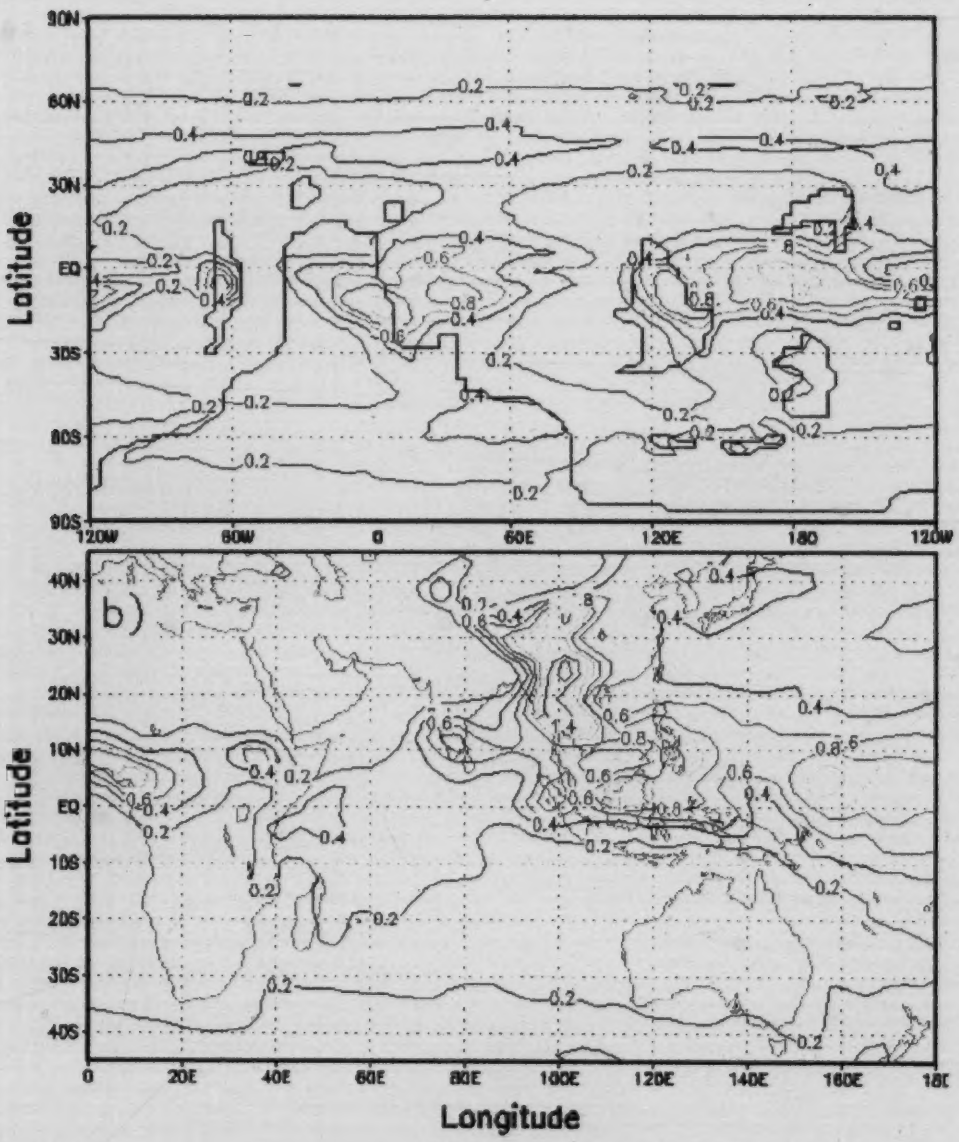

Figure 3-6-2 MAM Precipitation in the monsoon region for (a) the Ordovician and JJA precipitation in the monsoon region for (b) the present day. The contour interval is 0.2 cm/d.

3-7. Permanent Continental Ice

The simulated atmosphere in southern high latitudes has seasonal snow but no permanent snow indicated from a year round snow accumulation. The simulated annual mean snow accumulation is shown in Figure 3-7-1-a. The major snow accumulation is on S. Gondwana where maximum snowfall locally exceeds 18 cm water equivalent during JJA (boreal summer; Figure 3-7-1-c). Even Figure 3-7-1-b and –c have DJF (boreal winter) and JJA (boreal summer) averaged snow accumurations at the south pole, which are included in the unstable duration of the coupled simulations (1-15 years). Also, this coupled simulation did not exhibit even a single year round of snow accumulations (there are at least a couple of months free of snow per year).

Permanent sea ice was not simulated although there is seasonal sea ice during JJA in the northern hemisphere (Figure 3-7-2-a). However it is quite thin compared to modern sea ice (Figure 3-7-2-b). Moreover, in the northern hemisphere sea ice was simulated in the earlier years (up to 15 years) of the Ordovician simulations and as time progressed the northern hemisphere became free of sea ice world as well as the southern hemisphere, which was sea ice free through all of the 65 years of coupled model simulations. Therefore even where there is sea ice formation in the northern hemisphere (Figure 3-7-2-a), it is not accepted as permanent ice.

Although the coupled model used in this study does not transform snow into ice, and thus there can be no buildup of continental ice, permanent snow

cover can nevertheless be used as a proxy for ice build up. However below freezing temperatures do not persist through a year given the strong seasonal cycle over Gondwana and hence the initiation of glacial buildup is precluded since snow completely melts seasonally. I can therefore conclude that, since a relatively low value of CO_2 was used here, orbital parameters must have played a primary role in triggering the Late Ordovician glaciations.

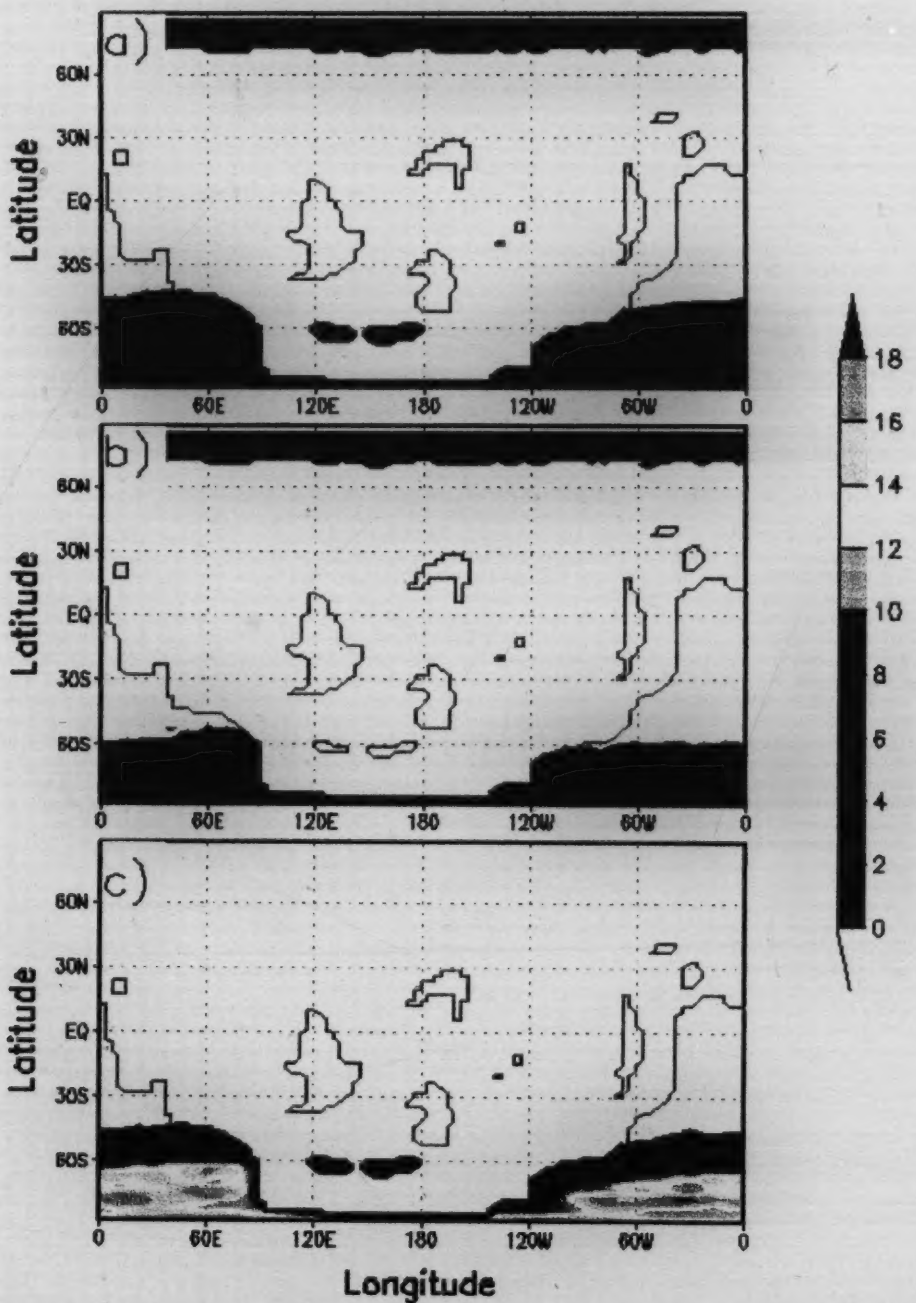

Figure 3-7-1 Spatial distribution of the Ordovician snow accumulation in cm of water equivalent. The annual mean is shown in (a), DJF (boreal winter) average in (b), and the JJA (boreal summer) averages in (c). Contour intervals are 2 cm.

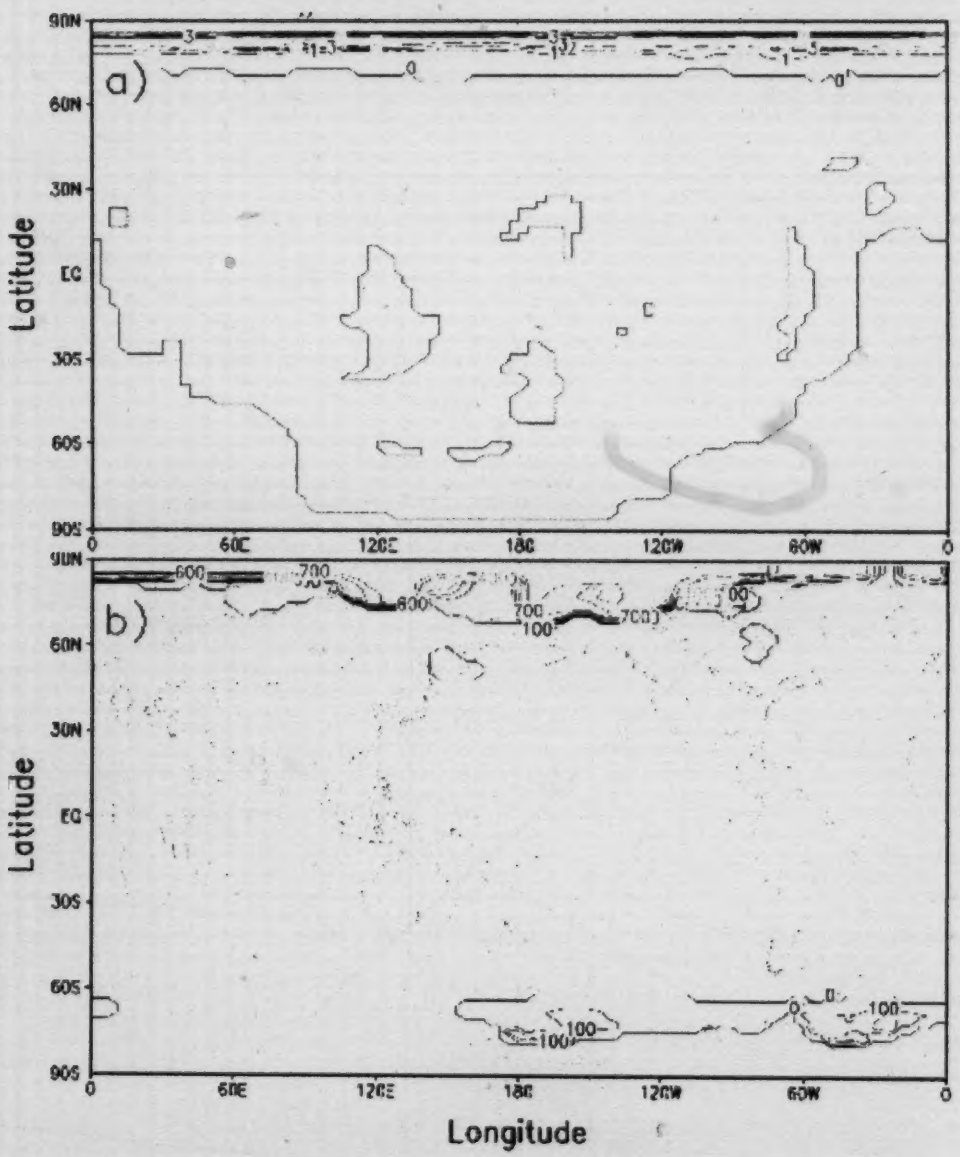

Figure 3-7-2. DJF averaged sea ice thickness for (a) Ordovician and (b) the present day. The contour intervals are 1 cm for (a) and 100 cm for (b).

4. DISCUSSION AND CONCLUSIONS

4-1. CORRELATION BETWEEN THE MODELING RESULTS AND GEOLOGICAL AND PALAEONTOLOGICAL EVIDENCE

Most of the trilobites and brachiopods used in constructing Figure 1-4 were found in the tropical region of the Ordovician (with a few exceptions). The simulated annual mean near surface atmospheric temperature in the southern high latitudes is lower than the freezing point, thereby precluding most higher forms of life at that location. *Ampyxina* (trilobites) favoured the tropical oceans with SST over 27°C. A few exceptions were found on the continental shelf of Baltica where simulated SST is 18-21°C and also in the shallow ocean north of Avalonia where simulated SST is almost 3°C. *Calyptaulax* trilobites also favoured the tropical oceans where SST is over 24°C, though there are a couple of exceptions found in Avalonia (SST 0°C). *Panderia* trilobites are more commonly found in the sub-tropical realm with SST 3-21°C although an exception has been found from the shallow waters of the Gondwana continental shelf where SST reached 27-30°C. *Carolinites*, trilobites, however, are the most tolerant to ranges of SST because they have been found in regions where simulated SST ranged between 0 and 30°C Trilobites found in Avalonia may have had a greater tolerance for seasonal cycle fluctuations since the simulated amplitude of the seasonal cycle around Avalonia is up to 25 degrees.

Brachiopods listed in the map of Figure 1-4-b are generally tolerant to

tropical and subtropical SST, although some were located in the higher latitude regions in the southern hemisphere where SST could drop below 3°C.

The ocean currents simulated for the southern hemisphere (Figure 4-1-1) are likely to have helped transport brachiopods (benthic), and trilobites (many of them are benthic; Figure 1-4) to different realms as Cocks and Fortey (1990) hypothesized. The ocean circulation delivered by the numerical simulation is therefore consistent with the idea that the observed faunal distribution is linked to ocean circulation.

Pacific graptolite faunas are less tolerant to SST changes, and likely could not adapt to the colder temperatures at the end of the Ordovician (Clarkson, 1986). The Atlantic graptolite faunas are believed to have migrated to the equatorial regions from the colder high latitudinal realms (Clarkson, 1986). Ordovician graptolites are found in the region between 30 N and 3S (Clarkson, 1986), where the simulated temperature is warm and the seasonal cycle has a lower magnitude. The simulated results suggest that the Walker circulation increased ocean upwelling in the eastern half of both ocean basins, leading to two semi-permanent cold regions from most of which graptolite recovery would therefore be unlikely. The graptolites that survived the Ordovician glaciation are Glyptograptidae and Diplograptidae (2 rows of theca and 1 stipe) but were subsequently replaced by monograptidae (1 row of thecae and 1 stipe) in the Silurian (Clarkson, 1986).

Bulman (1971) documented the early appearance of *Glyptograptus austrodentatus* graptolites in eastern Avalonia (earlier England; Atlantic faunal

provinces), though this is ambiguous because of the planktonic life mode. However, their palaeogeographic dispersions were influenced by ocean currents and they were transported to Avalonia, Baltica, and Gondwana (Figure 4-1-1). It is concluded that the ocean circulation delivered by the numerical simulation is consistent with the idea that observed faunal distribution is linked to ocean circulation.

The wind circulation of the Ordovician with flat topography (cf. Figure 3-5-1) was different from the present day primarily because of the distribution of the continents. Topography would not have affected northern hemisphere wind circulation because of the lack of continents. However, the end of the Ordovician is documented as being the first step of Appalachian mountain building (Windley, 1995), and crude estimates of Late Ordovician topography have been suggested (Scotese, 2001; Golonka, 2000). If this topography were used in the simulation, temperatures, wind circulations, and precipitation would be affected in those regional areas that had high topography. Nevertheless, the change in the simulated global mean general circulation between the Ordovician and today are likely to be robust as a first approximation.

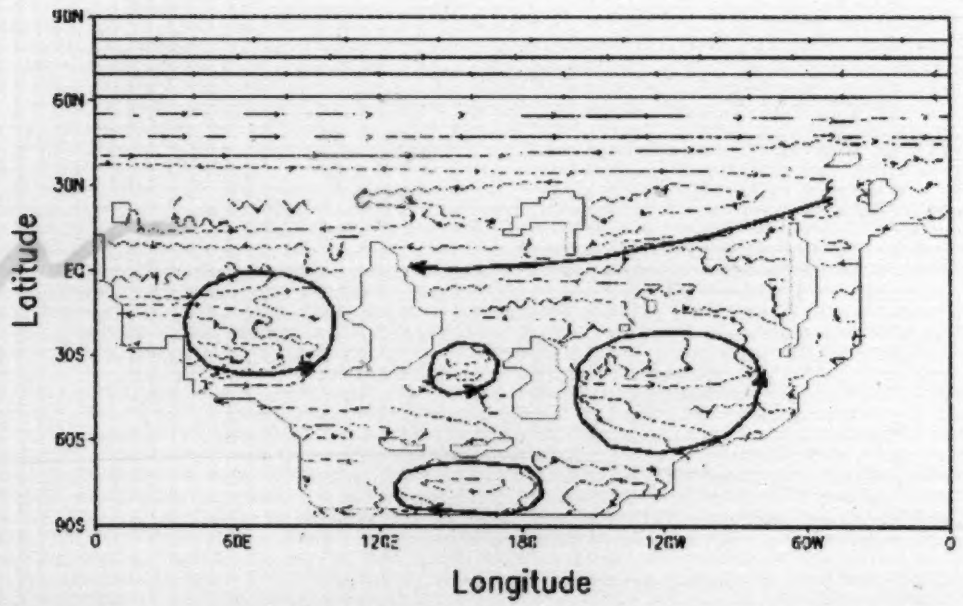

Figure 4-1-1. The southern hemisphere ocean currents. Bold arrows show the direction of current flows schematically.

The global temperature of late Ordovician climate is about 5°K higher than the present day through a combination of greatly enhanced CO_2 tempered by a reduced solar constant. Both atmospheric and oceanic tropical zones of the Ordovician are expanded poleward by about 10°-15° with consequences for marine biota habitats. Simulated temperatures in higher latitudes of the Ordovician are not as cold as the present day but can drop below freezing. Lack of permanent snow and ice sheets at the poles (unlike Antarctica and Greenland today) lead to high latitude warming of the Ordovician. The warmer Ordovician climate exhibits increased latent heat release in midlatitude synoptic events as well as over the two large western warm pools. Therefore the global annual average of the late Ordovician precipitation is ~12% more than the present day.

This decreases the regional salinity of the ocean under the Laurentia and Gondwana monsoon regions. Two zonal bands of high salinity (35-35.5 PSU) exist underneath the descending branches of the Hadley circulation.

The ocean circulation is strongly influenced by the atmospheric circulation. The jet stream and vertical atmospheric circulation are stronger even though the temperature gradients of the lower troposphere in the Ordovician are reduced. Therefore the strength of the ocean circulations is increased.

The South Pole seasonal cycle in the Ordovician is comparable with the modern seasonal cycle in the high latitude northern continental regions. Southern Gondwana temperatures drop below the freezing point during winter but the snow accumulation does not last through the antarctical summer months. Oceanic poleward heat transport is higher in the southern hemisphere where boundary currents exist. None of the above supports the formation of permanent snow and ice at the South Pole with this climate configuration. Considering the configuration of this simulation, I can conclude that the higher atmospheric CO_2 level and the lower luminosity are not sufficient conditions to induce the late Ordovician glaciation. At present, ice sheets are simply prescribed in GCMs. If ice sheets were introduced to this coupled model as an initial condition in a future study, the ice-albedo feedback would likely lower the atmospheric temperatures in Southern high latitudes such that permanent snow accumulation would occur. Other future studies of Late Ordovician climate also need to address the impact of orbital forcing on glacial inception in a series of coupled model sensitivity tests since both the atmospheric and oceanic heat transports will be affected and it may be the case that an altered orbit is the necessary condition

for glacial inception.

Nevertheless, the warmer simulated climate does correlate with the limited geological and palaeontological evidence. The simulations presented here show that there are new and interesting coupled atmosphere-ocean climatic phenomena, such as vast monsoons and ENSO-like events, that were likely in operation during the Late Ordovician. The higher atmospheric temperature over Ordovician continents drives the very strong Ordovician monsoons, thereby reducing ocean salinity regionally and influencing ocean currents and oceanic habitats. The Ordovician monsoons would be expected to be much stronger than the modern south Asian monsoon if high equatorial topography was introduced. Although the temporal resolution of any Ordovician proxy records precludes identifying interannual variability, the consistent dynamics simulated within the model make it highly likely that they did in fact occur and that biota living in the equatorial region suffered through infrequent but very long-lived ENSO events. These results for the Ordovician monsoons and ENSOs are new and are unique to the coupled atmosphere-ocean system that was simulated here.

REFERENCES

Barnes, C.R., and Zhang X., 1999. Pattern of conodont extinction and recovery across the Ordovician-Silurian boundary interval. ACTA UNIVERSITATIS CAROLINAE, GEOLOGICA 43, 211-212.

Barnes, C.R. 1999. Paleoceanography and paleoclimatology: an Earth system perspective. CHEMICAL GEOLOGY 161, 17-35.

Berner, R.A., 1994. 3GEOCARB II: A revised model of atmospheric CO_2 over Phanerozoic time. AMERICAN JOURNAL OF SCIENCE 294, 56-91.

Berner, R.A., 1998. The carbon cycle and CO_2 over Phanerozoic time: the role of land plants. PHILOSOPHICAL TRANSACTIONS OF THE ROYAL SOCIETY, SERIES B 353, 75-82.

Boer, G.J., McFarlane, N.A., and Lazare, M., 1992. Greenhouse gas induced climate change simulated with the CCC 2ned – generation general circulation model, JOURNAL OF CLIMATE 5(10), 1045-1077.

Brenchley, P.J., and Newall, G, 1980. A facies analysis of Upper Ordovician regressive sequences in the Oslo region, Norway – A record of glacio-eustatic changes. PALAEOGEOGRAPHY, PALAEOCLIMATOLOGY, PALAEOECOLOGY 31, 1-38.

Brenchley, P.J., and Newall, G, 1984. Late Ordovician environmental changes and their effect on faunas. In: Aspects of the Ordovician System, Bruton, D.L., (ed), University of Oslo, Oslo, Norway. 65-79 pp.

Brenchley, P.J., Marshall, J.D., Carden, G.A.F., Robertson, D.B.R., Long, D.G.F., Meidla, T., Hints, L., and Anderson, T.F, 1994. Bathymetric and isotopic evidence for a short-lived Late Ordovician glaciation in a greenhouse period. GEOLOGY 22, 295-298.

Brenchley, P.J., Marshall, J.D., and Underwood, C.J., 2001. Do all mass extinctions represent an ecological crisis? Evidence from the Late Ordovician. GEOLOGICAL JOURNAL 36, 329-340.

Brenchley, P.J., Carden, G.A., Hints, L., Kaljo, D., Marchall, J.D., Martma, T., Meidla, T., Nolvak, J., 2003. High-resolution stable isotope stratigraphy

of Upper Ordovician sequences: Constraints on the timing of bioevents and environmental changes associated with mass extinction and glaciation. GEOLOGICAL SOCIETY OF AMERICA BULLETIN 115 (1), 89-104

Bryan, K., 1969. A numerical method for the study of the circulation of the World Ocean. JOURNAL OF COMPUTATIONAL PHYSICS 4, 347-376.

Bulman, O.M.B., 1971. Graptolite faunal distribution. In: Middlemiss, F.A., Rawson, P.F., and Newell, G., (eds), Faunal provinces in space and time. The Seel House press, Liverpool, 236 pp.

Bush, A.B.G, and Philander, S.G.H., 1997. The late Cretaceous: Simulation with a coupled atmosphere-ocean general circulation model. PALEOCEANOGRAPHY 12 (3), 495-516.

Bush, A.B.G., and Philander, S.G.H., 1999. The climate of the Last Glacial Maximum: Results from a coupled atmosphere-ocean general circulation model. JOURNAL OF GEOPHYSICAL RESEARCH – ATMOSPHERES 104 (D20) 24509-24525.

Bush, A.B.G., 2006. Extra-tropical influences on the El Nino Southern Oscillation through the Late Quaternary. JOURNAL OF CLIMATE, in press.

Caputo, M.V., 1998. Ordovician-Silurian glaciations and global sea-level changes. NEW YORK STATE MUSEUM BULLETIN 491, 15-25.

Clarkson, E.N.K., 1986. Invertebrate palaeontology and evolution. Chapman & Hall, London, 434 pp.

Cocks, L.R.M., and Fortey, R.A., 1990. Biogeography of Ordovician and Silurian faunas. In: Scotese, C.R., and McKerrow, W.S., (eds), Palaeozoic Palaeogeography and Biogeography, GEOLOGICAL SOCIETY MEMOIR No.12, 97-104.

Cocks, L.R.M., 2001. Ordovician and Silurian global geography, JOURNAL OF THE GEOLOGICAL SOCIETY 158, 197-21.

Coorough, P.J., 1986. Brachiopod provinciality in the Late Ordovician-Early

Silurian. MSc Thesis. University of Wisconsin, Milwaukee.

Cox, M.D., 1984. A primitive equation three-dimensional model of the ocean. GFDL Ocean Group Technical Report No. 1, Geophysical Fluid Dynamics Laboratory / NOAA, Princeton University, Princeton 250 pp.

Crowley, T.J., and Baum, S.K., 1995. Reconciling Late Ordovician (440 Ma) glaciation with very high (14X) CO_2 levels. JOURNAL OF GEOPHYSICAL RESEARCH 100 (D1), 1093-1101.

Crowley, T.J., and North, G.R., 1991. Palaeoclimatology. Oxford University Press, Oxford, 349 pp.

Doty, B.E. and Kinter III, J.L., 1995. Geophysical Data Analysis and Visualization using GrADS. In: Visualization Techniques in Space and Atmospheric Sciences. E.P. Szuszczewicz and J.H. Bredekamp, (eds), NASA, Washington, D.C., 209-219.

Endal, A.S., and Schatten, K.H., 1982. The faint young sun – Climate paradox – Continental influences. JOURNAL OF GEOPHYSICAL RESEARCH–OCEANS AND ATMOSPHERES 87 (NC9), 7295-7302.

Fortey, R.A., and Cocks, L.R.M., 2005. Late Ordovician global warming-The Boda event. GEOLOGY 33 (5), 405-408.

Frakes, L.A., Francis, J.E., Syktus, J.I., 1992. Climate modes of the Phanerozoic. Cambridge University Press, Cambridge, 274pp.

Golonka, J., 2000. Cambrian-neogen : plate tectonic maps. Wyd 1 – Krakow b Wydawn, Uniwersytetu Jagiello/nskiego, 1-125 (36 plates). http://www.dinodata.net/Golonka/Golonka.htm.

Gordon, C.T., and Stern, W., 1982. A description of the GFDL global spectral model. MONTHLY WEATHER REVIEW 110, 625-644.

Gibbs, M.T., Barron, E.J., and Kump L.R., 1997. An atmospheric PCO_2 threshold for glaciation in the late Ordovician. GEOLOGY 25, 447-450.

Gibbs, M.T., Bice, K.L., Barron, E.J., and Kump, L.R., 2000. Glaciation in the early Paleozoic "greenhouse"; the roles of palaeogeography and atmospheric CO_2. In: Huber, T., MacLeod, K.G, and Wing, S.L., (eds),

Warm Climates in Earth History. Cambridge University Press, Cambridge, 386-422pp.

Hahn, D.G., and Manabe, S., 1975. The role of mountains in the south Asian monsoon circulation. JOURNAL OF THE ATMOSPHERIC SCIENCES 32(8), 1515-1541.

Hallam, A., 1994. An outline of Phanerozoic biogeography. Oxford University Press, Oxford, 246 pp.

Handoh, I.C., Matthews, A.J., Bigg, G.R., and Stevens, D.P., 2006. Interannual variability of the tropical Atlantic independent of and associated with ENSO'Part I. The North Tropical Atlantic. INTERNATIONAL JOURNAL OF CLIMATOLOGY, in press.

Harland, W.B., Armstrong, R.L., Cox, A.V., Craig, L.E., Smith, A.G., and Smith, D.G., 1990. A Geological Time Scale, 1990 edition, Cambridge university press, Cambridge, 263 pp.

Harper, D.A.T., and Owen, A.W., 1996. Fossils of the upper Ordovician. The Palaeontological Association, Field guides to fossils: no. 7., London, 312 pp.

Herrmann, A.D., and Patzkowsky, M.E., 2003. Obliquity forcing with 8-12 times preindustrial levels of atmospheric pCO_2 during the late Ordovician glaciation. GEOLOGY 31(6), 485-488.

Herrmann, A.D., Patzkowsky, M.E., and Pollard, D., 2004a. The impact of paleogeography, pCO_2, poleward ocean heat transport and sea level change on global cooling during the Late Ordovician. PALAEOGEOGRAPHY, PALAEOCLIMATOLOGY, PALAEOECOLOGY 206, 59-74.

Herrmann, A.D., Haupt, B.J., Patzkowsky, M.E., Seidov, D., and Slingerland, R.L., 2004b. Response of Late Ordovician paleoceanography to changes in sea level, continental drift, and atmospheric pCO_2: potential causes for long-term cooling and glaciation. PALAEOGEOGRAPHY, PALAEOCLIMATOLOGY, PALAEOECOLOGY 210, 385-401.

Kim, H.K., and Lee, S., 2001. Hadley cell dynamics in a primitive equation

model. Part II: Nonaxisymmetric flow. JOURNAL OF THE ATMOSPHERIC SCIENCES 58(19), 2859-2871.

Kutzbach, J.E., and Gallimore, R.G., 1989. Pangean climates: megamonsoons of the megacontinent. JOURNAL OF GEOGHYSICAL RESEARCH 94(D3), 3341-3357.

Lambeck, K., Esat, T.M., and Potter, E.K., 2002. Links between climate and sea levels for the past three million years. NATURE 419, 199-206.

Lee, S., 1997. Maintenance of multiple jets in a baroclinic flow. JOURNAL OF THE ATMOSPHERIC SCIENCES 54(13), 1726-1738.

Levitus, S., and Boyer, T.P., 1994. World Ocean Atlas 1994: Temperature. U.S. Department of Commerce, National Oceanic and Atmospheric Administration, Washington, D.C., 117 pp.

Lowe, D., and Etheridge D., 2001. Antarctic ice: the world's air museum, NIWA, WATER & ATMOSPHERE 9(1), 22-23.

Manabe, S., and Holloway, J.L.Jr., 1975. The seasonal variation of the hydrologic cycle as simulated by a global model of the atmosphere. JOURNAL OF GEOPHYSICAL RESEARCH 80(12), 1617-1649.

Manabe, S., and Wetherald, R.T., 1975. The effect of doubling the CO_2 concentration on the Climate of a General Circulation Model. JOURNAL OF THE ATMOSPHERIC SCIENCES 32 (1), 3-15.

Marshall, J.D., Brenchley, P.J., Mason, P., Wolff, G.A., Astini, R.A., Hints, L., Meidla, T., 1997. Global carbon isotopic events associated with mass extinction and glaciation in the Late Ordovician. PALAEGEGOGRAPHY, PALAEOCLIMATOLOGY, PALAEOECOLOGY 132(1-4), 195-210.

McCormick, T., and Fortey, R.A., 1999. The most widely distributed trilobite species: Ordovician Carolinites genacinaca. JOURNAL OF PALEONTOLOGY 73(2), 202-18.

McFarlane, N., and Manzini, E., 1997. Parameterization of gravity wave drag in comprehensive models of the middle atmosphere. ADVANCES IN

SPACE RESEARCH 20(6), 1241-1251.

McKerrow, W.S., Dewey, J.F., and Scotese, C.R., 1991. The Ordovician and Silurian development of the Iapetus Ocean. In: Bassett, MG., Lane, PD., and Edwards, D., (eds), The Murchison Symposium: Palaeontological Association of London, SPECIAL PAPERS IN PALAEONTOLOGY 44, 165-178.

Molnar, G.I., and Gutowski, W.J., 1995. The faint young sun paradox – further exploration of the role of dynamical heat-flux feed backs in maintaining global climate stability. JOURNAL OF GLACIOLOGY 41, 87-90.

Nichols, G., 1999. Sedimentology and stratigraphy. Blackwell Science, Oxford, 355 pp.

Pacanowski, R.C., and Philander, S.GH., 1981. Parameterization of vertical mixing in numerical models of tropical oceans. JOURNAL OF PHYSICAL OCEANOGRAPHY 11, 1443-1451.

Pacanowski, R.C., Dixon, K., and Rosati, A., 1991. The GFDL modular ocean model user guide. GFDL Ocean Group Technical Report 2, NOAA/Geophysical Fluid Dynamics Laboratory, Princeton, NJ, 46 pp.

Palmer, A.R., and Geissman, J., 1999. Geological time scale. The Geological Society of America, Product code CTS004

Paris, F., Elaouad-Debbaj, Z., Jaglin, J.C., Massa, D., and Oulebsir, L., 1995. Chitinozoans and Late Ordovician glacial events on Gondwana, In: Ordovician Odyssey: Short papers for the 7th international symposium on the Ordovician system, Cooper, J.D., Drose, M.L., and Finney, S.L., (eds.), 171-176.

Petit, J.R., Jouzel, J., Raynaud, D., Barkov, N.I., Barnola, J.M., Basile, I., Bender, M., Chappellaz, J., Davis, M., Delaygue, G., Delmotte, M., Kotlyakov, V.M., Legrand, M., Lipenkov, V.Y., Lorius, C., Pepin, L., Ritz, C., Saltzman, E., & Stievenard, M., 1999. Climate and atmospheric history of the past 420,000 years from the Vostok ice core, Antarctica. NATURE 399, 429-436.

Philander, S.G, 1990. El Niño and La Niña, and the southern oscillation. San

Diego, Academic Press, 293pp.

Poussart, P.F., Weaver, A.J., and Barnes, C.R., 1999. Late Ordovician glaciation under high atmospheric CO_2: A coupled model analysis. PALEOCEANOGRAPHY 14, 542-558.

Qing, H., Barnes, C.R., Buhl, D., and Veizer, J., 1998. The strontium isotopic composition of Ordovician and Silurian brachiopods and conodonts' Relationships to geological events and implications for coeval seawater. GEOCHIMICA ET COSMOCHIMICA ACTA 62(10), 1721-1733.

Ronov, A.B., Khain, V.Y., and Balukhovskiy, A.N., 1980. A comparative estimate of volcanism intensity on continents. INTERNATIONAL GEOLOGY REVIEW 22(12), 1383-1389.

Ronov, A.B., Khain, V.E., and Seslavinskii, K.B., 1984. Atlas of litholigal-paleogeographical maps of the world: late Precambrian and Paleozoic of continents. Leningrad, Ministerstvo Geologii SSSR, 70 pp.

Royer, D.L., Berner, R.A., Montanez, I.P., Tabor, N.J., and Beerling, D.J., 2004. CO_2 as a primary driver of Phanerozoic climate. GEOLOGICAL SOCIETY OF AMERICA TODAY 14, 4-10.

Saltzman, M.R., and Young, S.A., 2005. Long-lived glaciation in the Late Ordovician? Isotopic and sequence-stratigraphic evidence from western Laurentia. GEOLOGICAL SOCIETY OF AMERICA 33 (2), 109-112.

Scotese, C.R., 1997. PALEOMAP Paleogeographic Atlas. PALEOMAP progress report 90, University of Texas Arlington, USA, 22 pp.

Scotese, C.R., 2001. Atlas of Earth History, Volume 1, Paleogeography, PALEOMAP Project, Arlington, Texas, 52 pp.

Scotese, C.R., 2002. http://www.scotese.com, (PALEOMAP website)

Scotese, C.R., Boucot, A.J., and McKerrow, W.S., 1999. Gondwanan palaeogeography and Palaeoclimatology. JOURNAL OF AFRICAN EARTH SCIENCES 28(1), 99-114.

Scotese, C.R., and McKerrow, W.S., 1990. Revised world maps and introduction. In: Scotese, CR., and McKerrow, WS. (eds), Palaeozoic Palaeogeography

and Biogeography, GEOLOGICAL SOCIETY MEMOIR 12, 1-12.

Scotese, C.R., and McKerrow, W.S., 1991. Ordovician plate tectonic reconstructions. In: Barnes, CR., Williams, SH. (eds), Advances in Ordovician Geology. CANADIAN GEOLOGICAL SURVEY PAPER 90, 271-282.

Sepkoski, J.J., 1981. A factor analytic description of the Phanerozoic marine fossil record. PALEOBIOLOGY 7, 36-53.

Sepkoski, J.J., 1998. Biodiversity: past, present and future. JOURNAL OF PALAEONTOLOGY 71, 533-539.

Sheehan, P.M., 2001a. History of marine biodiversity. GEOLOGICAL JOURNAL, 36, 231-249.

Sheehan, P.M., 2001b. The Late Ordovician mass extinction. ANNUAL REVIEWS OF EARTH PLANET SCIENCES 29, 331-364.

Sheehan, P.M., and Coorough, P.J., 1990. Brachiopod zoogeography across the Ordovician-Silurian extinction event. In: Scotese, CR., and McKerrow, WS. (eds), Palaeozoic Palaeogeography and Biogeography, GEOLOGICAL SOCIETY MEMOIR 12, 181-187.

Skinner, B.J., and Porter, S.C., 1987. Physical Geology. John Wiley and Sons, Inc., 750 pp.

Smit, J., 2006. Crises in the History of life and the record of large impacts. European Space Agency, First international conference on impact cratering in the solar system, ESTEC, Noordwijk, The Netherlands, S.12 – Catastrophes and extinctions, No. 306480.

Stormont, J.C., 2003. Evaluation of analytical models for surface temperature differences in Sun and shade with field data. http://www.unm.edu/~jcstorm/model.pdf

Sutcliffe, O.E., Dowdeswell, J.A., Whittington, R.J., Theron, J.N., and Craig, J., 2000. Calibrating the late Ordovician glaciation and mass extinction by the eccentricity of Earth's orbit. GEOLOGY 28, 967-970.

Sweet, W.C., 1990. The Conodonta: Morphology, Taxonomiy, Paleoecology and

Evolutionary History of a Long-Extinct Animal Phylum. Oxford, UK, Clarendon. 212 pp.

Trenberth, K.E., 1997a. Short-term climate variations: Recent Accomplishments and issues for future progress. BULLETIN OF THE AMERICAN METEOROLOGICAL SOCIETY 78(6), 1081-1096.

Trenberth, K.E., 1997b. The definition of El Niño. BULLETIN OF THE AMERICAN METEOROLOGICAL SOCIETY 78(12), 2771-2777.

Trenberth, K.E., and Caron, J.M., 2001. Estimates of meridional atmosphere and ocean heat transports. JOURNAL OF CLIMATE 14(16), 3433-3443.

Trenberth, K.E., and Stepaniak, D.P., 2001. Indices of El Niño evolution. JOURNAL OF CLIMATE 14, 1697-1701.

Villas, E., Vennin, E., Álvaro J.J., Hamman, W., Herrera, Z.A., and Piovano, E.L., 2002. The late Ordovician carbonate sedimentation as a major triggering factor of the Hirnantian glaciation. BULLETIN DE LA SOCIÉTÉ GÉOLOGIQUE DE FRANCE 173(6), 569-578.

Wang, K., Chatterton, B.D.E., and Wang, Y., 1997. An organic carbon isotope record of Late Ordovician to Early Silurian marine sedimentary rocks, Yangtze Sea, South China: Implications for CO_2 changes during the Hirnantian glaciation. PALAEOGEOGRAPHY, PALAEOCLIMATOLOGY, PALAEOECOLOGY 132, 147-158.

Wellman, C.H., and Gray, J., 2000. The microfossil record of early land plants. PHILOSOPHICAL TRANSACTIONS OF THE ROYAL SOCIETY OF LONDON SERIES B-BIOLOGICAL SCIENCES 355, 717-732.

Wellman, C.H., Osterloff, P.L., and Mohiuddin, U., 2003. Fragments of the earliest land plants. NATURE 425, 282-285.

Williams, G.E., 1991. Milankovitch-band cyclicity in bedded halite deposits contemporaneous with Late Ordovician – Early Silurian glaciation, Canning Basin, Western Australia. EARTH AND PLANETARY SCIENCE LETTERS 103, 143-155.

Windley, B.F., 1995. The evolving continents third edition. John Wiley and

Sons Ltd., England, 526 pp.

Yapp, C.J., and Poths, H. 1992. Ancient atmospheric CO_2 pressures inferred from natural goethites. NATURE 355, 342-344.

Yeh, S.W., Park, Y.G, and Kirtman, B.P., 2006. ENSO amplitude changes in climate change commitment to atmospheric CO_2 doubling. GEOPHYSICACL RESEARCH LETTERS 33, L13711.

Young, E.M., 2004. Modeling and field data analysis of frost penetration depth frost heave potential and soil erosion due to frozen ground in the flagstaff area. Thesis proposal, Arizona, Northern Arizona University

Ziegler, A. M., Barrett, S.F., and Scotese, C.R., 1981. Palaeoclimate, sedimentation and continental accretion. PHILOSOPHICAL TRANSACTIONS OF THE ROYAL SOCIETY OF LONDON. SERIES A, MATHEMATICAL AND PHYSICAL SCIENCES, 301 (1461), 253-264

Ziegler, P.A., 1988. Evolution of the Arctic-North Atlantic and the western Tethys. AAPG MEMOIR 43, 164-196.